

Brake Caliper Design and Optimisation for a Formula Student Vehicle

Diogo Paulo Martins Ferreira

Thesis to obtain the Master of Science Degree in

Mechanical Engineering

Supervisor(s): Prof. Luís Alberto Gonçalves de Sousa
Prof. Hélder Carriço Rodrigues

Examination Committee

Chairperson: Prof. João Orlando Marques Gameiro Folgado

Supervisor: Prof. Hélder Carriço Rodrigues

Member of the Committee: Prof. Aurélio Lima Araújo

November 2019

To my beloved parents, brother, girlfriend and friends.

Thanks for feeding my dreams.

Acknowledgments

First of all, I would like to thank my master thesis supervisors, Prof. Luis Sousa and Prof. Helder Rodrigues, for all the advice, patience and counsel provided during this work.

To Altair, for the given software licenses during this master thesis research.

To all my family, especially to my Mother, Father and Brother for all the support during this five years journey and all the sacrifice made for me to be able to study and achieve what they could not achieve. I can not be thankful enough, promising to pay you back with my presence, love and care.

To Patrícia, for all the never-ending support, the patience, the motivational speeches, the hours sleeping alone waiting for me, all the dinners, the escape rides, the weekends away from Lisbon, all the love. It would be worse without you.

To Patrícia's parents and family, for all the support and availability, being a second family to me, without asking in return.

To all the former and current team of FST Lisboa, for the friendship and concern showed towards this work.

Special thanks to Bogdan Sandu, João Formiga, Pedro Mendonça, Miguel Lino, Pedro Neves, Migdon, João Guapo, Tomás Bastos e Inês Carrondo for all the shared moments and friendship.

Not less important, to those who have been following me almost since the beginning: Xana, Adriana, Tomás, Ajuda, Hélder, Mariana, Pedro, Ribeiro, Rego, Chico, Milton, Franco.

To my dog, Salsa, for all the given company during the writing stages of this thesis.

Resumo

Encontrar a melhor solução compatível para cada componente do carro tem sido o objetivo de muitas equipa de *formula student*, tal como acontece na indústria automobilística. Este trabalho aborda a substituição do travão atual do carro, por uma solução otimizada produzida por fabrico aditivo.

O sistema atual foi analisado, resultando num valor de *compliance* de 10000 *Nmm*. Foi estabelecido um diâmetro de 25mm para os êmbolos. A interpretação dos resultados da otimização topológica terminou numa solução 12.5% mais leve.

Um modelo de transmissão de calor determinou uma temperatura de estabilização do sistema de 480°C após duas voltas em circuito, tolerável pelo material da pinça e dos discos.

O fabrico da pinça foi introduzido com referência às mudanças necessárias que permitam a maquinação das zonas com toleranciamento dimensional.

Foi proposta uma solução alternativa, com o suporte de um software de edição de malhas, resultando numa recriação mais precisa do design topológico e 23% mais leve.

Estabeleceu-se uma comparação entre os três componentes, focada na rigidez, redução de peso e comparação de custos do ponto de vista da produção. A solução final tem um custo de produção de 550€. Já a solução atual é vendida por 634€.

Palavras-chave: Travões, Fabrico aditivo, *Formula Student*, Otimização topológica, Projeto mecânico, *Selective Laser Melting*

Abstract

Finding the best suitable solution for each component of the car has been the objective of many formula student teams, similarly to the professional motorsport industry. This research is focused on the car's brake caliper replacement by an additive manufactured solution.

The current system was analysed, resulting in a 10000 Nmm compliance objective for the new design. The new piston diameter was specified as 25mm . The topology optimisation results interpretation ended in a 12.5% lighter caliper.

A transient heat transfer model has shown a settling temperature of 480°C after two circuit laps, bearable for both the caliper and discs.

The manufacturing of the caliper was introduced with the necessary changes to be made on the caliper to allow the later post-processing machining with tolerance dimensions.

An alternative solution was proposed, created with facets editing capable software, resulting in a most accurate topology recreation and in a 23% lighter component.

The conclusions between the three components were made, focusing on compliance maintenance, percentage of weight reduction and cost comparison from the production point of view. The final solution production cost is around 550€ , while the current solution selling price is 634€ .

Keywords: Calipers, Additive manufacturing, Formula Student, Topology optimisation, Mechanical design, Selective Laser Melting

Contents

- Acknowledgments v
- Resumo vii
- Abstract ix
- List of Tables xv
- List of Figures xvii
- Nomenclature xxi
- Glossary xxv

- 1 Introduction 1**
- 1.1 Motivation 1
- 1.2 Objectives 3
- 1.3 Thesis Outline 3
- 1.4 Methodology 4

- 2 Important concepts and theoretical background 5**
- 2.1 Formula Student Competition 5
 - 2.1.1 Competition Description 5
 - 2.1.2 Competition Rules about Brake design 5
- 2.2 FST Lisboa Team 6
 - 2.2.1 Relevant Car Specifications 6
 - 2.2.2 Design Constraints 7
 - 2.2.3 Actual Brake Design Description 9
- 2.3 Brakes 9
 - 2.3.1 Types of Brake Caliper 10
 - 2.3.2 Usual Components 11
 - 2.3.3 Brake Pads 12
 - 2.3.4 Lubrication 13
 - 2.3.5 Brake Fluid 13
- 2.4 Tires 14
 - 2.4.1 Friction Model - Coulomb model 14
 - 2.4.2 Important Loads 15

2.5	Additive Manufacturing	15
2.5.1	Available Technologies and Materials	16
2.5.2	Geometric Tolerances	16
3	Mechanical Analysis	19
3.1	Free Body Diagram Analysis	19
3.1.1	Free Body Diagram with Aerodynamic Influence	21
3.2	Forces Calculation	22
4	Design Process	27
4.1	Initial Design	27
4.2	Optimisation Model Setup	31
4.2.1	Topology Optimisation Formulation	32
4.2.2	Model Description	34
4.3	Convergence analysis	35
4.4	Optimisation parameters	36
4.5	Post Processing of Optimisation Results	38
4.5.1	First Design	40
4.5.2	Second Design	42
4.5.3	Third Design	43
4.6	Assembly checks	44
4.7	Assembly example with Bill of Materials (BOM)	44
5	Thermal Analysis	47
5.1	Theoretical Model	47
5.2	Transient heat transfer model setup	48
5.2.1	Initial Results	52
5.3	Second Model - Aerodynamics and Hub influence	54
5.3.1	Second Model Temperatures	55
5.4	Third Model - Aerodynamics and Regeneration influence	56
5.4.1	Third Model Temperatures	57
5.5	Convergent Temperature	59
6	Manufacturing Approach	61
6.1	3D Printing Design Adjustments	61
6.2	Geometrical and Dimensional Tolerances	63
6.2.1	Thread Holes	63
6.2.2	Piston boreholes	63

7 Alternative Design	65
7.1 Alternative design obtained by STL editing	65
7.2 Final renders	68
8 Conclusions	71
8.1 Results Discussion	71
8.1.1 Detailed comparison between solutions	71
8.1.2 Weight Reduction	73
8.1.3 Alternative Solution	74
8.2 Spare Parts Cost	74
8.3 Final Conclusions	75
8.4 Future Work	76
Bibliography	77
A Sculpteo Quote	81

List of Tables

2.1	DOT Standards	14
2.2	Additive manufacturing processes and suitable materials [18].	16
2.3	SLM process accuracy according to IT grade [21]	17
3.1	FST 09e car's specifications	22
4.1	Finite elements model properties	36
4.2	Ti6Al4V material properties	36
4.3	BOM example for the caliper assembly	45
5.1	Friction couple properties	47
5.2	Titanium thermal properties	49
8.1	AP Racing caliper analysis	72
8.2	Third design caliper analysis	72
8.3	SLM optimal parameters for quality [35]	72
8.4	AM final design cost analysis	73
8.5	Alternative design caliper analysis	74
8.6	AM alternative design cost analysis	74
8.7	Spare parts cost	75

List of Figures

1.1	Specific Strength of the commonly used materials against temperature [6]	2
1.2	Bugatti first 3D printed brake caliper [7]	2
1.3	Work methodology flow chart	4
2.1	FST 09 line specifications	7
2.2	OZ Formula Student Magnesium CL 10 inch wheel [10]	8
2.3	FST 09e wheel knuckle	8
2.4	FST 09e brake pads from AP Racing	8
2.5	Disc brakes	9
2.6	Drum brakes	10
2.7	Fixed Caliper vs Float Caliper	10
2.8	Exploded view of a typical caliper	11
2.9	Wide variety of attachments for brake pads [16]	12
2.10	Manufacturing processes IT grades	17
3.1	Car under braking diagram [15]	19
3.2	Free body diagram	20
3.3	Free body diagram with aerodynamics	21
3.4	Real rolling radius due to tire load and pressure [15]	23
3.5	Excel spreadsheet	24
3.6	Pedal Ratio meaning [15]	24
3.7	Balance Bar setup [15]	25
4.1	Compatibility design approach	27
4.2	Caliper design and space definitions	28
4.3	Caliper halves attachment points	28
4.4	Knuckle attachment points	29
4.5	Piston placement in caliper	29
4.6	O-ring deformation range in function of the cross-section [22]	30
4.7	25mm diameter size atching o-rings (left); Schematic for hydraulic rod seals (right) [22]	30
4.8	Another groove parameters (left); Roughness tolerances (right) [22]	30
4.9	Brake fluid trajectory inside the caliper	31

4.10 Banjo fitting (left); Bleeding screws (right)	31
4.11 Finite Element Method (FEM) Model	32
4.12 Shared faces between the design and non-design space bodies	32
4.13 SIMP method curves with different penalty factors [23]	33
4.14 The influence of using member size filters [24]	34
4.15 Line pressure represented on FEM model	34
4.16 Brake torque represented on FEM model	35
4.17 Bolt pretension represented on FEM model	35
4.18 Convergence of displacement result at two reference points	36
4.19 Cyclic Load	37
4.20 Approaches for non fully reversed cyclic fatigue loading [27]	37
4.21 Volume fraction response at each iteration	38
4.22 Compliance response at each iteration	39
4.23 Different threshold plot results	39
4.24 NURBS design approach	40
4.25 First design rendered view	40
4.26 von Mises stress plot for first design attempt	41
4.27 First design close-up views	41
4.28 Energy error density plot for first design attempt	42
4.29 von Mises stress plot for second design attempt	42
4.30 Second design close-up views	42
4.31 Energy error density plot for second design attempt	43
4.32 von Mises stress plot for third design attempt	43
4.33 Energy error density plot for third design attempt	44
4.34 Interferences location of the assembly	44
4.35 Full assembly with fittings	45
4.36 Representation of the aluminium piston	45
5.1 Thermal model scheme	49
5.2 Defined areas for heat flux application	50
5.3 Convection relevant faces	50
5.4 In plane GPS position	51
5.5 Vertical GPS position	51
5.6 Grid temperature Vs Time during a autocross event - Model 1	52
5.7 The reduction factor for effective yield strength with temperature [31]	53
5.8 Temperature plot at different stages of autocross - Model 1	53
5.9 Second thermal model scheme	54
5.10 Aerodynamics Influence on Braking Total Power	55
5.11 Grid temperature Vs Time during a autocross event - Model 2	55

5.12	Temperature plot at different stages of autocross - Model 2	56
5.13	Aerodynamics and Regeneration Influence on Braking Total Power	57
5.14	Grid temperature Vs Time during a autocross event - Model 3	57
5.15	Temperature plot at different stages of autocross - Model 3	58
5.16	Convergence of Disc Temperature	59
6.1	Fine tolerance faces of half capiler	61
6.2	Design adaption with excessive material for 3D printing	62
6.3	Design adaption with excessive material for 3D printing (2)	62
6.4	Shoulder bolts drill scheme	63
6.5	Piston boreholes	64
7.1	Volume fraction response of the alternative optimisation	65
7.2	Compliance response of the alternative optimisation	66
7.3	Alternative design optimisation isosurface	66
7.4	Facets geometry representation	67
7.5	SpaceClaim 0.3 density threshold isosurface	67
7.6	Smoothing and wrapping of the design space mesh with the non-design space	67
7.7	Final faceted part	68
7.8	Faceted design reanalysis	68
7.9	Faceted design render view	69
7.10	Faceted design render view (2)	69
8.1	AP Racing Caliper	71
A.1	Sculpeo Quote for the caliper 3D printing	81

Nomenclature

α	Thermal effusivity
a	Acceleration
A_{disc}	Disc contact area
$A_{fpiston}$	Front piston area
A_{pads}	Pads contact area
A_{prof}	Aerodynamics projected area
BB	Brake bias
C	Compliance
c	Specific heat capacity
C_D	Coefficient of drag
C_L	Coefficient of lift
C_M	Coefficient of moment
$D_{fpiston}$	Front piston diameter
d_M	Maximum deceleration [m/s^2]
E	Element stiffness
E⁰	Standard element stiffness
F	Load vector
F_B	Balance bar force
F_f	Front axle total vertical force
F_L	Left master cylinder force
F_R	Right master cylinder force
F_{aero}	Aerodynamics drag force

$F_{balancebar}$	Balance bar force
F_{brake}	Brake force
$F_{frontMC}$	Front line master cylinder force
F_{fwheel}	Vertical force per wheel
F_{mt}	Vertical force component due to mass transfer
F_{pedal}	Pedal force
F_{v_f}	Front axle static vertical force
F_A	Aerodynamics vertical force
F_k	Kinetic friction force
F_N	Contact normal force
F_{s_i}	Each wheel friction force
F_{smax}	Maximum total friction force
F_s	Static friction force
g	Gravity acceleration
g_M	Maximum deceleration [$g's$]
H	Heat energy
$H_{caliper}$	Heat energy per caliper
H_{disc}	Heat energy dissipated on discs
h_{forced}	Forced convection coefficient
$h_{natural}$	Natural convection coefficient
H_{pad}	Heat energy dissipated on the pads
K	Stiffness matrix
κ	Thermal conductivity coefficient
L	Wheelbase
l	Tire width
m	Mass
n	Safety factor
p	Penalisation factor

p_D	Disc heat parcel
p_P	Pads heat parcel
P_{aero}	Aerodynamics power
$P_{braking}$	Braking power
P_{disc}	Dissipated power on disc
$P_{frontline}$	Front line pressure
$P_{mechanical}$	Mechanical power
P_{pad}	Dissipated power on pad
$P_{regeneration}$	Regeneration power
P_{tire}	Tire pressure
PR	Pedal ratio
ρ	Density
ρ_e	Elementary relative density
ρ_{air}	Air density
$\tilde{\rho}$	Elementary relative densities vector
R	Tire radius
r_m	Mean disc radius
R_{loaded}	Tire loaded radius
S_e	Fatigue endurance limit
S_y	Yield strength
S_{ut}	Ultimate strength
t	Time
T_{brake}	Brake torque
\mathbf{u}	Displacement vector
μ_k	Kinetic friction coefficient
μ_s	Static friction coefficient
μ_{disc}	Disc brakes efficiency factor
μ_{pad}	Pad friction coefficient

μ_{tire}	Tire friction coefficient
u_{max}	Maximum velocity
v	Velocity
V_0	Initial velocity
\tilde{V}_e	Elementary volume vector
W_c	Car's Weight
ϕ_{disc}	Disc heat flux
ϕ_{pads}	Pads heat flux
σ_a	Alternating stress
σ_{max}	Maximum stress
σ_{med}	Mean stress
σ_{vm}	von Mises stress
x_{CG}	Longitudinal position of gravity centre
x_{CP}	Longitudinal position of pressure centre
y_{CG}	Gravity centre height

Acronyms

AM Additive Manufacturing

BOM Bill of Materials

CAD Computed Aided Design

CEF Cost Explanation File

CG Center of Gravity

CNC Computer Numerical Control

CP Center of Pressure

DMLS Direct Metal Laser Sintering

DOT US Department of Transportation

ERBP Equilibrium Reflux Boiling Point

FEM Finite Element Method

FSS Formula Student Spain

GPS Global Positioning System

IT International Tolerance

MC Master Cylinders

NURBS Non Uniform Rational Basis Spline

RBE3 Rigid Body Element 3

SIMP Solid Isotropic Material with Penalisation

SLM Selective Laser Melting

SLS Selective Laser Sintering

STL Standard Triangle Language

Chapter 1

Introduction

1.1 Motivation

Additive manufacturing (AM) technologies, after more than 30 years of development, are starting to get along in almost all the sectors of production. Although the high-intensity use of this technology is only a recent situation, the first pieces of this technology gave signs of life some years ago. The manufacturing industry is still used to manufacture all sorts of parts and pieces using blocks of material, for consequential material removal. This is common within the metal industry. There were also alternatives, such as metal casting and forming to manufacture an almost shape finished part [1].

First of all, the AM technology development made it worth billions nowadays, so it is vital to evaluate where it could be implemented, to reduce the number of productions steps and time for a specific piece or even reduce the material waste on machining cycles.

Secondly, Formula Student plays an essential role in the engineering field, where a student can work as a real engineer and apply a significant part of his ideas. So there is a constant search for innovation in this competition, being one of the places, apart for other formula competitions, where innovative solutions came up in first place. As Ross Brawn has previously said in an interview to the Formula Student IMechE website - "There are two really innovative forms of motorsport left: Formula One and Formula Student" - and knowing his fantastic role in the motorsport competition, especially in F1, this statement has a lot more meaning to it than any other [2].

With this mindset, searching simultaneously for innovation and performance can be only achieved if the basic principles of vehicle performance are taken into consideration, such as the case of acceleration and deceleration. If these two characteristics become perfectly tuned, the car can get the most out of the track, since there is less time wasted on performing a brake to a corner or even reaching the top speed on a straight piece of track. To achieve those goals, the brake design can be optimised to increase the ratio performance/weight, when compared to standard automotive road brakes.

Braking is the transformation of kinetic energy into heat energy, due to the friction forces that act between the brake pads and the disc. In a road car, the carried kinetic energy is lower, and it is converted gradually. Statistically speaking, a road driver rarely exceeds 0.2 G's of braking, since they usually brake

earlier enough to keep a smooth ride [3]. However, in a race scenario, such as F1, the kinetic energy carried is enormous due to the speed, and the rate of deceleration is tremendous, being capable of reaching 4 G's [4]. The formula student competition is a small-sized kind of F1 competition, focused a bit more in innovative solutions. The tracks are very narrow and curvy, so brake performance and acceleration take more importance when compared to speed.

The link between the brake system and the AM implementation is a way of avoiding unnecessary body shapes constrained by the manufacturing techniques, allowing the achievement of a topologically optimised body, capable of handling the necessary loads and temperatures, while being simultaneously lightweight.

State of the art solutions in 3D printing are now exploring the versatility of the Ti6Al4V alloy, also called Titanium grade 5. There are several variants of titanium alloys, all of them with excellent properties. However, this alloy is known for its key features, such as the weldability, high-temperature resistance of up to 800°, the biocompatibility and the high strength-to-weight ratio [5]. It is an exceptional material with performance levels closer to the carbon fibre reinforced polymers and some extra commodities of the metal field, shown in figure 1.1.

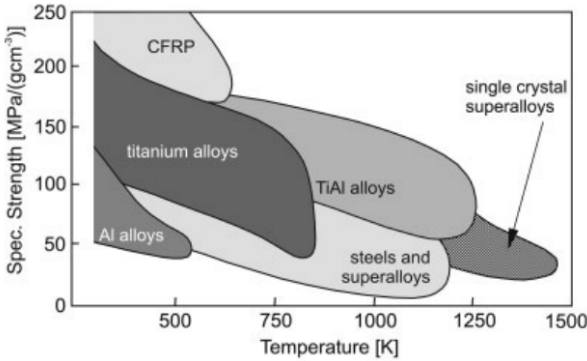


Figure 1.1: Specific Strength of the commonly used materials against temperature [6]

The automotive industry was marked by the combination of this fantastic alloy with the additive manufacturing, resulting in the Bugatti first 3D printed brake caliper (Figure 1.2), being considered the largest titanium functional component, printed with that alloy [7].



Figure 1.2: Bugatti first 3D printed brake caliper [7]

1.2 Objectives

This thesis' main goal is to bring the whole process of design and optimisation to a part, currently bought from a company. It can be split into several different milestones.

First of all, with this study, it is possible to bring a rapidly increasing technology, such as AM, closer to the team and prepare its future members to operate and develop parts with this field.

Secondly, there is an increase in design experience which can result in a better score at competitions if it is proven that this design and technology pay off on several levels. The performance level falls upon the final weight, stiffness and brake capabilities. The design level is about making things worth it, so the price and manufacturing process changes must be justifiable in terms of the gains it is getting in return.

1.3 Thesis Outline

The present thesis is divided into eight chapters:

- Chapter 1 - Targets the motivation, objectives and methodology that led to this thesis study.
- Chapter 2 - Defines the concepts and theory behind this type of part. Some concepts about the Formula Student rules and the FST Lisboa constraints are explained. Introduces the characteristics of the car that influence and help in defining the final parameters of a brake caliper. The several existent types of brakes, brake pads and other components are referred. Finishes with an introduction to the AM technologies and its geometric tolerances.
- Chapter 3 - Presents the mechanical analysis of the car that is relevant to determine some key parameters of the caliper and explains in which order it must be made.
- Chapter 4 - Exposes the design process and its development through time from the primordial base design to the final assembly. It is shown the finite elements model, the optimisation stage and its results. Several solutions are discussed, and a final one is established. With that solution comes up an example of an assembly with spare parts available on the market for sale.
- Chapter 5 - Consists in the thermal analysis of the brake system assembly to assess its working temperatures and if they conform with the material limits. The transient heat transfer model is explained, and its results discussed.
- Chapter 6 - A small chapter about the considerations that must be taken into account in order to print the part in a ready condition to be machined later.
- Chapter 7 - Approaches an alternative solution designed with another type of software techniques, based on STL (Standard Triangle Language) direct editing. Shows more accurately how much material can be actually removed, because of the more precise topology reproduction.
- Chapter 8 - Resumes all the results achieved by the previous solutions and correlate each result with a cost analysis in order to establish a comparison between the current and the new solutions.

1.4 Methodology

This work started with a set of specifications from the FST 09e car. The flow chart from figure 1.3 describes the methodology used during the present work. The final goal are the conclusions to evaluate if the new part is worth it in terms of cost, performance gained and knowledge.

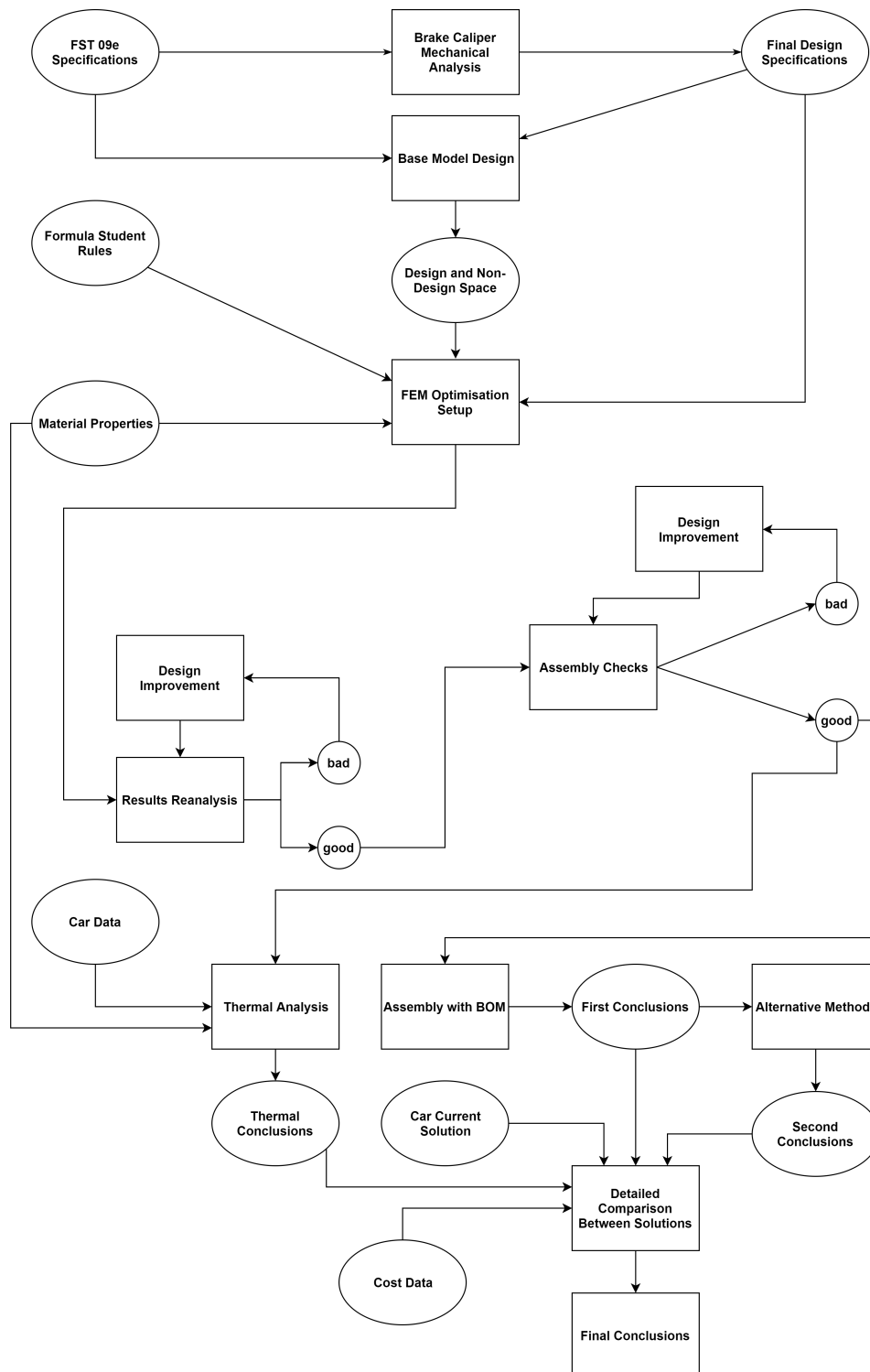


Figure 1.3: Work methodology flow chart

Chapter 2

Important concepts and theoretical background

2.1 Formula Student Competition

2.1.1 Competition Description

The Formula Student competition is a developed and known educational engineering competition, being more than 20 years old. The competitions are held and assisted by some of the greatest names of the engineering industry, also becoming a great way of launching a future career, while still being a student.

Despite being a student competition, it is frequently seen as an excellent asset to have, because of the work and development it takes to finish and compete with the prototype. It is also often compared with real industry working experience [8].

2.1.2 Competition Rules about Brake design

Due to the competition nature and being the prototypes entirely made by students, there is a set of rules to be strictly met while building the car. Therefore, there is some of them strictly made to affect the design process of the brake system, playing an important role to make sure the car fulfils all the security procedures related to minimum brake performance.

The most important rules to be taken into account are [9]:

- The brake system must be capable of locking all four wheels at the same time;
- The vehicle must be equipped with a hydraulic brake system acting on all wheels and operated by one single control/pedal.
- The brake pedal and all the system must be designed to withstand a force of 2 kN without the failure of any component.

- The brake system must have two independent hydraulic lines such that in the case of leak or failure, there is still braking power to be applied in, at least, two of the wheels.

2.2 FST Lisboa Team

The FST Lisboa team has a long history related to formula student competitions. The FST 09e is the team's ninth car with the development starting in September 2018 and ready to compete by June 2019. Since the thesis' intellectual product is to be applied to this or any future car, it makes sense to approach some of the car aspects and its influence on the design stage.

2.2.1 Relevant Car Specifications

The car specifications are critical to defining some reference values that play an important role in the design stage. Being this about the design of a brake system, the most important specifications to take into account are:

- **Weight and Center of Gravity (CG) position** - The weight of the car influences the amount of force exerted by the car on the floor, while the CG position defines the mass distribution.
- **Aerodynamic forces and Center of Pressure (CP) position** - The aerodynamic forces are another type of forces present on the vehicle free body diagram, assuming there is movement at a given speed and the car has a specific lift and drag coefficient. Because of the wings design, the car produces a vertical downforce and a horizontal drag force. The downforce influences, alongside the weight of the car, the amount of vertical reaction force produced on each wheel, contributing for the maximum brake torque available on the tire. The CP position, similar to the CG, determine the aerodynamic forces distribution on the car.
- **Wheelbase** - When the brakes are applied, it is imposed an acceleration and therefore a change in speed. Due to its weight, the car generates an inertial force, while braking. This force is responsible for the automotive phenomenon called "mass transfer" which is characterized by the weight change of each axle, decreasing on one of the axles and passed to the other.
- **Pedal Ratio** - The Pedal Ratio characterize the way the pedal is designed to transmit the forces to the Master Cylinders (MC). Briefly, it is a multiplication factor that is applied to the applied force in order to generate the MC Force. It is influenced by the connection point between the pedal and the Balance Bar and by the angle of the MC.
- **Tire Radius** - The tire radius affects the brake torque required to apply the needed amount of brake force. For a larger tire radius, the brake torque required is larger, to achieve a reference value of brake force.
- **Brake disc Effective Radius** - The brake disc effective radius affects the friction force necessary to apply the reference brake torque. The larger this radius is, the less required is the system to

apply the reference brake torque.

Both of these characteristics of the car are important to achieve a proper sizing of the system.

2.2.2 Design Constraints

The content produced by this thesis can be applied to an already design defined car, so some constraints could not be avoided. An entire brake system is constituted by:

- **Brake Pedal** - Which contain the pedal ratio characteristic
- **Master Cylinders** - The master cylinder has some properties that could influence the design process. The bore diameter of the cylinders influences the pressure on the line for a given amount a foot force. It is useful to tune the brake force feeling transmitted to the driver. There are some reference values for the ideal foot force required to apply 1g's of brake deceleration.
- **Brake Line** - The brake line is projected to withstand the pressure achieved on panic brake stops.
- **Brake Caliper** - The caliper contains the elements that exert the pressure on the disc.

It is assumed that the brake pedal is already finished in terms of design, so the pedal ratio is already defined. The master cylinders and the brake line are chosen as well, so the brake boundaries of pressure are already inevitable. Since the caliper is the object of study within this thesis, it may happen some changes on the caliper characteristics in order to achieve what the design demands.

In figure 2.1, it can be seen the type of brake line used by the team and the limit values of pressure those lines can withstand. The maximum working pressure is the pressure that should not be passed in normal operating conditions, while the burst pressure is the tested pressure at which the lines fail, being the absolute maximum value.



(a) Brake Line - 600-03BK

Part No	Bore Size		PTFE Wall		Braided O.D		Cover Wall		Cover O.D		Working Pres		Burst Pres		Weight		Temperature	
	MM	Inch	MM	Inch	MM	Inch	MM	Inch	MM	Inch	Bar	PSI	Bar	PSI	KG/M	L/FT	Min	Max
600-02	2.0	0.079	1.0	0.039	5.0	0.197	-	-	-	-	450	6600	1350	19800	0.045	0.03	-70°C (158°F)	260°C (500°F)
600-03	3.5	0.138	1.0	0.039	6.45	0.254	-	-	-	-	290	4250	870	12750	0.060	0.04	-70°C (158°F)	260°C (500°F)

(b) Pressure Limits

Figure 2.1: FST 09 line specifications

Although a significant part of the brake system constrains came from the system itself, some may occur due to other systems nearby. In this case, the FST 09e has a new rim (figure 2.2), that is slightly tighter when it comes to packaging. Due to that fact, it is paid particular attention to the inner contour of the rim, making sure there are no interferences between the caliper and the rim.

On another hand, the car's knuckle (figure 2.3) plays an important role either with the suspension links either with the brake system. It has some specific points where the caliper should fit and be secured. The knuckles' shape is itself a constraint, so compatibility must be assured with the current system on development.



Figure 2.2: OZ Formula Student Magnesium CL 10 inch wheel [10]



Figure 2.3: FST 09e wheel knuckle

For future compatibility and maintenance by the team, it was decided that the brake pads are the same of the current brake caliper package (figure 2.4), so they are easy to be bought and replaced in case of wear out. It is a good practice of engineering getting the most compatibility to the part under design, allowing a higher useful life for the part.

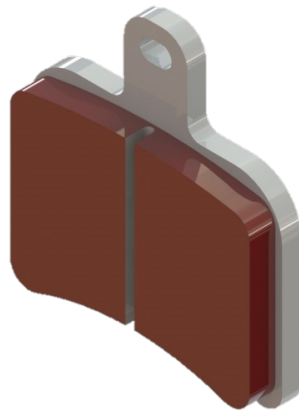


Figure 2.4: FST 09e brake pads from AP Racing

2.2.3 Actual Brake Design Description

Since its design stage, the FST 09e has a brake system projected to go into the car. The system has been reliable for the past few years, and it is composed by two calipers, with four pistons each, on the front axle and two calipers, with two pistons each, on the rear axle. There are also two master cylinders, each one for each axle, meaning two separate brake lines, acting as a backup plan in case of failure of one of them. It also allows the implementation of brake bias, splitting the force of the pedal unevenly for each of the master cylinders.

The components bought from AP Racing have a range of properties, in order to allow the proper sizing of each one of them, for example, there are several master cylinders with different diameters available. When it comes to the caliper, the pistons diameter are not customizable, so a compatible choice must be made.

2.3 Brakes

The nomenclature caliper is frequently applied to hydraulic disc brakes (figure 2.5). The structure of the caliper makes it similar to a clamp, that acts on the disc. The clamping force, combined with a friction couple, usually the pads and the disc itself, generates a friction force capable of producing a torque against the movement of the wheel. This phenomenon happens through the conversion of the kinetic energy of the vehicle to heat.



Figure 2.5: Disc brakes

There are, therefore, other types of hydraulic brakes, such as drum brakes (figure 2.6). The drum brakes generate the friction force by pressuring a couple of pads against the inner surface of the drum. The mechanism of force transmission is a hydraulic fluid. Those brakes are budget solutions for standard class road cars, but when it comes to racing performance, the heat generated by abusive braking causes the expansion of the drum, which leads to brake fading and less performance. They also tend to have a lower performance on wet scenarios [11].

For the hydraulic disc brakes, the brake disc is heated by the friction forces acting between the pads and the rotor, but there is typically much exposure to moving air, which makes the cooling process a lot easier and faster. The thermal expansion generated on the disc tendentially increases its volume against the pads, so brake fading is less propitious. These properties are crucial for racing vehicles since many cycles are happening and the endurance capability alongside with an even wear of the pads

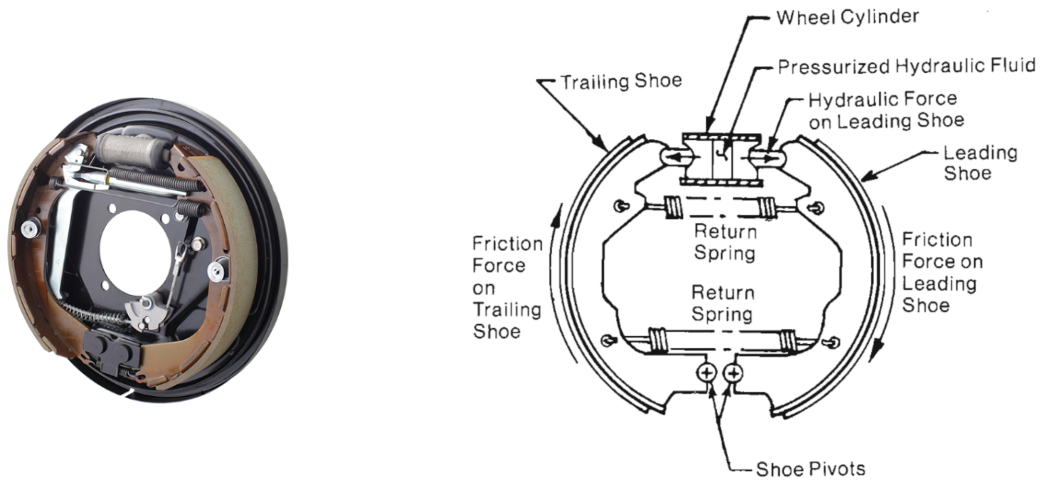


Figure 2.6: Drum brakes

is essential to maintain an excellent brake performance [11].

Despite the existence of several types of brakes, this thesis is focused on the development of a caliper to be applied on a hydraulic disc brake system, since they are the object of study, either for its greater performance either for the innovation team's philosophy.

2.3.1 Types of Brake Caliper

The figure 2.7 shows the two principal types of braking calipers.

A fixed caliper is a rigid clamp mounted on the wheel knuckle. The movable parts are the pistons and the pads and, as the brake pedal is pressed, they grip in both sides of the disc. They have an advantage over the floating type of caliper due to the even wear of the pads [12]. Those types of caliper have, at least, two pistons in total, one for each side [13].

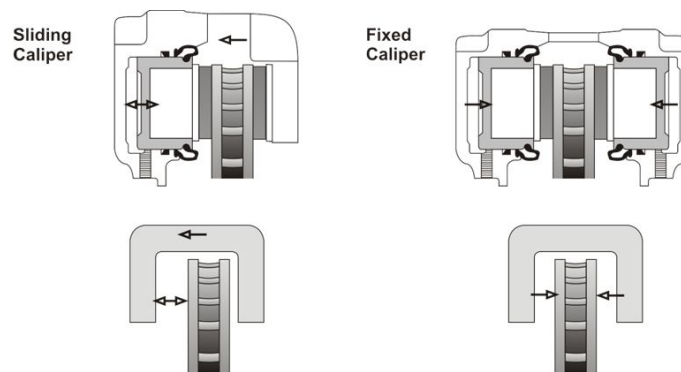


Figure 2.7: Fixed Caliper vs Float Caliper

A floating caliper is a sliding type of caliper. It only demands one piston. As the brake pedal is pressed, the piston moves and the pad contact the inner face of the disc. Sliding pins attach the other side, so when the disc is pressed on the inner side, the outer part is pushed against the disc. This guarantees the force is applied on both sides, even with just one piston. When compared to the fixed

calipers, this type requires less volume because of the only piston reservoir in the inner side [13].

2.3.2 Usual Components

There are several available configurations for the brake calipers design, but there are components that remain practically the same within each one.

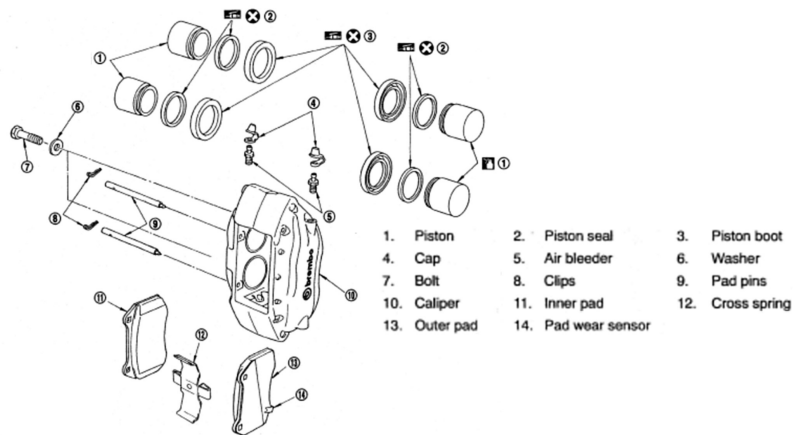


Figure 2.8: Exploded view of a typical caliper

Using the figure 2.8 model as an example, the major components are:

- **Housing/Caliper body** - The main structural body that gathers all the other components. It is tightly supported on the wheel knuckle.
- **Pistons** - The movable piece that exerts pressure on the pads and therefore on the disc.
- **Piston dust boot** - It is a rubber seal that prevents the penetration of debris and dust to the bore of the piston.
- **Piston retraction seal** - It is a rubber seal that prevents leakage of hydraulic fluid to outside of the bore, but it also has a function of retrieving the piston back, when pedal force is released. This seal has the capacity of deforming elastically, and due to that deformation, it is prevented the continuous wear of the pads, when pedal force is released.
- **Brake pad assembly** - It is the set of the brake pad and its backing plate. The backing plate is the point of contact with the piston and is used to guide the brake pad in a determined direction. It also protects the pistons of wearing out, in case of brake pad wear out. The brake pad is the friction material that contacts directly with the brake disc and is usually projected to have higher friction coefficients when rubbed against the disc material.
- **Bleeder screw** - This component has the function of bleeding the brake system, which consists on the filling stage of the brake system and consequent removal of air bubbles within the brake lines, to avoid compressive fluid behaviour. When the brake line has a compressive fluid on the line, such as air, the brake pedal feeling becomes spongy, which is undesirable [14].

2.3.3 Brake Pads

The brake pads are the material that rubs on the brake disc. In disc brakes, the friction material is attached to a backing plate, that contacts with the piston and the caliper. These backing plates can have several shapes and different ways of attachment to the pad material. The most common ways of attachment are a riveted connection or an adhesive one (figure 2.9).

The riveted connection is reliable, and an old technique, but some problems came up from its use, such as cracks on the pad, due to temperature changes. From another point of view, if the major part of the pad wears out, it can start scratching the brake disc [15].

A bonded connection is a modern approach being capable of handling high temperatures by the use of certain adhesives. Also, there is no tendency for the material to grow cracks, and in the case of complete wear out, there is less damage inflicted to the brake rotor. Because this is a surface attachment, there is a major percentage of the pad that is going to be consumed, compared to the riveted connection, being more efficient between pad changes [15].

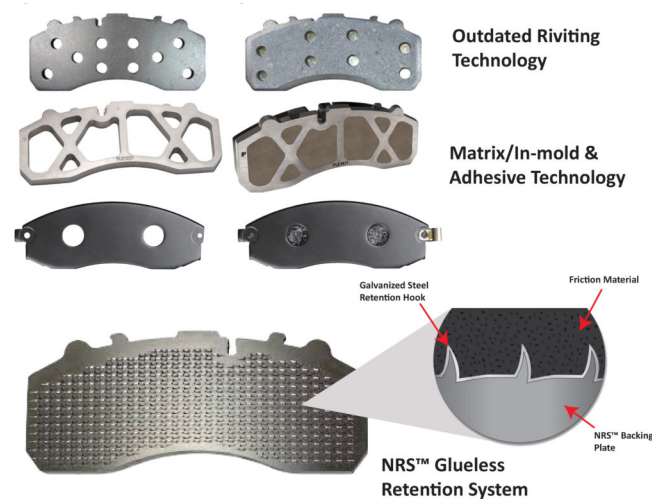


Figure 2.9: Wide variety of attachments for brake pads [16]

The brake pads material is a significant choice while designing a brake system. Depending on the estimated use and field of application, there are suitable materials to fulfil that function. Common types of brake pads materials are organic materials, metallic materials and semi-metallic materials [15].

Organic

Organic linings are widely used in the automotive industry when it comes to regular road performance. These linings have several varieties of components, such as:

- **Asbestos fibres** - for friction and heat resistance;
- **Friction modifiers** - To tune up the friction coefficient;
- **Fillers** - to reduce the noise on operation;
- **Binders** - Holding the material together;

- **Powdered elements** - to improve brake performance.

The major part of this linings have good friction properties at low temperature (204°C), but they wear fast and experience some fading when the temperature increases. That is why they are not suitable for racing purposes. However, there are some organic pads made specifically for high temperature (the best ones reach 670°C) and racing purposes. They tend to be highly constituted by metal particles, that increase the heat resistance and the friction coefficient.

Ceramic-Metallic

The ceramic-metallic linings came up as a manner of providing higher performance braking. The material of the pad is harder. Therefore it takes more time to wear out, but it is also more abrasive to the brake discs. This type of linings is designed to operate at higher temperatures, being potentially ineffective if not warmed up properly. For that reason, it is widely applied for racing purposes, and that is also the reason the drivers spend up some time heating the brakes to a desirable temperature on the warming up laps.

Semimetallic

This third category is a middle compromise to solve the issues that each type of brakes had. They are mainly made of steel fibres bonded with organic resins, to mix both of the characteristics. They handle temperatures pretty well (up to 540° C).

The hardness of the pads is an important property because a soft material tends to wear faster with temperature, than a harder one. Due to that, the choice may be different for every situation. Situations with low brake usage will not warm the brakes enough, so the best choice is semi-metallic or organic, while a brake intensive usage situation demands a ceramic-metallic, in order to handle the high temperatures and short cooling periods [15].

2.3.4 Lubrication

Lubrication is crucial for a good performance. The piston bores and all other moving parts must be well lubricated before the placement of the rubber seal, allowing the piston to slide relatively to those. In the case of a floating caliper, the guide pins must be in proper lubricated allowing the proper movement of the floating half of the caliper. The only place where lubricants are unwanted is between the friction pad and the rotor because they would reduce the originally designed friction coefficient of the pair [12].

2.3.5 Brake Fluid

The brake fluid maintains the car's reliability and safety. During a brake process, the energy dissipated heats the brake disks majorly. Therefore, some of that heat may be dissipated to the brake fluid, which can cause an impact on its performance.

The most important brake fluid characteristics are:

- **Boiling point** - There are two boiling points. The equilibrium reflux boiling point (ERBP) and the wet equilibrium reflux boiling point (Wet ERBP). The first one is tested with the fluid in brand new condition. The second one takes into account the moisture absorption that occurs over the time of use, which affects the properties and, therefore, the boiling point of the mixture.
- **Viscosity** - The viscosity is the resistance to deformation that the fluid presents. It is an important parameter especially at shallow temperatures, to avoid the excess of viscosity, which would cause a delayed action of the brake system.
- **pH** - The pH must be in agreement with the materials that are in direct contact with the fluid, to avoid corrosion.

There are vehicle standards defined for these fluids, called Department of Transportation (DOT) standards (table 2.1).

Table 2.1: DOT Standards

Brake Fluid	Dry Boiling Point	Wet Boiling Point	Viscosity at -40°C (mm^2/s)
DOT 3	205°C	140°C	1500
DOT 4	230°C	155°C	1800
DOT 5	260°C	180°C	900

2.4 Tires

The tires play a vital role in the conception of the brake system. They can transmit the moment exerted by the caliper, which acts against the moment caused by the inertia of the car, to the floor.

2.4.1 Friction Model - Coulomb model

There is a simple model that can be used to securely design a brake system, being the static friction Coulomb model. Coulomb has determined that the frictional force produced by the contact between two bodies depends if the bodies are in static or kinetic contact.

The friction force, F_s , depends on the contact normal force, F_N , by the following equation:

$$F_s = \mu_s F_N \quad (2.1)$$

The μ_s is called the static friction coefficient, being dependent on the material but almost independent on the contact area and surface roughness [17].

For the kinetic friction, the kinetic friction force, F_k is dependent on the contact force, F_N , and it is independent on the sliding speed. The equation is kept same except for the μ_s , being replaced by the kinetic friction coefficient, μ_k [17].

$$F_k = \mu_k F_N \quad (2.2)$$

The meaning of these coefficients is related to the difference between the apparent area of contact and the real area of contact, noticeable at a micro-scale analysis of the contact surfaces. For a wide range of magnitudes of the normal force, it can be considered that the material is usually stiff enough to maintain a reasonable difference between the two areas referred to earlier.

Often the change between static and sliding friction is considered to be discontinuous because of the friction coefficients difference. Therefore this is a rough approximation. For a broad spectrum of sliding speeds they can be considered pretty different, but it is also evident that when a static contact is loaded tangentially, there has to happen some sliding, even though it is just microscopic. This is the friction case between the tire and the road, but if the sliding speed increases dramatically, the "static friction" is lost. In that range of sliding speeds, it can be considered that $\mu_k \ll \mu_s$ [17].

2.4.2 Important Loads

Using these approximations, it can be calculated the maximum value of brake torque that is applied. Considering a critical scenario, it is needed an approximation for the maximum coefficient of static friction and a value for the maximum downforce acting on each wheel of the car. This value depends on several external factors, such as:

- Car weight
- Driver weight
- Aerodynamic produced downforce and its distribution for the axles.

Usually, the real usage conditions are softer than the critical ones, so the wheels are going to lock before reaching the critical brake torque, assuring that this value is suitable and a useful reference for a secure brake caliper design.

2.5 Additive Manufacturing

AM technologies are defined as processes based on material addition instead of the common subtractive machining techniques. It is present for the last 25 years, being early restricted to polymer materials, making most of the parts produced not suitable for heavy-duty engineering purposes.

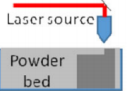


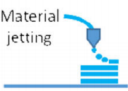
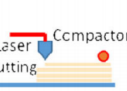
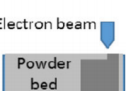
With this technology development, today, it is possible to see AM technologies incorporated in production and assembly lines of several industry fields [18]. The major benefits are those listed below:

- No tooling needed.
- Small production batches are economical - Setups are versatile.
- Reduced waste.
- Easy design changes and customization.

2.5.1 Available Technologies and Materials

The table 2.2 shows the currently available techniques used on the AM field. The most common polymer 3D printers use thermal extrusion processes. In the metal 3D printing, the most commonly used technologies are Laser Melting techniques, that use metal powders that are melted by a laser.

Table 2.2: Additive manufacturing processes and suitable materials [18].

Additive Manufacturing (AM) Processes														
Process	Laser Based AM Processes				Extrusion Thermal	Material Jetting	Material Adhesion	Electron Beam						
	Laser Melting		Laser Polymerization											
Process Schematic														
Name Material	SLS	Green	DMD	Green	SLA	Blue	FDM	Red	3DP	Green	LOM	Red	EBM	Green
	SLM	Green	LENS	Green	SGC	Blue	Robocasting	Red	IJP	Blue	SFP	Red		
	DMLS	Green	SLC	Green	LTP	Blue			MJM	Blue				
			LPD	Green	BIS	Blue			BPM	Blue				
					HIS	Blue			Thermojet	Blue				
Bulk Material Type		Powder	Green	Liquid	Blue	Solid	Red							

The most relevant processes for this master thesis purpose are the SLS (*Selective Laser Sintering*) or SLM (*Selective Laser Melting*).

The SLS process heats the powder to a specific point where the material grains start to fuse together. Enough to create a solid and robust piece with the loose powder being cleaned up and removed later [19].

The SLM process, which can also be called DMLS (*Direct Metal Laser Sintering*), is very similar, but the powder is fully melted so that the material binds in the liquid state. It allows better control of the part porosity and structural integrity, but also requires more support structures to prevent the warping due to high residual stresses. These residual stresses are relieved after the heat treatment of the part, which guarantees better properties of the material [19].

2.5.2 Geometric Tolerances

The dimensional accuracy of the process is an important characteristic which determines what types of parts can be directly manufactured to be used by the technology. Although additive manufacturing is not anywhere near being one of the most accurate processes in terms of dimensional precision, they are incredibly convenient if combined with other processes such as conventional milling. The functional faces and critical dimensional specifications of the part can be milled after the printing.

The dimensional accuracy of a process is defined by the International Tolerance grade (IT). The grade goes from 1 to 16 and the higher the number, the less accurate is the process. The equation for

the calculation is given below:

$$T = (0.45^3 \sqrt{X} + 0.001X)10^{(\frac{IT-16}{5})} \quad (2.3)$$

where T is the tolerance in mm , X is the nominal dimension in mm and IT is the grade value [20].

A study about the dimensional accuracy of the SLM process [21] tested the printing of several different features with various nominal dimensions. The analytical results are shown in the table 2.3.

Table 2.3: SLM process accuracy according to IT grade [21]

Nominal Dimension mm	Maximum deviation mm	IT grade
0.5	0.09	12
1	0.03	9/10
1.5	0.04	10
2	0.03	9/10
3	0.03	9/10
5	0.11	12
6	0.04	9/10
9	0.12	12
10	0.14	12
12	0.13	12
15	0.13	12
18	0.16	12

According to figure 2.10, the process has similar dimensional accuracy as rough milling or turning, which cannot be used for finishing operations but can be certainly used combined with fine milling to achieve the desirable specifications on the critical features of the part.

Manufacturing Process	IT Grade															
	2	3	4	5	6	7	8	9	10	11	12	13	14	15	16	
Lapping																
Honing																
Superfinishing																
Cylindrical grinding																
Diamond turning																
Plan grinding																
Broaching																
Reaming																
Boring, Turning																
Sawing																
Milling																
Planing, Shaping																
Extruding																
Cold Rolling, Drawing																
Drilling																
Die Casting																
Forging																
Sand Casting																
Hot rolling, Flame cutting																

Figure 2.10: Manufacturing processes IT grades

Chapter 3

Mechanical Analysis

In this chapter, a mechanical model of the car is used to evaluate the critical forces while braking.

Since a vehicle is a dynamic and complex system, it must be determined when the critical point happens. It depends indirectly on speed due to downforce effect. It all comes up to the tires and the vertical load that acts on them. Those factors determine the maximum deceleration that can be extracted from the car, independently of how massive are the brakes.

Knowing the maximum deceleration available, the process of designing the brakes is making the brake torque available at a certain amount of brake pedal force, to meet the driver requirements.

3.1 Free Body Diagram Analysis

When a car is moving, it can be said that the wheel is establishing a static contact with the floor and if there is no input coming from the engine, the cars start to slow down gently, due to the tires friction. That deceleration generates the inertial force, which is proportional to the body weight and acts against the resultant force. The inertia force keeps the wheels rolling, because a body in motion tends to stay in motion unless an outside force perturbs it. So when a car brakes the resultant force point backwards, in the opposite direction of the actual movement, but the inertial force points forward with the same value of the resultant force [15].

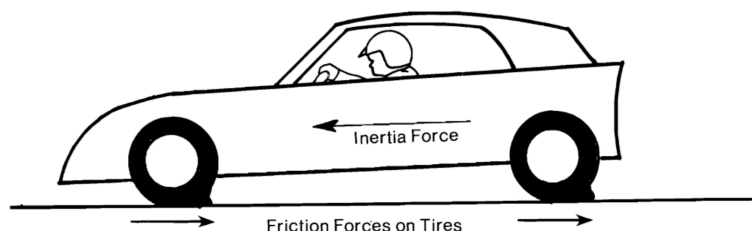


Figure 3.1: Car under braking diagram [15]

Generally, the rolling resistance of the bearings is low, which results in a lower friction force on the tires unless brakes are applied or there is strong aerodynamic resistance to the car's movement. Once the driver hits the brakes, the tires rolling resistance suddenly increases and therefore the friction force

on the contact patch also increases. The sum of the friction forces acting on the four contact patches generates the deceleration force.

There is also another critical phenomenon called mass transfer that occurs because the CG of the car is not at the same height comparing to the contact patches, where the brake force acts. This phenomenon is responsible for changing the weight distribution through the tires, and consequently, modifying their braking behaviour, since the maximum static friction force suffers changes (Equation 2.1). Once the brake torque applied overcomes the torque caused contact patch friction, the wheels lock and the friction force suffers a reduction which cause a brake capacity loss.

In order to obtain the critical loads for each tire, it has to be obtained first the maximum theoretical deceleration, d_M , that the car can achieve.

$$F_{smax} = \mu_s W_c = \sum_{i=1}^4 F_{s_i} \quad (3.1)$$

$$F_{smax} = \frac{W_c}{g} d_M \Leftrightarrow d_M = \mu_s g \quad (3.2)$$

where F_{smax} is the maximum total friction force, F_{s_i} are the friction forces of each wheel and W_c is the car weight. To express the maximum deceleration in g 's, g_M , then:

$$g_M = \mu_s \quad (3.3)$$

The figure 3.2 represents the free body diagram of the car under the maximum braking conditions. The force acting in the CG is the maximum inertial force of the car that is, as said before, pointing in the opposite direction of the force resultant in CG.

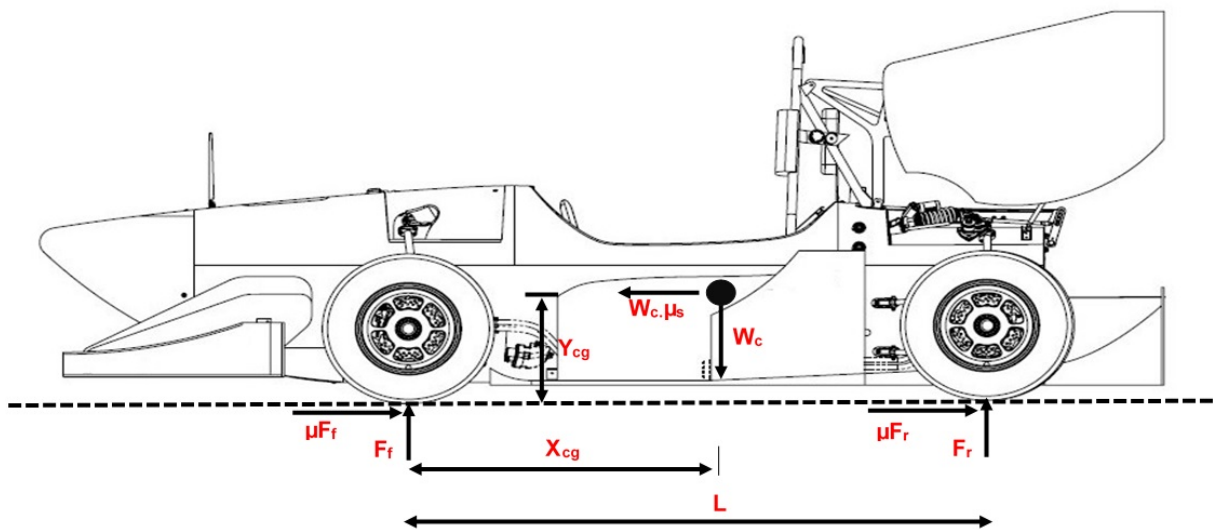


Figure 3.2: Free body diagram

3.1.1 Free Body Diagram with Aerodynamic Influence

The aerodynamic influence is usually shown as two components: Downforce and Drag.

Despite the drag being essential to the car brake performance at high speeds, it does not influence the brake system size and specifications. Therefore, the friction force that the tires are able to apply on the ground does not depend on drag. It means the brake performance of the car may be better than the maximum theoretical performance, due to drag reasons, but it does not mean that the brake system parts are being more requested. It just means that somehow that drag force is being summed to the tires brake force. Despite this, it can be considered that the drag force may influence the mass transfer and therefore, it influences the tire vertical load. From now on it is dismissed the drag force presence and only the downforce influence is taken into consideration.

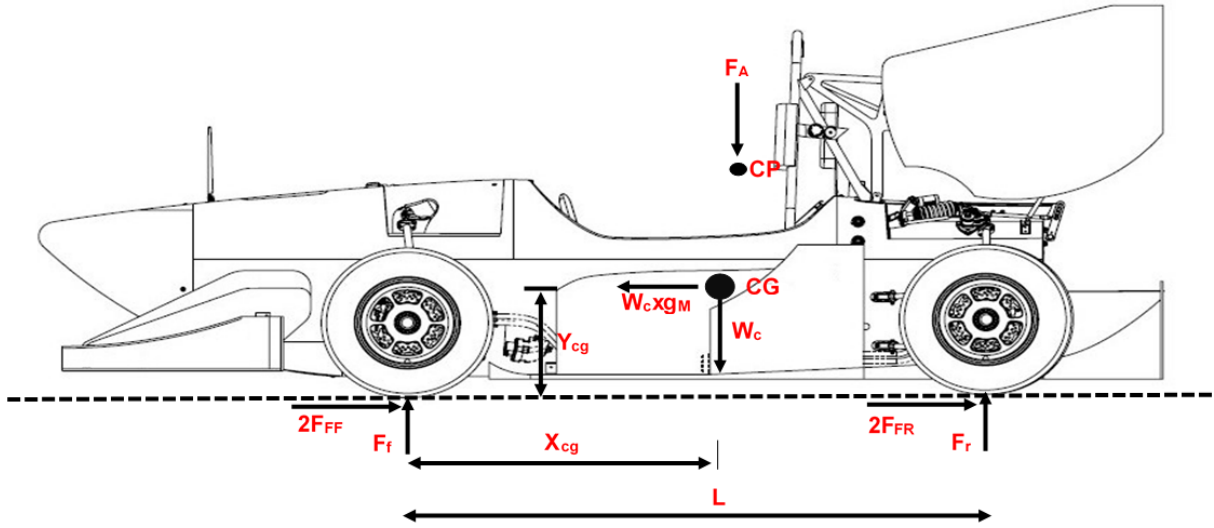


Figure 3.3: Free body diagram with aerodynamics

The figure 3.3 shows that the downforce acts as an alternative source of vertical load, which are applied to the tires. Recalling the equation 3.1, the new F_{smax} and d_M are given by:

$$F_{smax} = \mu_s (W_c + F_A) \quad (3.4)$$

$$F_{smax} = \frac{W_c}{g} d_M \Leftrightarrow d_M = \frac{\mu_s g}{W_c} (W_c + F_A) \quad (3.5)$$

where F_A is the aerodynamic downforce. To express the maximum deceleration in g' 's, then:

$$g_M = \frac{\mu_s}{W_c} (W_c + F_A) \quad (3.6)$$

Since the downforce is not real bodyweight, it is not taken into account when calculating the resultant or inertial forces. That is the reason why downforce plays a vital role in car performance, allowing the tire load to be higher, which impacts positively on acceleration, deceleration and handling. On the other hand, it does not increase the car's inertia, which also benefits those three mentioned characteristics.

3.2 Forces Calculation

Based on the maximum deceleration, g_M , calculated earlier, it is possible to estimate all the essential values necessary to the system design.

The table 3.1 shows some relevant car' specifications, quantitatively specified.

Table 3.1: FST 09e car's specifications

Specs.	Value
Car Weight with driver, W_c	300 kg = 2943N
CG Height, Y_{CG}	0.3 m
Tire Radius, R	0.22987 m
Tire Pressure, P_{tire}	14.5 psi = 99973.9 Pa
Tire Friction Coefficient, μ_{tire}	1.8
Wheelbase, L	1530 mm
Pad Friction Coefficient, μ_{pad}	0.56
Mean Brake Disc Radius, r_m	83 mm
Top Speed, u_{max}	105 km/h = 29.2 m/s
Coefficient of Lift, C_L	2.45
Frontal Projected Area, A_{proj}	1.182 m ²
CG Longitudinal Position (driver included), x_{CG}	48%Front 52%Rear
CP Longitudinal Position, x_{CP}	45%Front 55%Rear
Brake Pedal Ratio, PR	3.53
MC Bore Diameter	15 mm

Now, it is calculated the lift coefficient, C_L , and the theoretical maximum deceleration, g_M , of the car and then it is possible to define the static vertical load, Fv_f , on the front axle.

$$C_L = \frac{2F_A}{\rho_{air}u^2 A_{proj}} \Leftrightarrow F_A \approx 1481N \quad (3.7)$$

$$g_M = \frac{1.8}{2943}(2943 + 1481) = 2.7g's$$

$$Fv_f = 0.48W_c + 0.45F_A = 2079N$$

where ρ_{air} is the air density, u^2 is the square velocity and A_{proj} is the aerodynamic frontal projected area.

It is now determined the total front axle vertical force, F_f , as the sum of the static vertical force, Fv_f with the mass transfer force, F_{mt} .

$$F_f = Fv_f + F_{mt} \quad (3.8)$$

$$F_{mt} = \frac{F_{inertia}Y_{CG}}{L} \quad (3.9)$$

$$F_f = 2079N + \frac{W_c g_M Y_{CG}}{L} = 2079 + \frac{2943 \times 2.7 \times 0.3}{1530 \times 10^{-3}} \approx 3640N$$

$$F_{fwheel} = F_f/2 = 1820N$$

The F_{fwheel} is the vertical load on each front wheel, being basically the half split of F_f . Knowing the total wheel load, it can be calculated the maximum brake force, F_{brake} and then the maximum brake torque,

T_{brake} . To torque calculation, needs the real tire radius value, represented in figure 3.4.

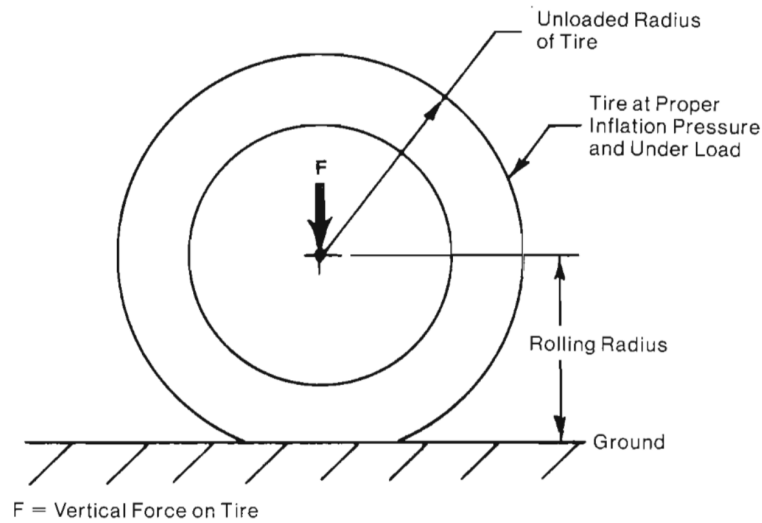


Figure 3.4: Real rolling radius due to tire load and pressure [15]

The equation 3.12 is an approximation used to calculate the tire real rolling radius, R_{loaded} , under load. It is dependent on the tire vertical load, but also on the tire pressure.

$$F_{brake} = \mu_{tire} F_{wheel} \quad (3.10)$$

$$F_{brake} = 1.8 \times 1820 = 3276N$$

$$T_{brake} = F_{brake} R_{loaded} \quad (3.11)$$

$$R_{loaded} = \sqrt{-\left(\frac{F_{wheel}}{2P_{tire}l}\right)^2 + R^2} \quad (3.12)$$

$$R_{loaded} = \sqrt{-\left(\frac{1820}{2 \times 99973.9 \times 0.1778}\right)^2 + 0.22987^2} = 0.224m$$

$$T_{brake} = 734.2Nm$$

At this stage, it is known the exact amount of brake torque that the calipers have to be capable of producing to achieve the maximum brake force. The caliper clamping force is a function of the total piston area and the line pressure. It is specified, as a design constraint, that the pedal ratio, PR , and the master cylinder bore diameter are equal to 3.53 and 15mm, respectively.

According to R. Limpert [3], for the female and male fifth percentile, the maximum pedal force is 445N and 823N, respectively. However, the maximum pedal force in agreement with the Formula Student competitions rules is 2000N. It is also stated that drivers considered a brake pedal force/deceleration ratio to be very good between 267 to 445N/g. For the on going design, the goal level of this ratio is set between 200 to 250N/g. The figure 3.5 shows the spreadsheet used on the calculations.

For a chosen driver's foot force of 600N to achieve the maximum deceleration, the ratio is 221N/g which is between the boundaries imposed. The pedal ratio, explained in figure 3.6 shows that the multiplication comes from the balance of moments on the pedal.

Car Specifications									
Vehicle Mass (kg)	230		Front						
CG Height (m)	0,3		Static Axle Weight (kg)	144,0					
Tire width (mm)	177,8		Aerodynamic Forces (N)	666,7					
Tire Radius (m)	0,22987		Total (N)	2079,3					
Tire Pressure (Psi)	14,5		Vertical Force with mass transfer (N)	3640,3					
Tire Pressure (Pa)	99974		Vertical Reaction on Wheel (N)	1820,1					
Tire Pressure (Bar)	0,99974		Loaded Wheel Radius (m)	0,2					
Deceleration (m/s ²)	26,5		Braking friction force required (N)	3276,2					
Tire Friction Coefficient	1,8		Rear						
Driver Mass (kg)	70		Static Axle Weight (kg)	156,0					
Wheelbase (mm)	1530		Aerodynamic Forces (N)	814,8					
Pad Friction Coefficient	0,56		Total (N)	2345,2					
Effective disc Radius fr (mm)	83		Vertical Force with mass transfer (N)	784,2					
CL	2,45		Vertical Reaction on Wheel (N)	392,1					
Aero projected area	1,182		Loaded Wheel Radius (m)	0,2					
Air density	1,2		Braking friction force required (N)	705,8					
CP Position	0,45	0,55							
CG Position	0,48	0,52							
Max speed	29,2								
Pedal Ratio	3,537								
			BRAKE BIAS		0,7				
			Drivers' foot force			Balance Bar force		Front Line Force	Rear Line Force
			61,2	600	2121,9	1485,3	636,6		
			kg	N	N	N	N		
			N/g Ratio		221,8				
			Front (pressure)		8405248,4	Pa	MC Diameter		mm
			Rear (Pressure)		3602249,3		15		
			Front Piston Area		0,000489396	m ²			
			Front Piston Diameter		0,024962345	m	25,0		mm
			Rear Piston Area		0,000504117	m ²			
			Rear Piston Diameter		0,025334993	m	25,3		mm

Figure 3.5: Excel spreadsheet

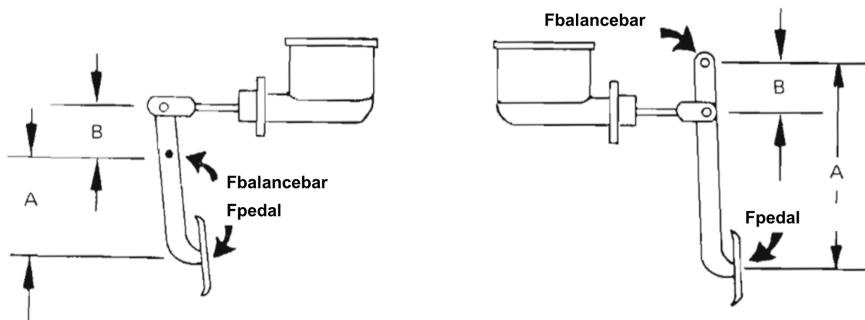


Figure 3.6: Pedal Ratio meaning [15]

Therefore, the force applied on the balance bar is given by:

$$PR = \frac{A}{B} \quad (3.13)$$

$$F_{balancebar} = F_{pedal} PR \quad (3.14)$$

$$F_{balancebar} = 600 \times 3.53 = 2121.9N$$

The balance bar is the middle term between the brake pedal and the master cylinders. It also plays an important role in the brake bias adjustment. The brake bias is the split ratio of the $F_{balancebar}$ amongst the MC. The balance bar mechanism is explained in figure 3.7.

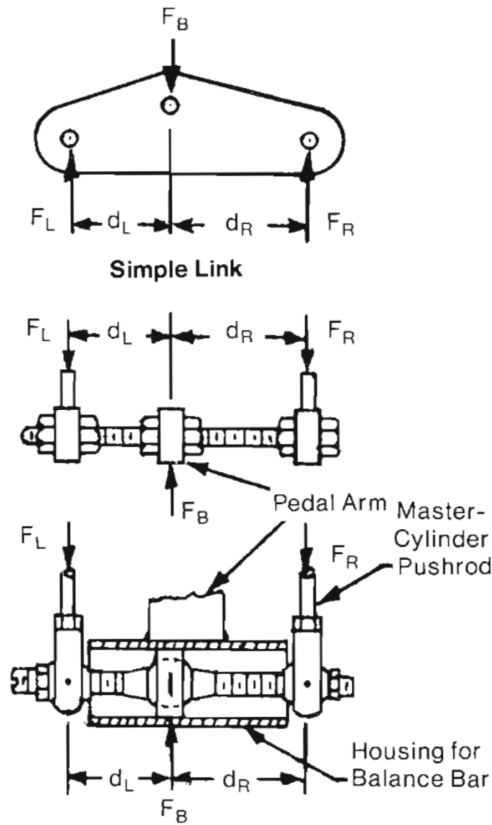


Figure 3.7: Balance Bar setup [15]

Adjusting the brake bias to 70% at the front and 30% at the rear, the force on the front MC, $F_{frontMC}$, is $1485.3N$. This adjustment decreases the rear brake line pressure, which may not be used due to smaller brake capabilities of the rear tires. The front line pressure, $P_{frontline}$ can be obtained by:

$$P_{frontline} = \frac{F_{frontMC}}{\pi r^2} \quad (3.18)$$

$$P_{frontline} = 8.405 \text{ MPa}$$

Now, as it is defined that there are four pistons on the front caliper, to assure a smoother and even friction on the pads, it is possible to determine their diameter.

$$A_{fpiston} = \frac{T_{brake}}{2 \times 2 \times \mu_{pad} \times \mu_{disc} \times P_{frontline} \times r_m} \quad (3.19)$$

$$D_{fpiston} = \sqrt{\frac{4A_{fpiston}}{\pi}} \quad (3.20)$$

where the r_m is the disc mean radius, $A_{fpiston}$ is the piston contact area and μ_{disc} is an efficiency factor used for disc brake systems that is usually 0.96. The result is a $D_{fpiston}$ equal to $25mm$.

¹Right MC force (figure 3.7)

²Left MC force (figure 3.7)

³Balance bar force (figure 3.7)

Chapter 4

Design Process

This chapter represents the design stage of the caliper. Similarly to a simulate driven design approach, beginning with a functional start base part and making it evolve to the optimised design, evaluating several types of boundary conditions the part has to face.

4.1 Initial Design

At this stage, it is designed a part that can perform exactly the same function with excessive material to be taken care of after. The maximum dimensions of the part are influenced by the space between the knuckle and the rim. For the part to work on the FST 09e, some of its features were merged to the design. That was accomplished by the use of several sketches available from the parts of FST 09e, as it can be seen in figure 4.1. The final result for the base model was a part where a non-design space

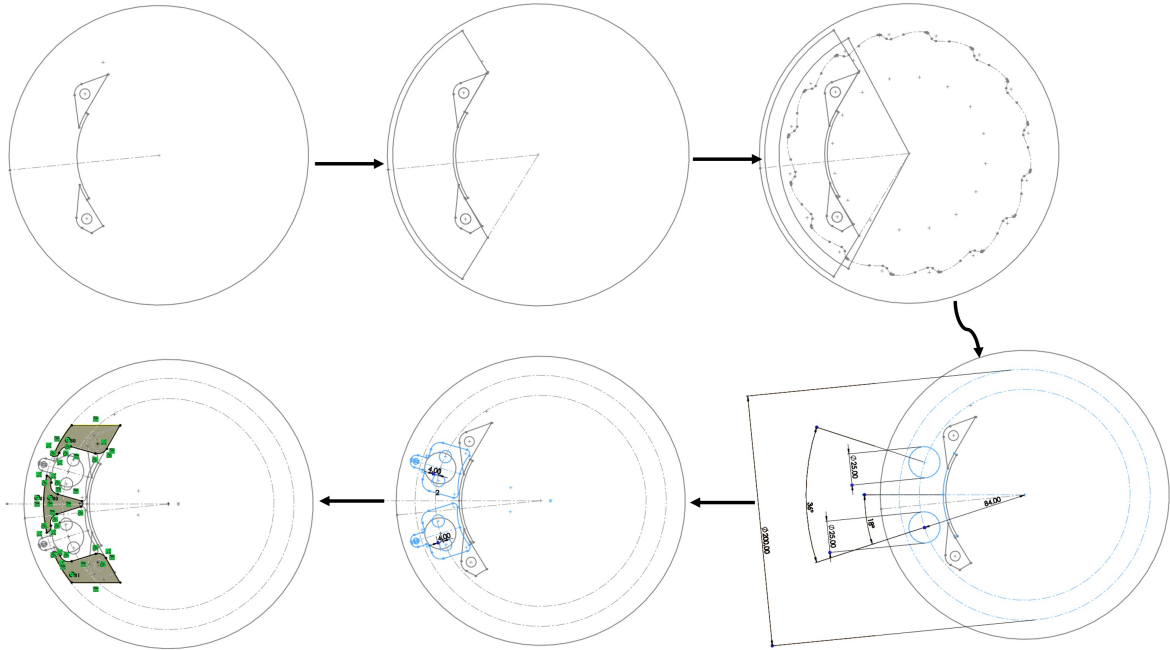


Figure 4.1: Compatibility design approach

had to be defined in order to keep the minimum necessary characteristics while optimising topologically, shown in figure 4.2.

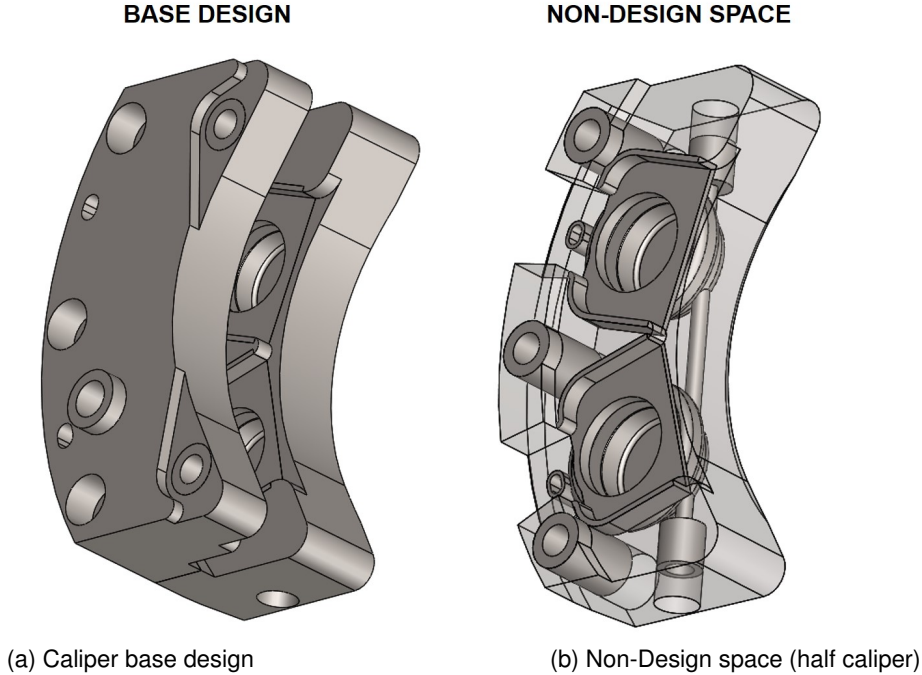


Figure 4.2: Caliper design and space definitions

The decision of making two halves of a caliper is required for interior access, with high tolerances required. With a single piece, there would be no wide-open access for the milling tools, causing interferences.

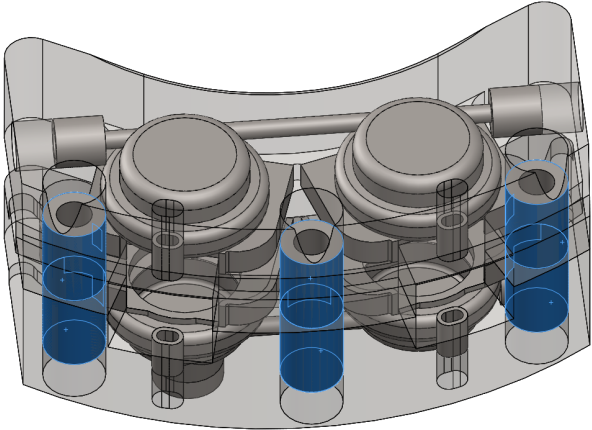


Figure 4.3: Caliper halves attachment points

The connection of the caliper's halves is assured by three screws (figure 4.3). This points also serve as anchor structures between the topology shapes and the non-design space. Another two attachment points are presently designated to fix the caliper on the knuckle (Figure 4.4). Finally, four boreholes, one for each piston (Figure 4.5).

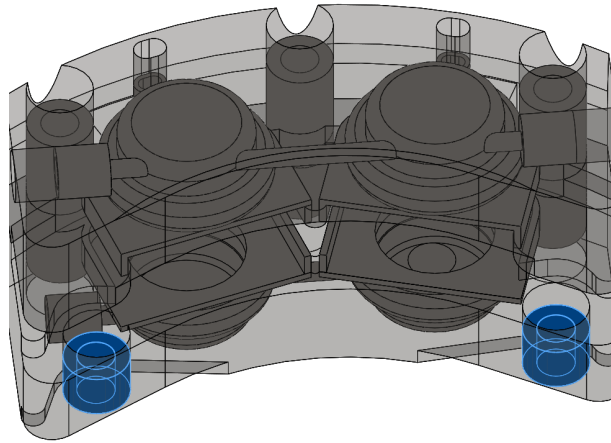


Figure 4.4: Knuckle attachment points

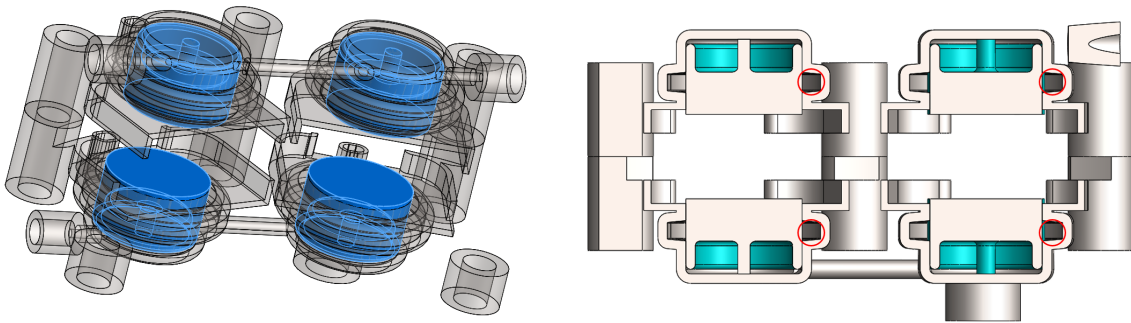


Figure 4.5: Piston placement in caliper

The piston bores have a hollow (represented by the red circle in figure 4.5) on the cylindrical interior wall made for the seal rubbers, preventing oil leakages between the piston and the bore walls. This o-ring is also responsible for the retraction of the pistons when the brake pedal is released. It has specific dimensions according to the type of seal and nominal dimensions of the piston. According to [22], the o-ring must deform and compress to make a proper seal. For hydraulic dynamic applications, the compression should be between 10 and 15%, never going below than the lower margin of 8%. The figure 4.6 shows the range of deformation that the o-rings can handle depending on their cross-section.

The used o-ring catalogue [22] states that for piston and bore sizes of $25mm$ there are two matches, being d_5 and d_{10} the piston and borehole diameters respectively (Figure 4.7). All the parameters, such as nominal dimensions, finish tolerances and dimensional tolerances, are defined and must be met to assure a good seal (figure 4.8).

The remaining characteristics are represented in the figure 4.9, that shows the brake fluid path, entering inside the caliper through a banjo screw connection. It spreads through the existent interior canals reaching the end of the half. There is a line connection between each half and, at the end of the trajectory, there is a bleeding valve that is used to remove air trapped on the line. The banjo fitting with copper crush washers and an exemplar bleeding valve are represented in figure 4.10.

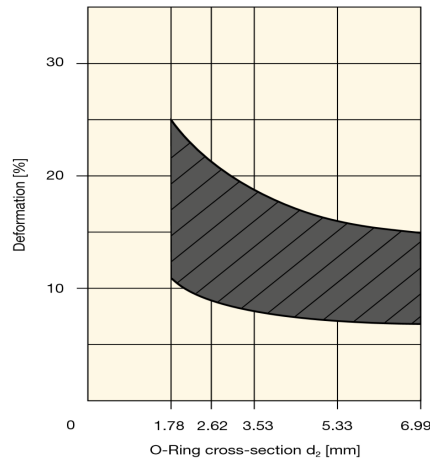


Figure 4.6: O-ring deformation range in function of the cross-section [22]

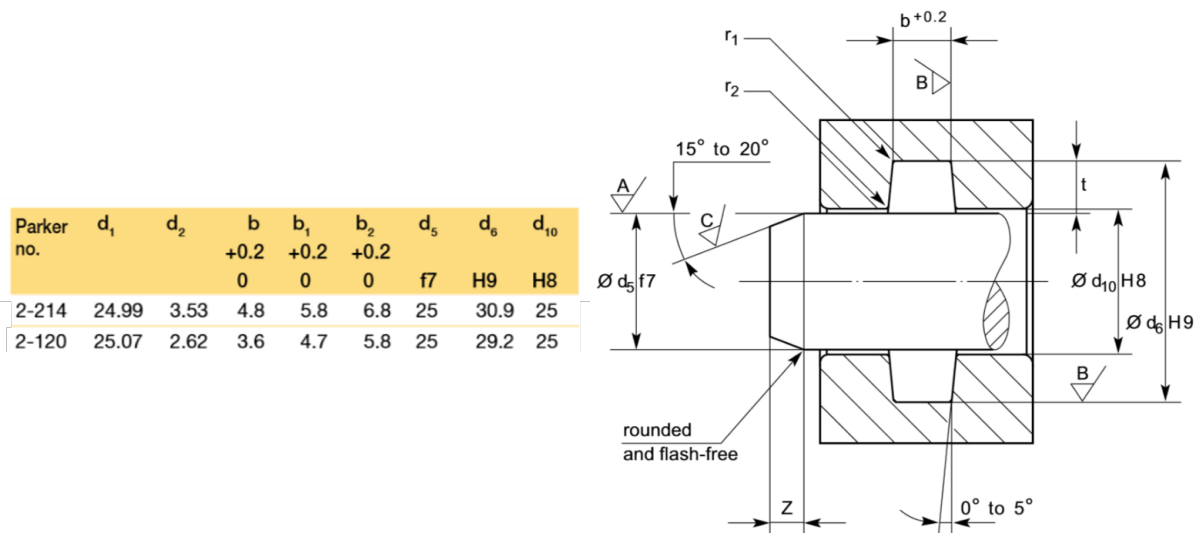


Figure 4.7: 25mm diameter size atching o-rings (left); Schematic for hydraulic rod seals (right) [22]

d_2	$t^{(1)}$	$b^{+0.20}$	z	r_1	r_2	Surface	Surface finish roughness, percentage contact area $t_p > 50\%$
1.50	1.30	1.90	1.50	0,20 - 0,40	0,10 - 0,30		R_a R_{max}
1.78	1.45	2.40	1.50	0,20 - 0,40	0,10 - 0,30		[μm]
2.00	1.70	2.60	1.50	0,20 - 0,40	0,10 - 0,30	A contact surface	0.40 1.60
2.50	2.10	3.30	1.50	0,20 - 0,40	0,10 - 0,30	B groove base and sides	1.60 6.30
2.62	2.20	3.60	1.50	0,20 - 0,40	0,10 - 0,30	C surface finish of lead-in edge chamfer	3.20 12.50
3.00	2.60	3.90	1.80	0,40 - 0,80	0,10 - 0,30		
3.53	3.05	4.80	1.80	0,40 - 0,80	0,10 - 0,30		
4.00	3.50	5.30	1.80	0,40 - 0,80	0,10 - 0,30		
5.00	4.45	6.70	2.70	0,40 - 0,80	0,10 - 0,30		
5.33	4.65	7.10	2.70	0,40 - 0,80	0,10 - 0,30		
6.00	5.40	8.00	3.60	0,40 - 0,80	0,10 - 0,30		
6.99	6.20	9.50	3.60	0,40 - 0,80	0,10 - 0,30		

Figure 4.8: Another groove parameters (left); Roughness tolerances (right) [22]

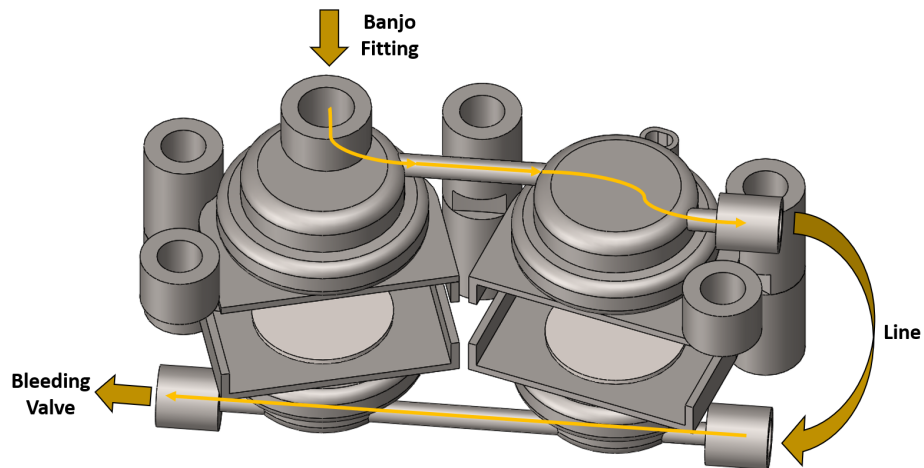


Figure 4.9: Brake fluid trajectory inside the caliper



Figure 4.10: Banjo fitting (left); Bleeding screws (right)

4.2 Optimisation Model Setup

For this purpose, it was used the latest version of Altair SimLab with the solver OptiStruct, which uses the SIMP (Solid Isotropic Material with Penalisation) method algorithm during optimisations. The model is represented in figure 4.11.

As explained in section 4.1, the CAD has split bodies that represent either the design and non-design space (do not misunderstand these separated bodies by the two halves but as separated bodies on each half - design and non-design space). They are different bodies, but, in the fundamental point of view, they are the same body. Their separation comes from the need to set their design variables differently. The shared faces have to be mesh coincident, shown in figure 4.12.

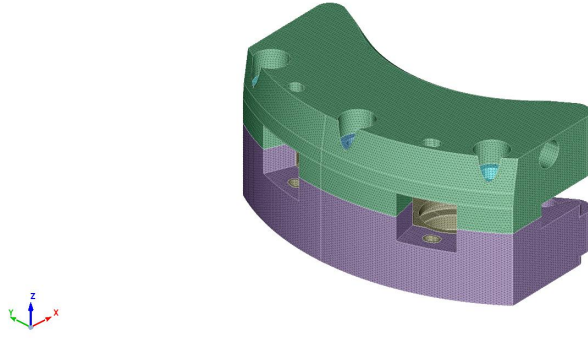


Figure 4.11: Finite Element Method (FEM) Model

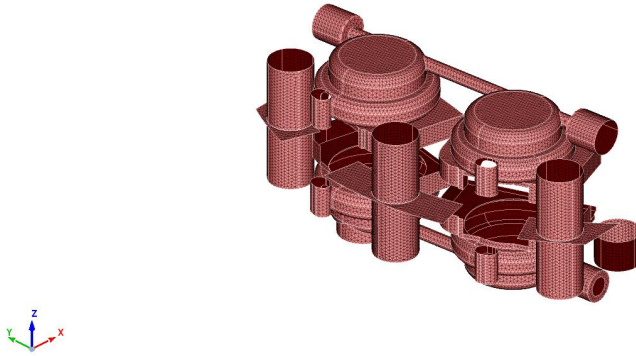


Figure 4.12: Shared faces between the design and non-design space bodies

4.2.1 Topology Optimisation Formulation

For a structural problem like this the design variable is the element relative density, ρ_e , that defines basically the existence or the absence of that element. The problem formulation is stated below in the system 4.1.

$$\left\{ \begin{array}{l} \min \quad f(\tilde{\rho}, \mathbf{u}(\tilde{\rho})) \\ \text{subjected to} \quad \left\{ \begin{array}{l} \text{equilibrium equation} \\ \text{design constraints} \\ \text{manufacturing constraints} \end{array} \right. \end{array} \right. \quad (4.1)$$

The function f is the objective function of the problem, that in this case will be the volume of the structure. The volume is given by the the internal product between the elementary volume vector and the elementary density vector.

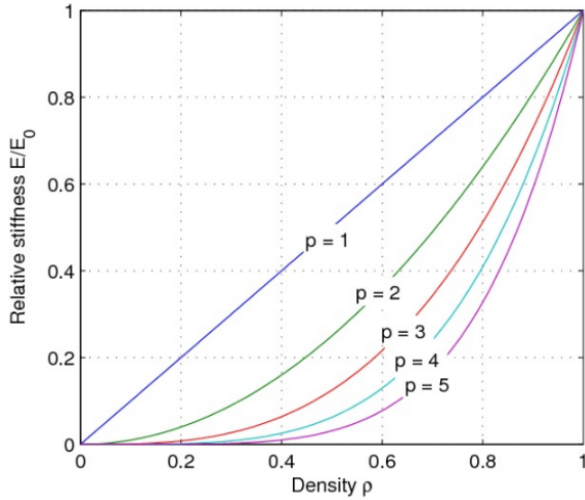
$$\min f = \min \tilde{V}_e \cdot \tilde{\rho} \quad (4.2)$$

The vector \mathbf{u} is the displacement vector of the mesh nodes that is dependent of the $\tilde{\rho}$ vector, which contains all the element relative densities. The equilibrium equation is given by:

$$\mathbf{K}(\tilde{\rho}) \mathbf{u}(\tilde{\rho}) = \mathbf{F} \quad (4.3)$$

where \mathbf{K} is the stiffness matrix of the problem and \mathbf{F} is the global load vector.

To evaluate the effect of intermediate densities in the structural integrity of the model, there is an interpolation of the element stiffness, according to the figure 4.13 and equation 4.4. The p is the penalty



$$\mathbf{E} = \mathbf{E}^0 \rho_e^p, \quad \rho_e \in [0, 1], \quad p \geq 1 \quad (4.4)$$

Figure 4.13: SIMP method curves with different penalty factors [23]

factor and those curves are the SIMP method curves, whose method is described by the equation 4.4. For the same density, the relative stiffness of the element gets lower with the increase of the penalty factor. This will merge the result to a more discrete solution with element densities closer to 1 or to 0. The design and non-design space are defined through a constraint applied to this variable.

$$\rho_e = \begin{cases} 1, & \text{if } e \in \text{non-design space} \\ [0, 1], & \text{if } e \in \text{design space} \end{cases} \quad (4.5)$$

To guarantee that the volume minimisation problem do not result in a very fragile solution, there is a constraint applied to the compliance. The compliance is a way of define the structure stiffness, that is defined by the equation 4.6. The larger the compliance, the less stiff is the structure.

$$\mathbf{C} = \mathbf{F}^T \mathbf{u}(\bar{\rho}) \quad (4.6)$$

A structural analysis made to the AP Racing solution, lead this study to a maximum compliance value equal to $10^4 N.mm$, applied as a constraint.

The manufacturing constraints that act in the form of filters or other conditions. These constraints may be such as extrude direction, symmetry plans or even maximum and minimum member size. Since this part is supposed to be 3D printed, there is much freedom allied with the manufacturing performance. The only issue that may stand out is the small members printing that is more susceptible to warping. In that case, a filter like minimum member size or thickness can be defined to prevent the nominated checkerboard scenario of topology optimisation (figure 4.14).



Figure 4.14: The influence of using member size filters [24]

4.2.2 Model Description

The model is as complex as it can be because it is an assembly, so the boundary conditions between each half are vital to guarantee that the effort is evenly spread through the whole part. So the model was idealised with caution to avoid stiffened elements that may hide the hot spots in the assembly when it comes to stresses. There are necessarily three loads present on the model, such as the line pressure, the brake torque and the bolts pretension.

Line Pressure

The line pressure is applied on each borehole until the O-ring's grooves and inside the channels made for bore connections and brake fluid flow inside the caliper. The pressure value is roughly 28 MPa , derived from the maximum pedal force applied of 2000 N .

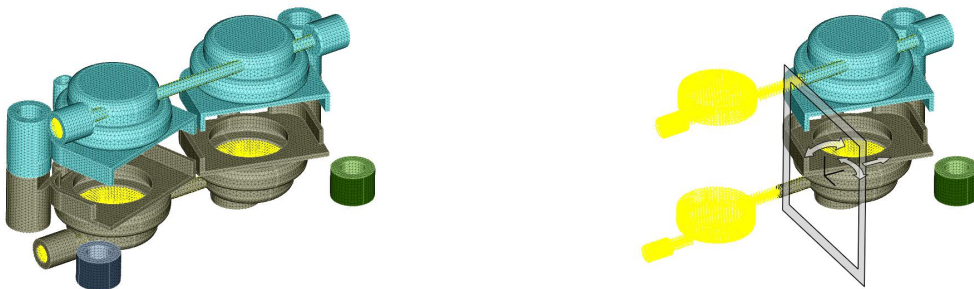


Figure 4.15: Line pressure represented on FEM model

Brake Torque

For the brake torque application (figure 4.16), it was used an element called RBE3. This is a non-rigid element that is commonly used to apply forces distributed by a set of nodes. So it was created an RBE3 with the dependent node in the brake disc centre position. This node is connected to the independent nodes located on the brake pad guiding walls, which receives all the effort that comes from the braking action.

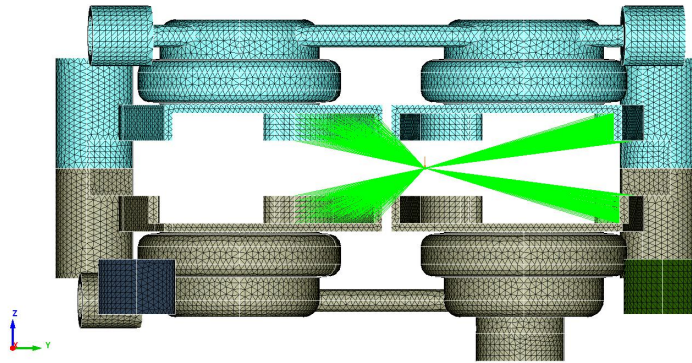


Figure 4.16: Brake torque represented on FEM model

Bolt Pretension

The pretension load for an M6 grade 12.9 thread that is used to restrain it on the knuckle and keep that halves connected is approximately $16000N$ [25], so there is a huge compressing effort applied to the part.

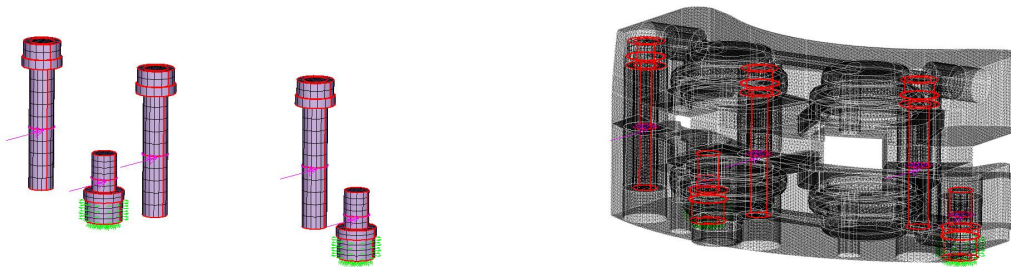


Figure 4.17: Bolt pretension represented on FEM model

The small bolts are the ones that fix the caliper to the knuckle therefore they have a displacement constraint applied on their head, represented by the green elements on figure 4.17, fixing all the six degrees of freedom of those nodes.

4.3 Convergence analysis

A convergence analysis was made to assure an accurate solution. The problem was repeated several times for different mesh sizes, establishing a pattern that leads the solution to a convergence region where the decrease of mesh size only increases the computational time and do so little over the solution. The convergence analysis was made with the displacement results in two reference points because they tend to converge more accurately than the stress responses. As an example, a stress concentration point hardly converges while refining the mesh, but at the same time, if the analysis falls upon the displacement result, it converges. The conclusion drawn from the figure 4.18 is that a 1mm mesh size fits the problems needs to get an accurate solution. It would be arguable if the 1.5mm or 2mm mesh size are good enough and, in terms of results, they are, but since the topology optimisation results were

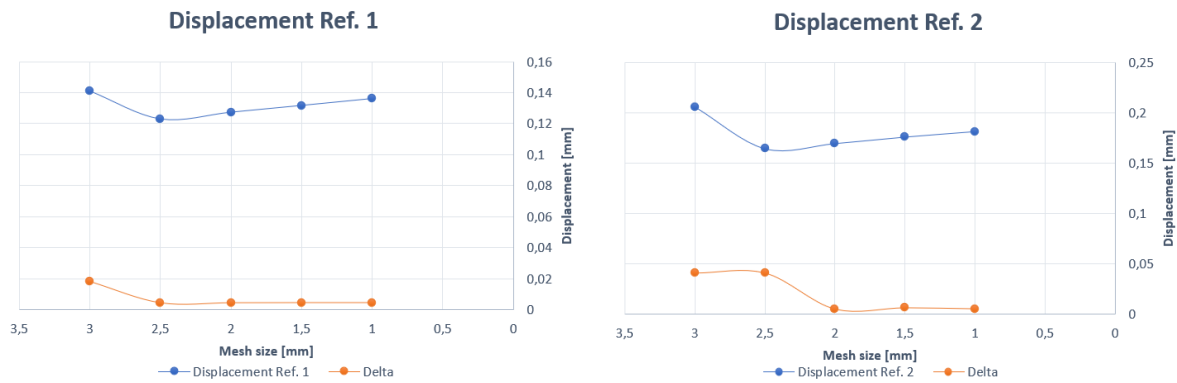


Figure 4.18: Convergence of displacement result at two reference points

used to replicate the a complex shape, a fine mesh makes it easier and smoother to understand the shape topology. The table 4.1 shows the properties of the model, for that mesh size.

Table 4.1: Finite elements model properties

Properties	Value
Number of Nodes	202962
Number of Elements	1018758
Iterations until converge	50
Total computational time	60 min.
Computational time per iteration	1.2 min.

4.4 Optimisation parameters

In order to achieve a level of optimisation where the part still withstands the loads, boundaries are set up for the maximum stresses the part can achieve at any point, otherwise it would start to yield. The table below shows the material properties expected for this 3D printed material after the heat treatment to relieve the residual stresses.

Table 4.2: Ti6Al4V material properties

Properties	Value
E-Modulus	104-124 <i>GPa</i>
Yield strength, S_y	min. 860 <i>MPa</i>
Ultimate Tensile strength, S_{ut}	min. 930 <i>MPa</i>
Density, ρ	4.41 <i>g/cm³</i>
Air and Watertight	yes
Max. Operating Temperature	350°C

Using a safety factor of 1.5 and always using the minimum properties values to get the most secure result as possible, the maximum allowable stress is around 570*MPa*. In this stage, the optimisation is based on static analysis that only considers a static maximum load case, but since this part is loaded cyclically, fatigue may happen. Being this a safety system, it is safer to design it to achieve infinite life, leaving more room for all the usage of the car after it has completed all the competitions listed for that year.

In what concerns fatigue loading, it is considered that the part is always being submitted to full load over the time, as represented in figure 4.19.

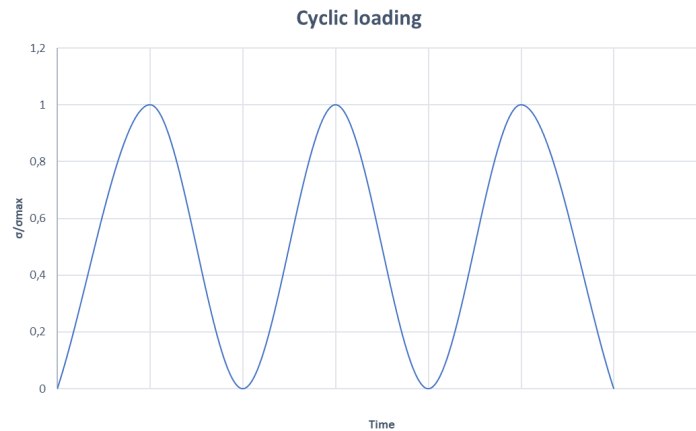


Figure 4.19: Cyclic Load

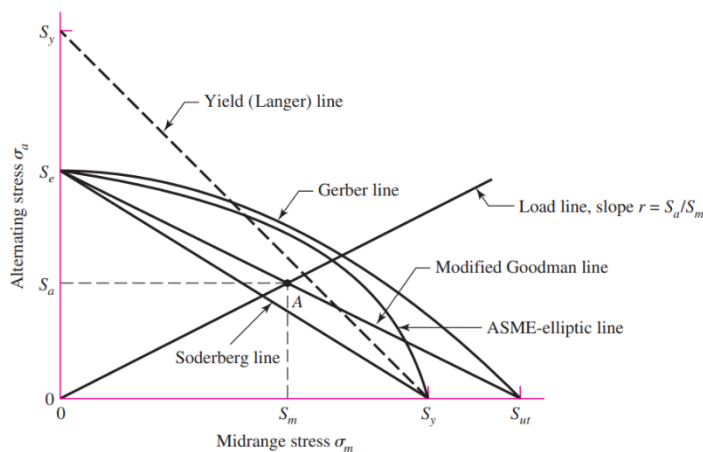
According to [26], the fatigue curve for the Ti6Al4V alloy, for high cycle fatigue behaviour, is represented by the equation:

$$\sigma(N) = 1700N^{-0.2} + 440 \text{ MPa} \quad (4.7)$$

where N is the number of cycles. It considers the fatigue limit is in the range of $10^7 - 10^8$ cycles. Using the 10^7 as the fatigue cycle limit, the fatigue strength, S_e , of the material is:

$$\sigma(10^7) = S_e = 507 \text{ MPa}$$

The S-N curves are well suited for fully reversed cycle loading, where $R = -1$ or $\sigma_{med} = 0$. As explained above, that is not the case of the loading problem, so several approximations can be used to estimate the influence of the mean stress, σ_{med} , in the fatigue problem. The approach used is the modified Goodman line.



$$\frac{\sigma_a}{S_e} + \frac{\sigma_{med}}{S_{ut}} = \frac{1}{n} \quad (4.8)$$

Figure 4.20: Approaches for non fully reversed cyclic fatigue loading [27]

Looking to the figure 4.19 it can be concluded:

$$\sigma_a = \frac{\sigma_{max}}{2} \quad \text{and} \quad \sigma_{med} = \frac{\sigma_{max}}{2} \quad (4.9)$$

so the equation 4.8 quickly turns to:

$$\frac{\sigma_{max}}{2S_e} + \frac{\sigma_{max}}{2S_{ut}} = \frac{1}{n} \quad (4.10)$$

where n is the safety factor. The variables S_e and S_{ut} are already known, so using a safety factor of 1.5 the $\sigma_{max} = 437 \text{ MPa} \approx 440 \text{ MPa}$. That being said, the actual maximum stress allowed in the optimisation problem is then lowered due to fatigue reasons. Summing up all the optimisation problem is defined by:

$$\left\{ \begin{array}{l} \min \quad \tilde{V}_e \cdot \tilde{\rho} \\ \text{subjected to} \quad \left\{ \begin{array}{l} \mathbf{K}\mathbf{u} = \mathbf{F} \\ \mathbf{C} - 10^4 \leq 0 \\ \sigma_{vm} - 440 \leq 0 \end{array} \right. \end{array} \right.$$

4.5 Post Processing of Optimisation Results

The results obtained by the program came in form of a density plot for each iteration. In the graphics shown during the optimisation run it can be analysed if the solution is converging and what is the best solution because, sometimes, a middle iteration can achieve a better solution than the last one, where it converges.

From the plots on the figures 4.21 and 4.22, it is safe to say that the problem converges and the last iteration/solution can be assumed as the best one in terms of volume fraction reduction. The optimisation explores the design as much as it can until compliance constraint is active. As a result, there is a 93.3% of volume reduction in the design space with 0% of any constraint violation.

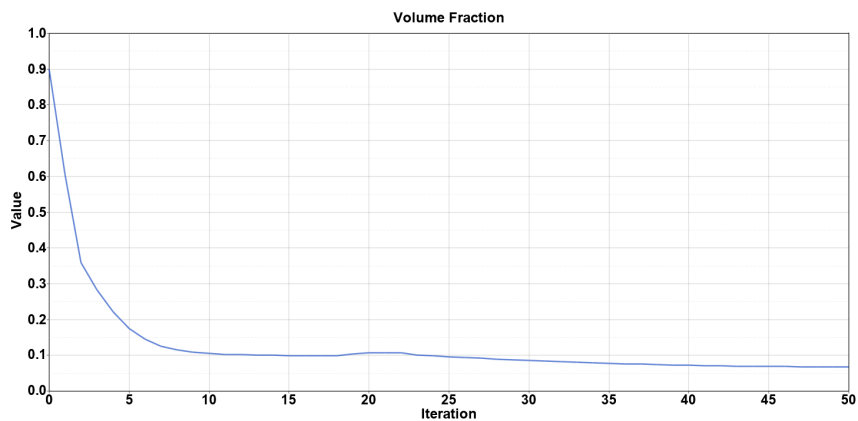


Figure 4.21: Volume fraction response at each iteration

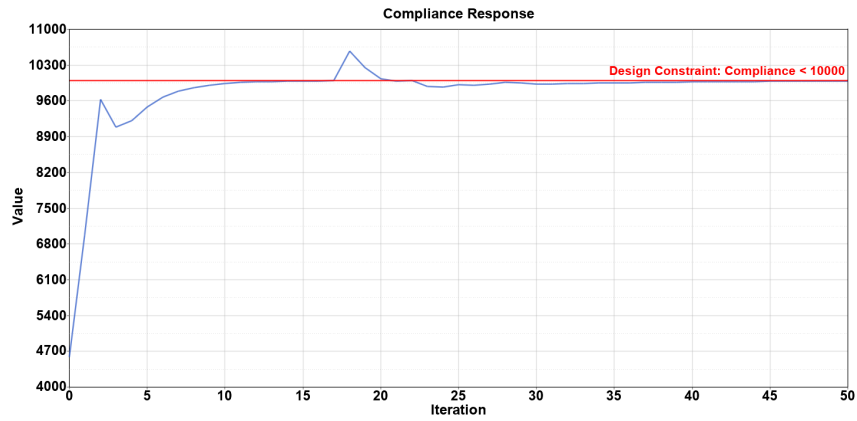


Figure 4.22: Compliance response at each iteration

The plot that contains the geometry of the topology optimisation varies with the threshold value used. This threshold value is the minimum relative density shown in the plot. The lower the threshold value, the more material is shown in the plot and higher is the probability of having excessive material. This is explained because lower density elements do not influence the stiffness of the part that much, due to the penalisation factor explained in equation 4.4.

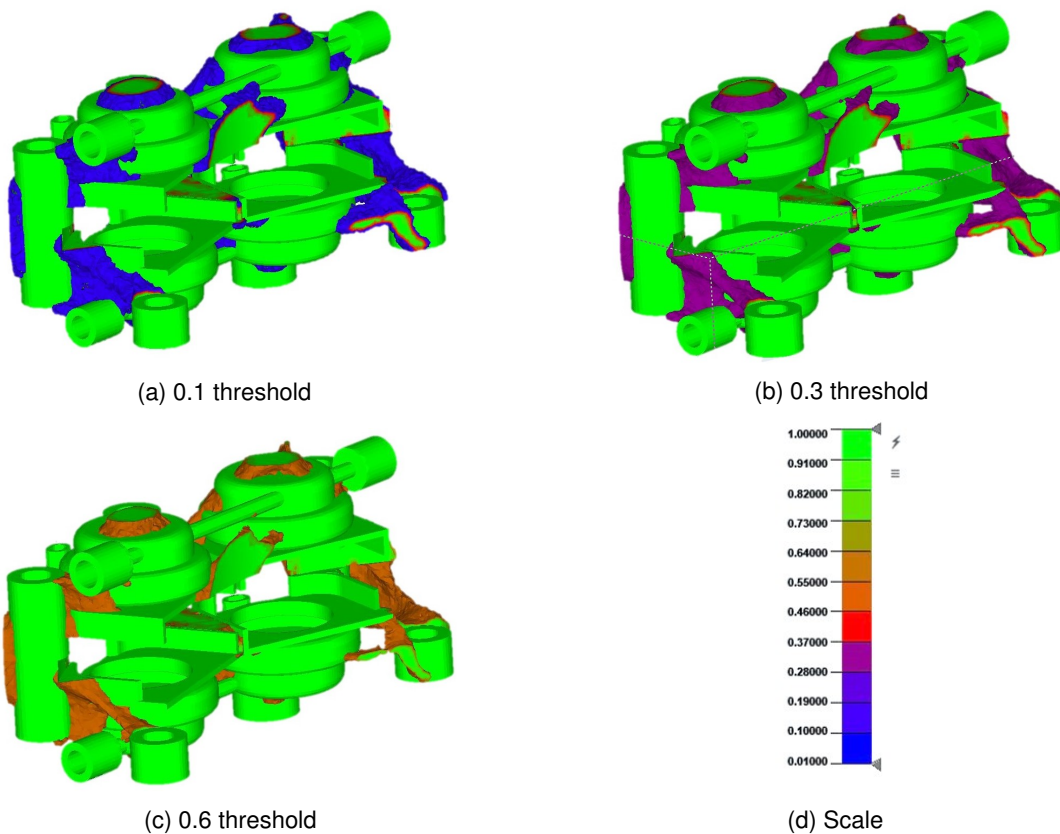


Figure 4.23: Different threshold plot results

The threshold was analysed from an engineering point of view. The solution represented by the figure 4.23c shows some links with very tiny connections where the solution's plausibility starts to be questionable. As a safe approach, it was decided to proceed with the 0.3 threshold value, that appears

to have continuous links and a smooth appearance.

To create such an intricate design, especially with this kind of flexibility, without many plane faces and sharp angles, standard CAD software would be a bad option. The Altair company has outstanding software that is capable of producing those type of features using NURBS (Non Uniform Rational Basis Spline) algorithms. Altair calls their algorithm by PolyNURBS, represented by figure 4.24, that can approximate the geometry to the mesh and discrete optimised results by splines that can be continuously adjusted until the design becomes very similar to the discrete optimised one, that will, at first sight, withstand the loading problem.

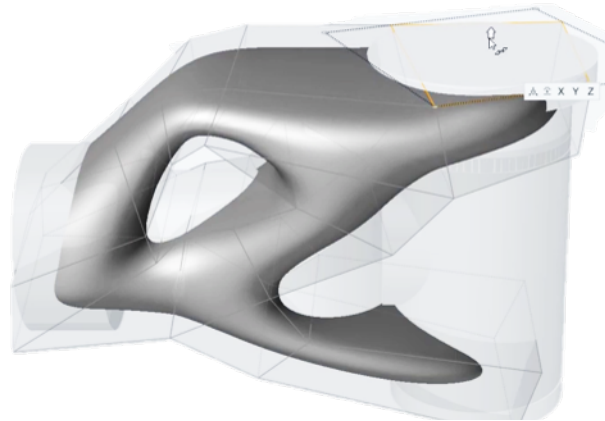


Figure 4.24: NURBS design approach

In the next subsections, it is presented the several designs obtained that suffered changes due to reanalysis processes. Normally, it is a good practice to perform a reanalysis of the problem over the obtained designs with a better-refined mesh. With this practice, there are some highlighted areas of the part that are performing under expected due to the approximation of the design and, with that knowledge it is possible to define what are the necessary changes the part should take.

4.5.1 First Design



Figure 4.25: First design rendered view

The figure 4.25 shows a rendered view of the first design solution made with the topology results' interpretation. To properly assess the design capability to withstand the required specifications it is

plotted the von Mises stress distribution above the limit and the energy error distribution which may be helpful to determine some stress peaks due to mesh errors.

The figure 4.26 shows the plot of von Mises stress above the actual limit of design of 440 MPa . The close-up 4.27a shows a member that is currently lacking material with a stress level that would probably cause the yield of the material leading to a critical fail. The close-up 4.27b shows some areas where material can be added as well, not to prevent yield mechanisms but to assure the fatigue desired performance. On the other hand, the close-up 4.27c represents some stress concentration due to the problem constraints. The hole represented on that close up is the attachment point between the caliper and the knuckle of the car, resulting in several conditions applied on that inner face of the hole, such as contact elements. Those contact definitions may influence and cause some mathematical errors on that inner face because of the non-relative motion nature of the contact elements used (TIE contact definition).

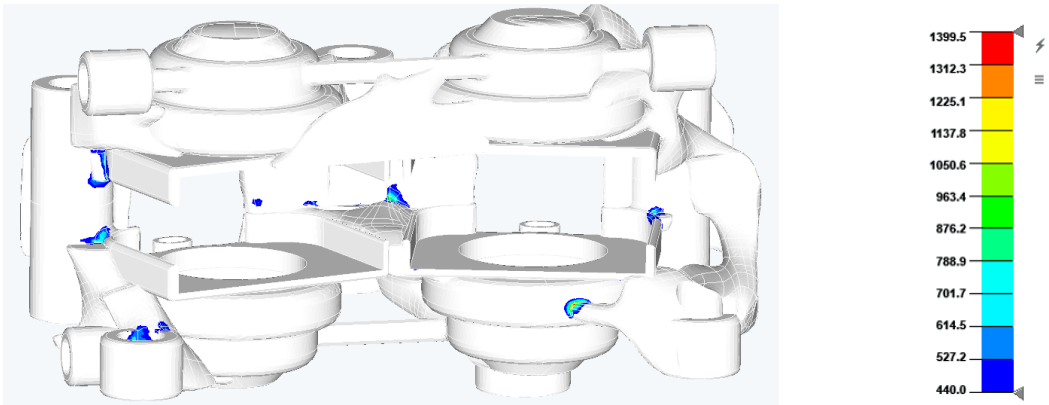


Figure 4.26: von Mises stress plot for first design attempt

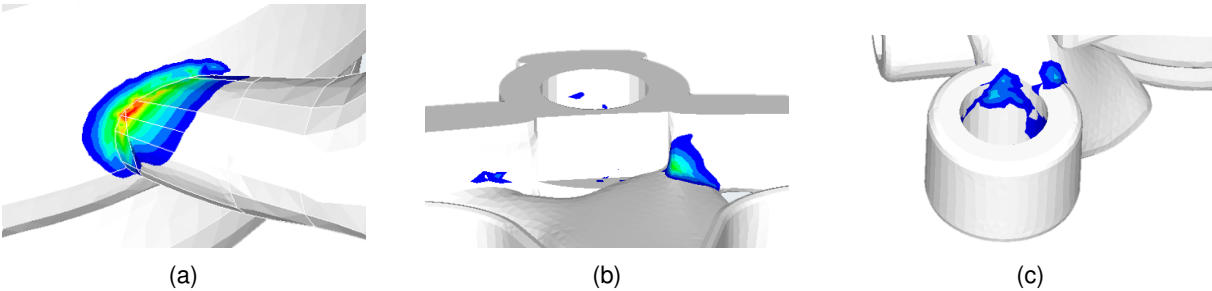


Figure 4.27: First design close-up views

The energy error density plot (4.28) shows some error happening in the already discussed zones of the caliper, raising suspicious thoughts about some of those stress concentration points because usually, a stress field presents a wide gradient zone between the loaded areas and the non-loaded ones. There are zones with the error reaching almost 40%.

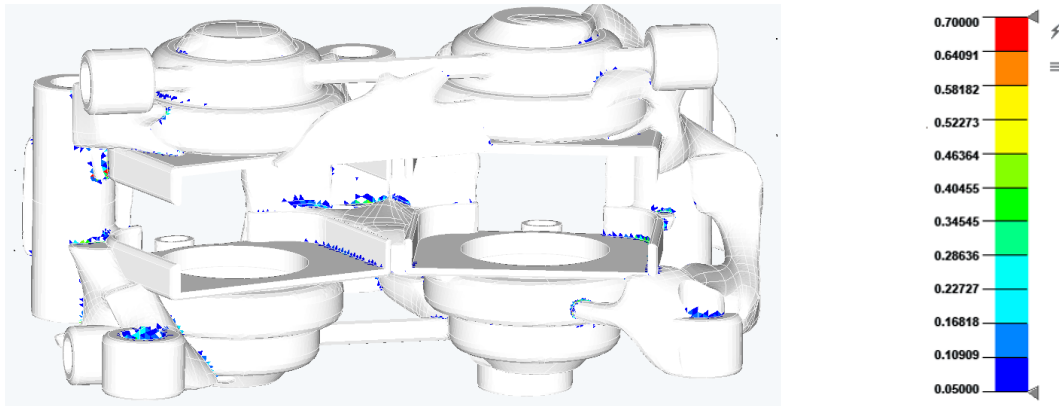


Figure 4.28: Energy error density plot for first design attempt

4.5.2 Second Design

For this second design, several areas were worked on in order to achieve a better overall result. All the highlighted zones were improved in terms of mesh and material presence so, when a new analysis was made, the results were those on figures 4.29 and 4.31.

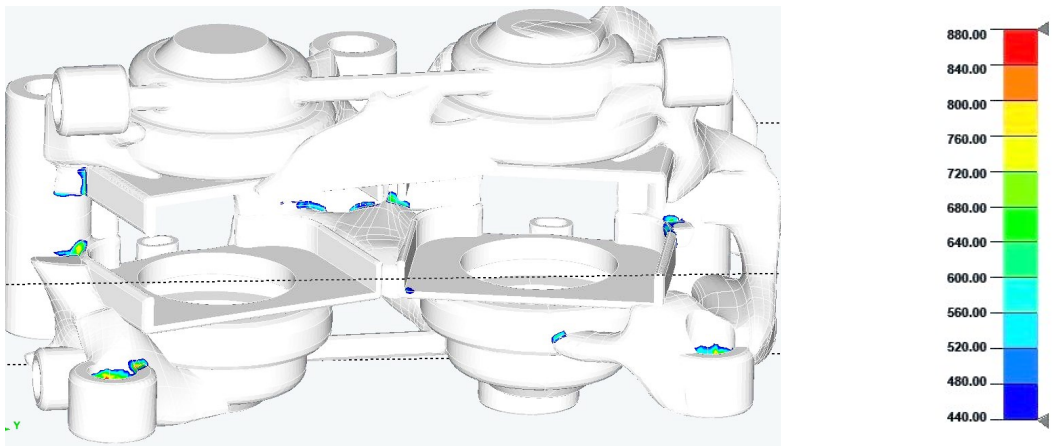


Figure 4.29: von Mises stress plot for second design attempt

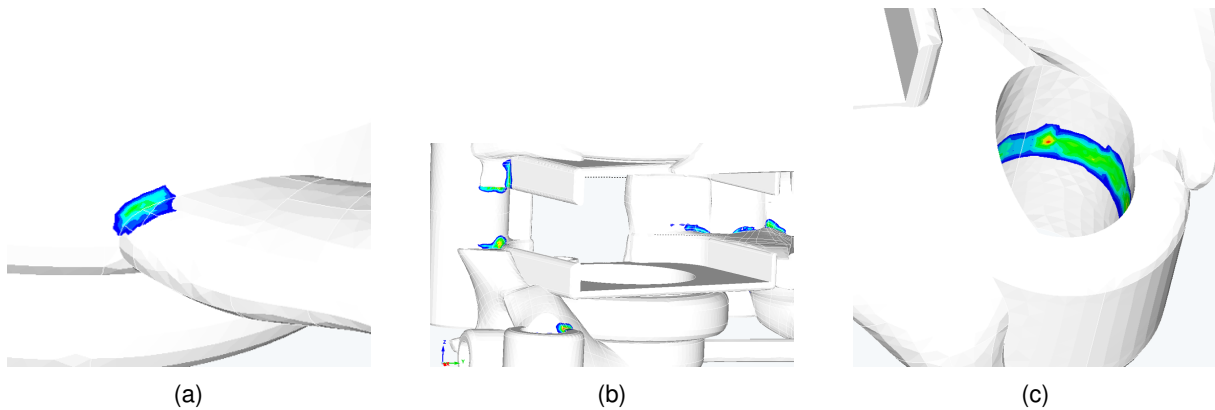


Figure 4.30: Second design close-up views

The overall level of stress on this design was decreased, leaving all the values under the material

yield stress limit. For the effects of comparison, there are plotted with colour only the elements with the stress above the optimisation limit. Despite the part being already secure to handle the static load case, there is still improvement to be made. The stresses shown in figure 4.30c can be neglected because its origin is already discussed above.

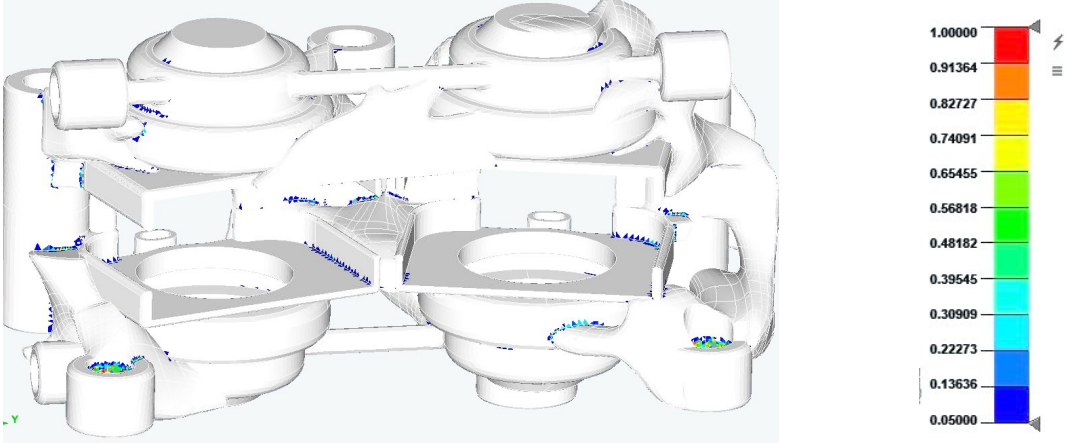


Figure 4.31: Energy error density plot for second design attempt

In terms of energy error, the plotted elements are those with an error between 5% and 100%.

4.5.3 Third Design

The third and last design results from a tweak given to the second design, which met all the design specifications. The figure 4.32 shows a clean stress plot.

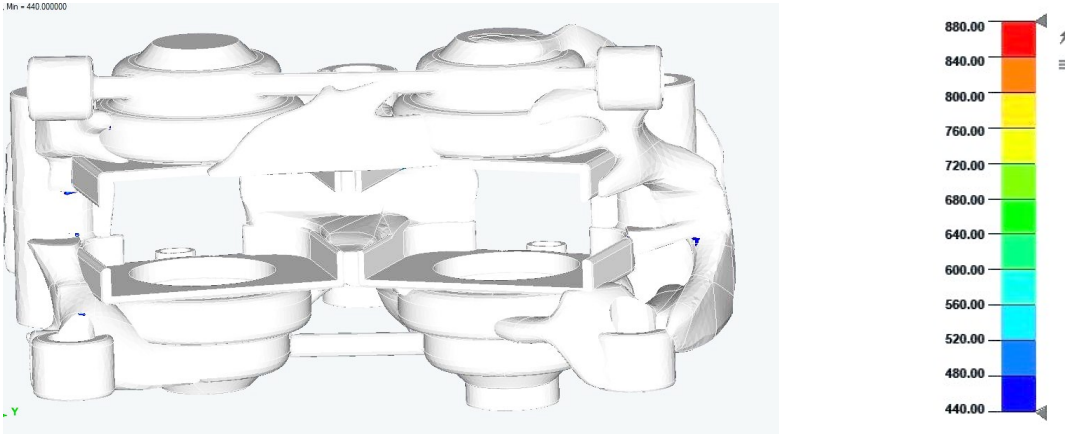


Figure 4.32: von Mises stress plot for third design attempt

With the inclusion of fillets and the elimination of sharp edges, those stresses suffer a reduction. In terms of energy, there is still residual errors present that are difficult to abolish without doing some close mesh refinement or without removing the sharp leading edges.

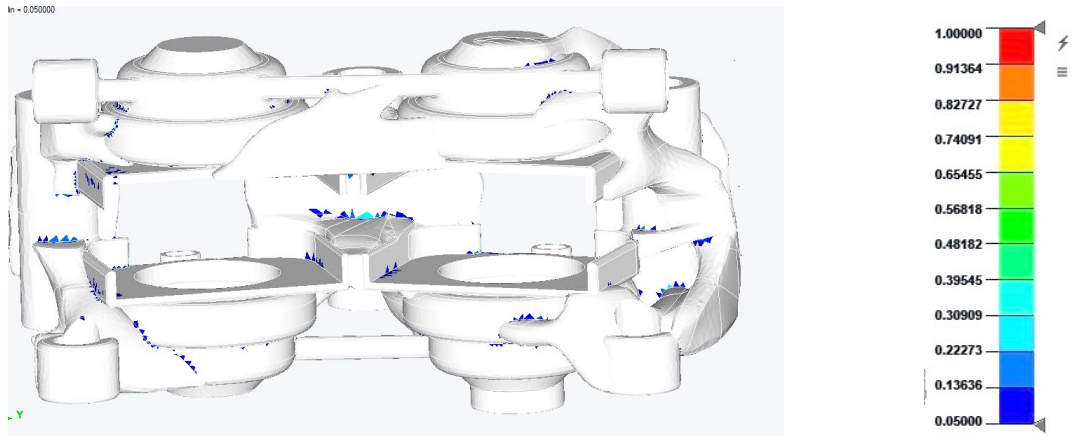


Figure 4.33: Energy error density plot for third design attempt

4.6 Assembly checks

The final part has to be assembled with all the drive train components of the car to see if there is any interference that may need to be solved. There are some interferences between the caliper, knuckle and rim. The rim CAD model is, intentionally, 5mm thicker to the inner side than in reality to make sure that the drive train design does not get very tight and has enough space to allow a clear assembly. Those interferences are within that extra added thickness, but must comply with the logic behind the design. Therefore, the interfering material was removed.

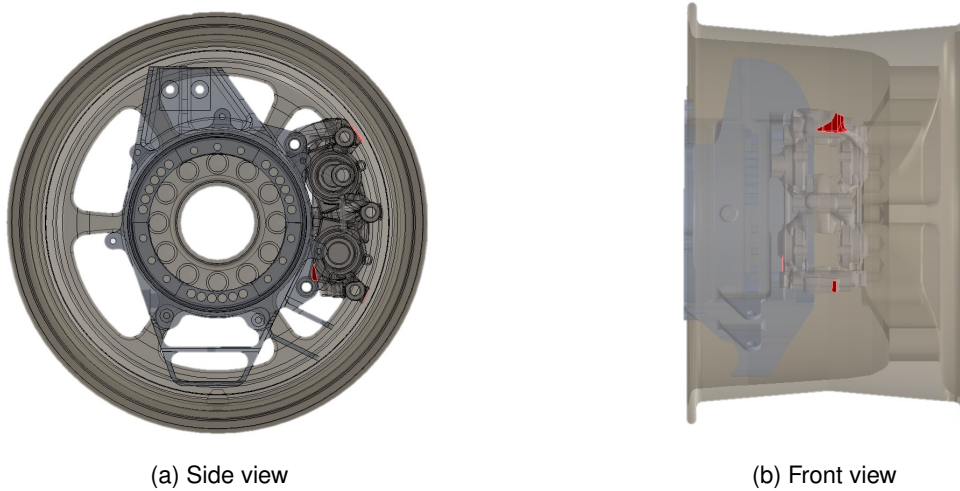


Figure 4.34: Interferences location of the assembly

4.7 Assembly example with Bill of Materials (BOM)

Here it is shown an example of a possible assembly with the list of parts that are compatible with this build, which can be changed to another setup depending on the usage and preferences.

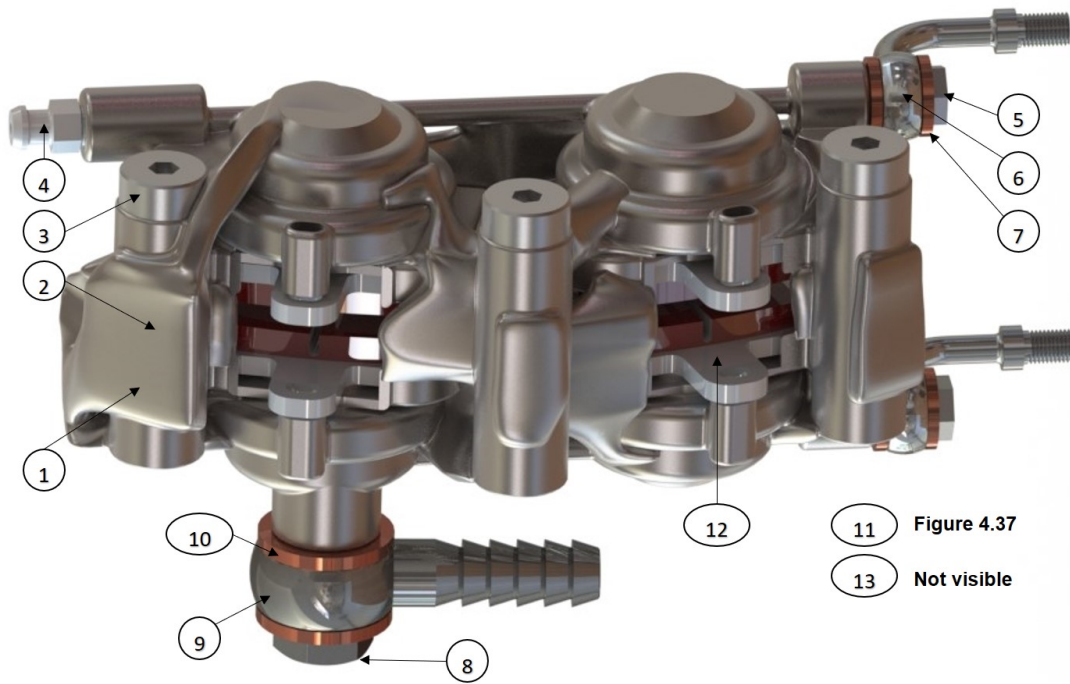


Figure 4.35: Full assembly with fittings

Table 4.3: BOM example for the caliper assembly

Number	Reference	Description	Quantity
1	-	Inner Caliper Half	1
2	-	Outer Caliper Half	1
3	ISO 7379 8x25	Connection Shoulder Bolt 8mm diameter M6 thread	3
4	Sealey BS6129 M6x1.0 29mm	Bleeding Screw M6	1
5	Goodridge 992-02-21C M8X1.0	Banjo Bolts M8	2
6	Venhill 3/60094C	Banjo 8mm with 90 degrees curvature	2
7	ISO 7089 M8	Copper Crush Washer M8	4
8	Goodridge SBK992-03-31SC	Banjo Bolt M10x1.0	1
9	Goodridge SBK592-03C	Banjo 10mm	1
10	ISO 7089 M10	Copper Crush Washer	2
11	Represented on fig. 4.36	Piston 25mm diameter	4
12	CP4226D27-RX	Brake Pads	4
13	Parker 2-214 N0552-90	O-ring seals 25mm	4

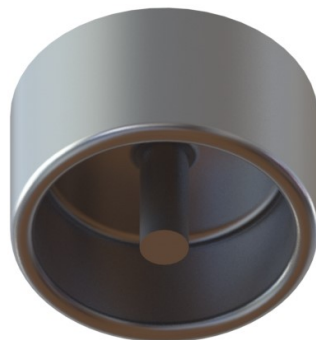


Figure 4.36: Representation of the aluminium piston

Chapter 5

Thermal Analysis

To assess the operating temperature and to evaluate the compatibility with the type of material and brake fluid used, a transient heat transfer analysis was performed. The assembly created before contains only the caliper, the pistons, the brake pads and the brake disc, being the only parts that matter for heat transfer purposes.

5.1 Theoretical Model

The brake torque generation implies the conversion of kinetic energy into heat. The energy generated in the interface between the pad and the disc is dissipated by conduction for each part. For an accurate analysis, it is important to evaluate the split percentage of this energy to both the components. The thermal effusivity, α , is a measure for the capability of a material to exchange thermal energy with its surroundings.

$$\alpha = \sqrt{k\rho c} \quad (5.1)$$

A theoretical model to determine the heat distribution for an imperfect contact [28], is given by:

$$p_D = \frac{\alpha_D A_D}{\alpha_D A_D + \alpha_P A_P} \quad (5.2)$$

$$p_P = 1 - p_D \quad (5.3)$$

where p_D is the percentage of heat dissipated to the brake disc and p_P is the fraction dissipated to the pad.

Table 5.1: Friction couple properties

Specs.	Disc	Pad
Density, ρ	7860 kg/m ³	2600 kg/m ³
Thermal Conductivity, k	50 W/m K	12 W/m K
Specific heat capacity, c	500 J/kg K	1465 J/kg K
Area of friction	19512 mm ²	3755 mm ²

The values for the p_D are around 90%, which means that the major part of the energy is dissipated

to the disc and only a small percentage is dissipated to the pad, which follows the data obtained by F. Talati and S. Jalalifar [29]. The Ap Racing pads thermal properties were not provided. Using several values for racing brake pads thermal properties, the values of p_D fall frequently on the same range.

The energy dissipated to the brake system is equal to the kinetic energy of the car (equation 5.4) and looking to the previous calculation sheet (figure 3.5) each front caliper assembly absorbs 35% of the energy dissipated under braking.

$$H = \frac{1}{2}mV_0^2 \quad (5.4)$$

The car's top speed is referred before in the chapter 3, so the maximum energy release for one full brake event is:

$$H = 1/2 \times 300 \times 29.2^2 = 127896 \text{ J}$$

$$H_{caliper} = 0.35 \times 44764 \text{ J}$$

$$H_{disc} = 0.9 \times H_{caliper} \text{ and } H_{pad} = 0.1 \times H_{caliper}$$

The maximum theoretical deceleration is also shown in chapter 3 so it is possible to calculate the time it takes to stop the car at maximum speed, considering the deceleration is constant.

$$V = V_0 + at \quad (5.5)$$

$$0 = 29.2 - 26.5 \times t \equiv t = 1.1s$$

In this type of analysis, the accurate value of the time used on braking is not very important. The difference between the initial velocity and final velocity influences the energy dissipated, and that is the critical factor when it comes to evaluating the disc temperature properly. The only thing that the time spent under braking influences is the power component of the heat flux. So under these statements, it is safe to say that the time spent in full brake conditions is rounded to 2 seconds, due to other exterior factors that may reduce the friction conditions. With that being assumed, the heat flux is given by:

$$\Psi = \frac{H}{tA} \left[\frac{J}{s \cdot m^2} \right] \equiv \left[\frac{W}{m^2} \right] \quad (5.6)$$

5.2 Transient heat transfer model setup

For this type of problem, the computational times were smaller than the topology optimisation runs, so the mesh size was maintained for two reasons: first of all, the geometry of the problem has a right level of accuracy and secondly the results are prone to be accurate, as they were for the structural analysis.

The model is represented in figure 5.1 and each colour represents a different material. There are three materials used: The titanium Ti6Al4V alloy for the caliper, the steel for the brake disc and the pads' backing plates and the pad composite. Each one of those materials has different thermal properties. The disc and pad properties are defined in table 5.1 and the titanium alloy properties are specified in

table 5.2.

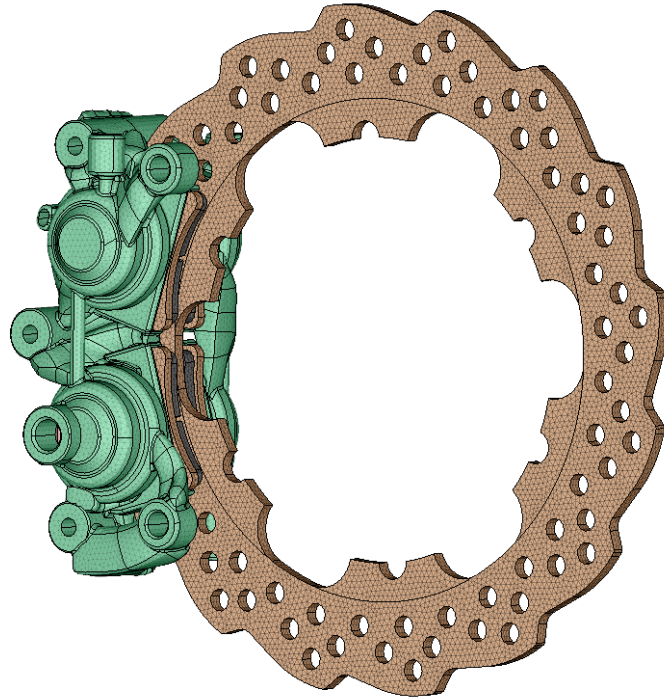


Figure 5.1: Thermal model scheme

Table 5.2: Titanium thermal properties

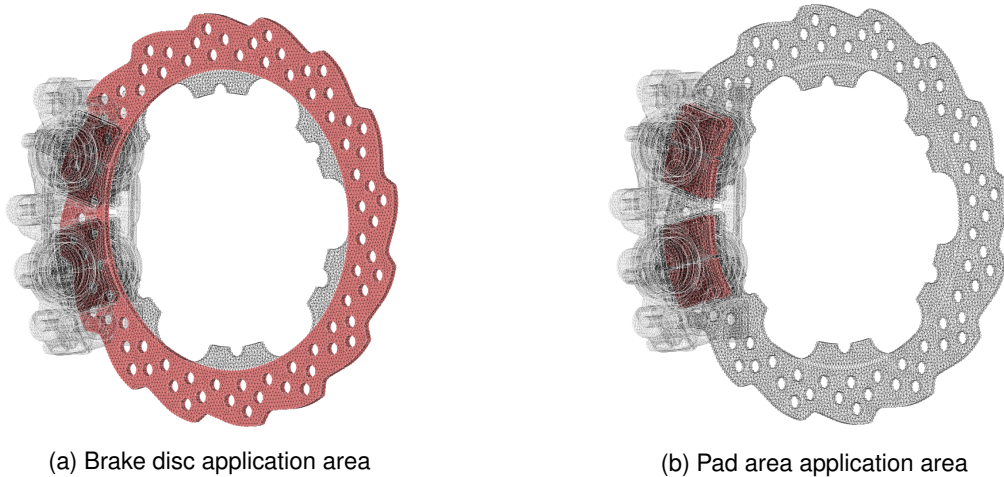
Specs.	Value
Thermal Conductivity, k	$7.1 W/m K$
Specific heat capacity, c	$550 J/kg K$

Once the materials are defined, it is important to define the areas where the heat fluxes are applied (figure 5.2). The mesh coincidence in the contact areas of different materials assures the conductivity of the heat to the caliper and the pistons, so there is no setup needed for the conductive process between parts.

There is still the need of imposing some initial boundary conditions which are mainly the initial temperature, that was set to 300K. The convection load is also important, being the primary heat dissipation process guaranteeing the system is capable of cooling down between uses. Therefore, the areas in contact with the air flux are defined (figure 5.3) together with the convection coefficient for the fluid. Only the external surfaces of the caliper and the surfaces of the disc represent an active and consistent contact with the surrounding air flux.

A radiation flux is applied only to the disc because of its higher temperatures and emissivity. At higher disc temperatures, the irradiated energy is higher and therefore, the influence in the total cooling rate is higher. Nevertheless, it can be discarded.

According to [30], a study to assess the convection coefficient around the discs of typical formula



(a) Brake disc application area

(b) Pad area application area

Figure 5.2: Defined areas for heat flux application

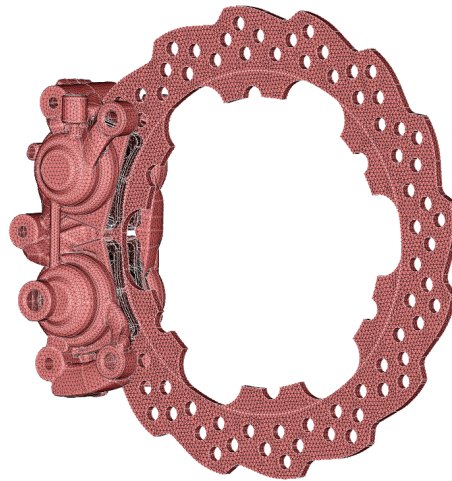


Figure 5.3: Convection relevant faces

student cars and its dependency on velocity follows the expression:

$$h_{forced} = 17v + h_{natural} \quad (5.7)$$

Being this a transient heat transfer study, variables may change with time. The goal is to gather car's data to establish a velocity profile during a lap.

The data was gathered from the 2019 FSS (Formula Student Spain) competition at the autocross event. This event pushes the car to its peak performance since there is no management being made during this one lap circuit. So it is expected the fastest lap times, which is for sure more demanding to the brake system. The car was equipped with a camera capable of collecting GPS (Global Positioning System) and accelerometer data. This specific autocross event has two laps (two allowed attempts for each driver) in a row, but only the fastest lap is used, for now.

The figures 5.4, 5.5 show the position data and its precision, by concluding that the GPS track is very similar to the original and this data is accurate enough for this analysis. The plot of the track indicates the car's position and its speed at each frame. A second plot shows the vertical position of the car. It is



Figure 5.4: In plane GPS position

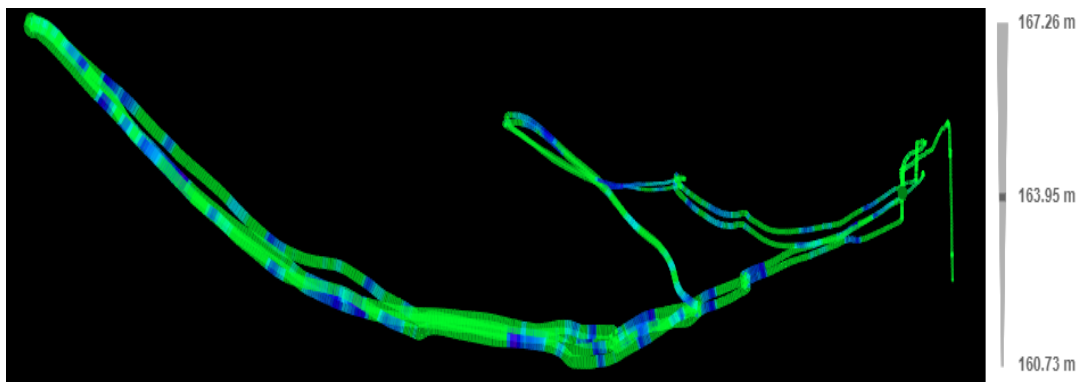


Figure 5.5: Vertical GPS position

vital to capture the 3D dimensional velocity value and not just the in-plane velocity value.

The treatment of this data determined a transient response for the pads and disc heat fluxes.

Knowing the acceleration and velocity at each point the braking power can be calculated by:

$$F_{braking} = m \times a \quad (5.8)$$

$$P_{braking} = F_{braking} \times v \quad (5.9)$$

It is assumed all the braking power is going to the brake system of the car, but there are four wheels, all of them equipped with braking systems that can split the power. Using the brake bias assumption made in sections 3.2 and 5.1:

$$P_{disc} = \frac{P_{braking} \times BB \times p_D}{2} \quad (5.10)$$

$$P_{pads} = \frac{P_{braking} \times BB \times p_P}{2} \quad (5.11)$$

The heat fluxes are obtained with:

$$\Psi_{disc} = \frac{P_{disc}}{A_{disc}} \quad (5.12)$$

$$\Psi_{pads} = \frac{P_{pads}}{A_{pads}} \quad (5.13)$$

5.2.1 Initial Results

The results were retrieved from 4 locations on the brake system. The grid node 60093 is located at the external surface of the caliper; the node 5082 is located at the end of the backing plate, the node 3991 is placed at the interface surface of the brake pads and, finally, the node 18720 represents the disc surface temperature.

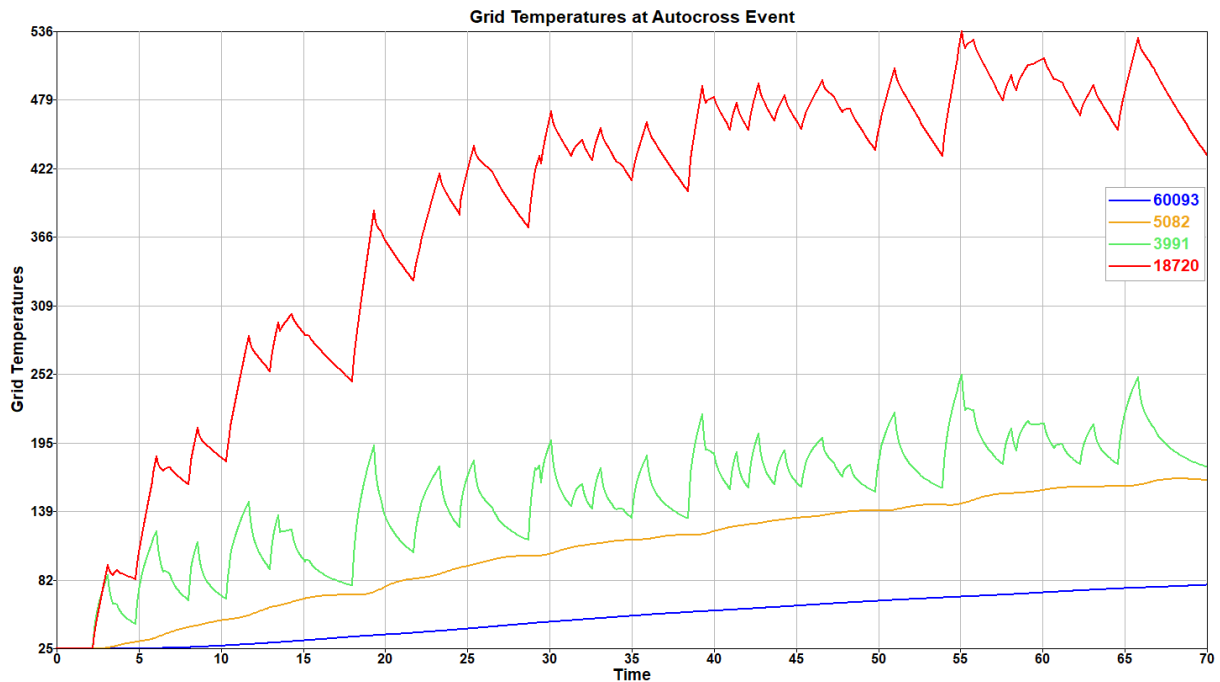


Figure 5.6: Grid temperature Vs Time during a autocross event - Model 1

The temperature increase at the lap beginning is higher, but tends to stabilise over time, due to the difference between the disc temperature and the surroundings, which increases the heat losses. The pad surface also presents the thermal spikes due to the brake application being inconstant, and its temperature loss is majorly caused by conduction to the other parts since there is little room for convection. The backing plate and the caliper became gradually hotter in a stable way since the heat input came from conduction. It is essential to recognise the brake fluid is not defined in this simulation, and it would be safe to assume that it would absorb some of that energy and keep the system even more stable.

The maximum temperature is around 530° C which is bearable for the brake disc's material. It is made from structural steel suited for high strength and wear resistance purposes with a melting point of 1400-1500° C.

Despite the high melting points, steels tend to loose their mechanical properties with rising temperatures. The temperature influence starts to be noticeable above the 400-500° C temperature range. [31]

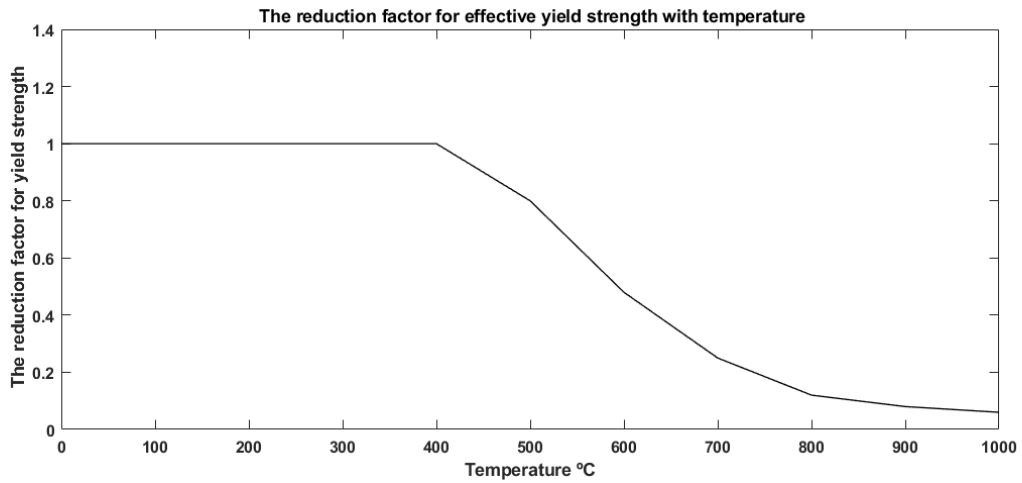


Figure 5.7: The reduction factor for effective yield strength with temperature [31]

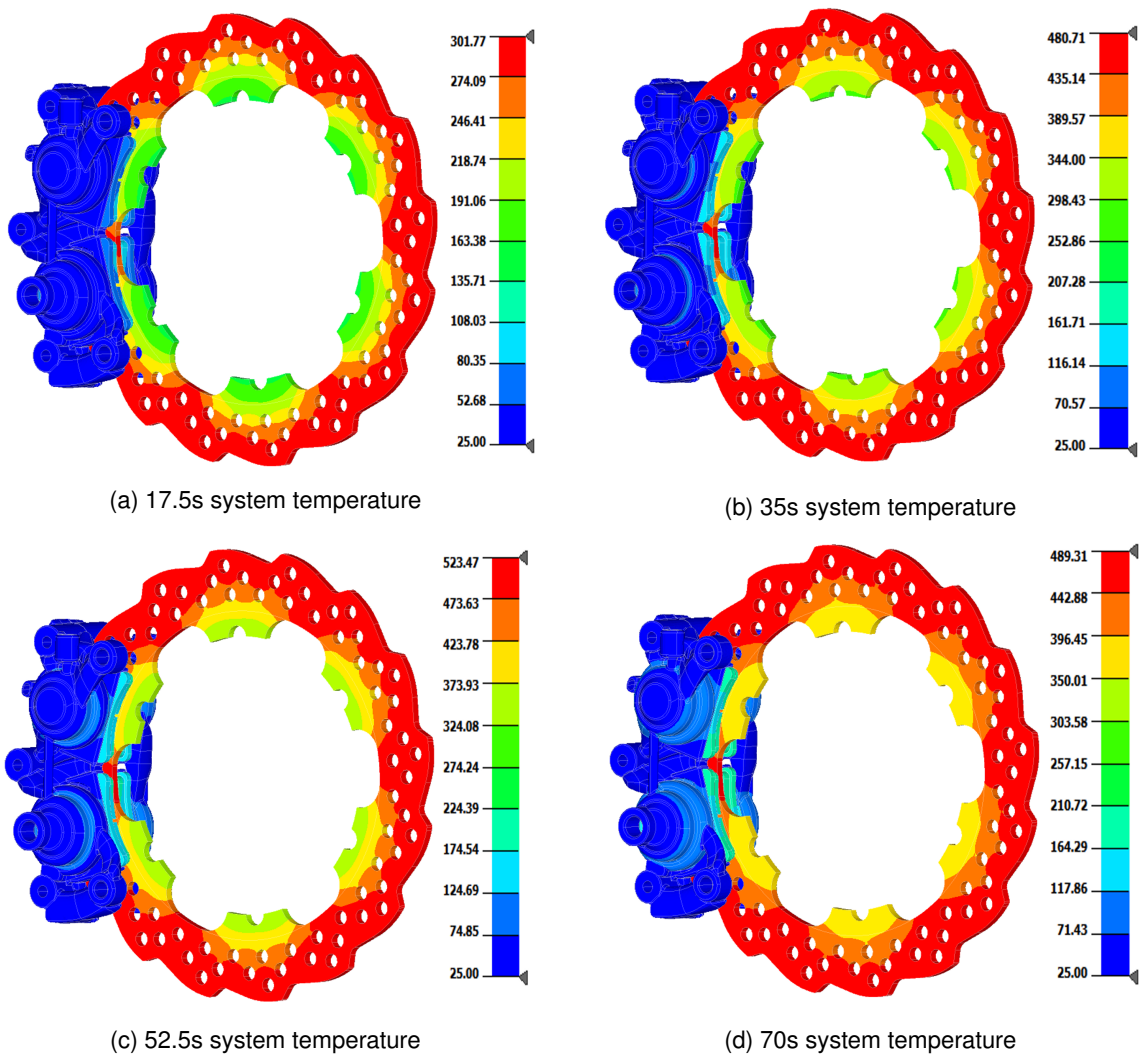


Figure 5.8: Temperature plot at different stages of autocross - Model 1

5.3 Second Model - Aerodynamics and Hub influence

The temperatures achieved in the first model were bearable but still high when compared to what was expected. Before, it was considered that all the energy spent in slowing down was transferred to the brake system, which is not precisely the truth. For a formula student car, aerodynamics play an essential role, which makes the drag force a relevant influence. Another change to get more accurate results is considering the other parts in contact with the disc, such as is the case of the hub. The hub is made from aluminium, being a high thermal conductivity material and responsible for absorbing some of the disc energy. This second model kept all its past features, suffering a tuning on the heat fluxes, due to aerodynamics. Also the hub was added, according to the figure 5.9a and the contact nodes were made equivalent.

The hub's inclusion as a dissipation medium had to be carefully thought since there is an operating temperature at specific faces of the hub. Those faces are close or in direct contact with the transmission and its lubricant, where heat is being generated. Its initial overall temperature was set to be at ambient temperature, but all the faces that are in contact with the transmission lubricant and other elements were set to an operating temperature of $75^{\circ} C$, according to [32].

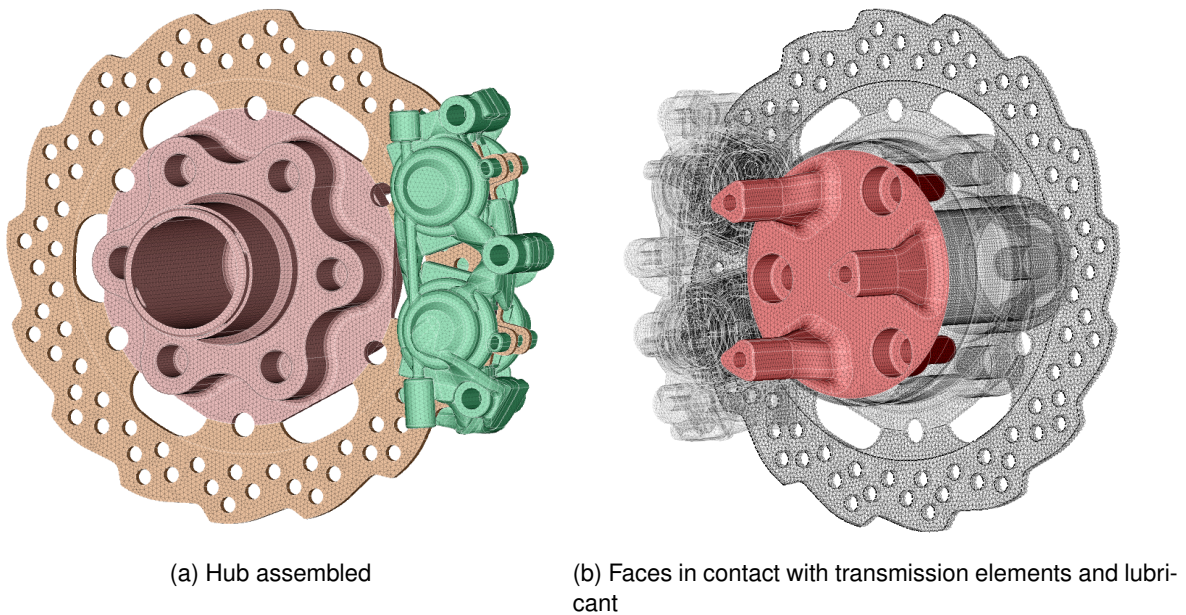


Figure 5.9: Second thermal model scheme

The corrected heat fluxes were obtained with the new mechanical braking power, $P_{mechanical}$, according to equations 5.14, 5.15 and 5.16.

$$P_{braking} = P_{aero} + P_{mechanical} \quad (5.14)$$

$$F_{aero} = \frac{C_D \times v^2 \times \rho_{air} \times A_{proj}}{2} \quad (5.15)$$

$$P_{aero} = F_{aero} \times v \quad (5.16)$$

where the F_{aero} and P_{aero} are the drag force and power, respectively. The figure 5.10 shows the influence of this correction method, in the effective mechanical braking power. It is observed that at higher velocities, the resistance power created by aerodynamics effects are dominant, which reduce the curve's peaks. This reduction in power is, of course, translated into a reduction of the heat fluxes. The power is considered negative because it is acting against the car's movement.

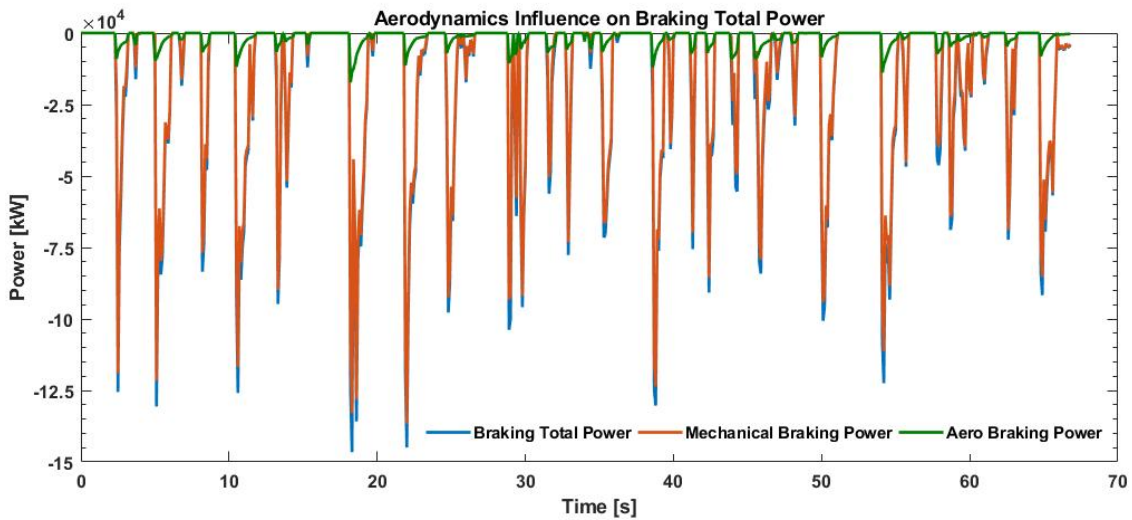


Figure 5.10: Aerodynamics Influence on Braking Total Power

5.3.1 Second Model Temperatures

The temperatures lowered as expected (figure 5.11), with the maximum temperature falling to $480^{\circ}C$. The main reason is that the aerodynamics effects acted upon the power curve peaks by lowering them.

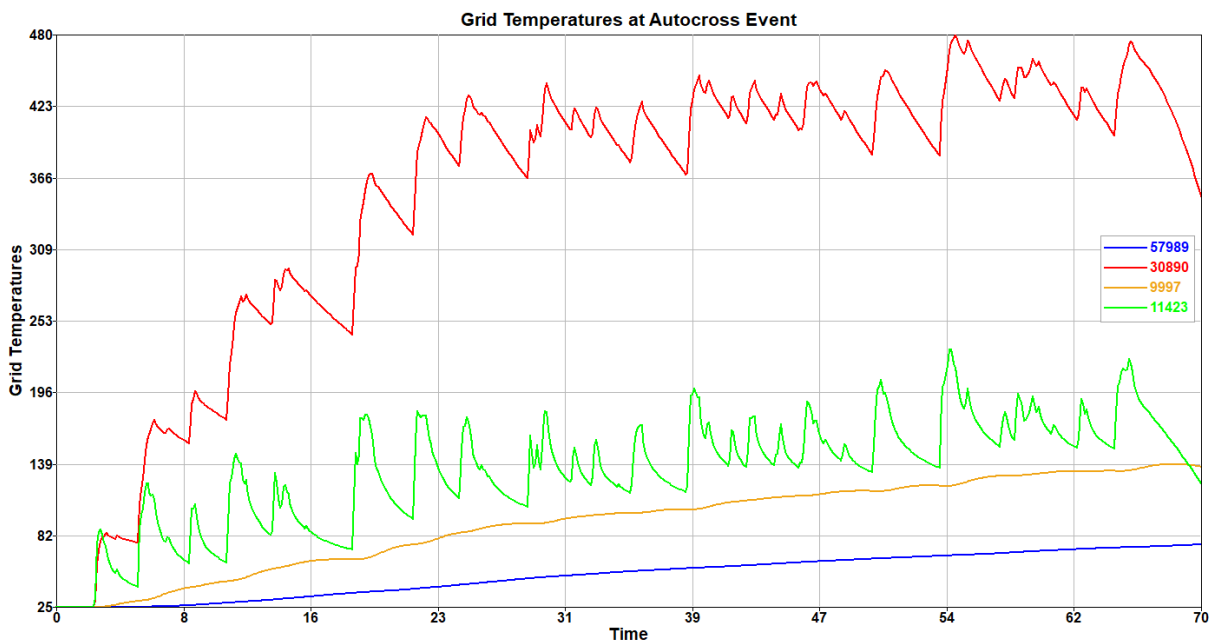


Figure 5.11: Grid temperature Vs Time during an autocross event - Model 2

The figure 5.12 shows the evolution of temperatures with the inclusion of the hub and its inherent constraints. The areas in contact with the drivetrain assembly start at the operating temperature. At the end the minimum hub temperature becomes $75^{\circ}C$, with hotter points close to the disc.

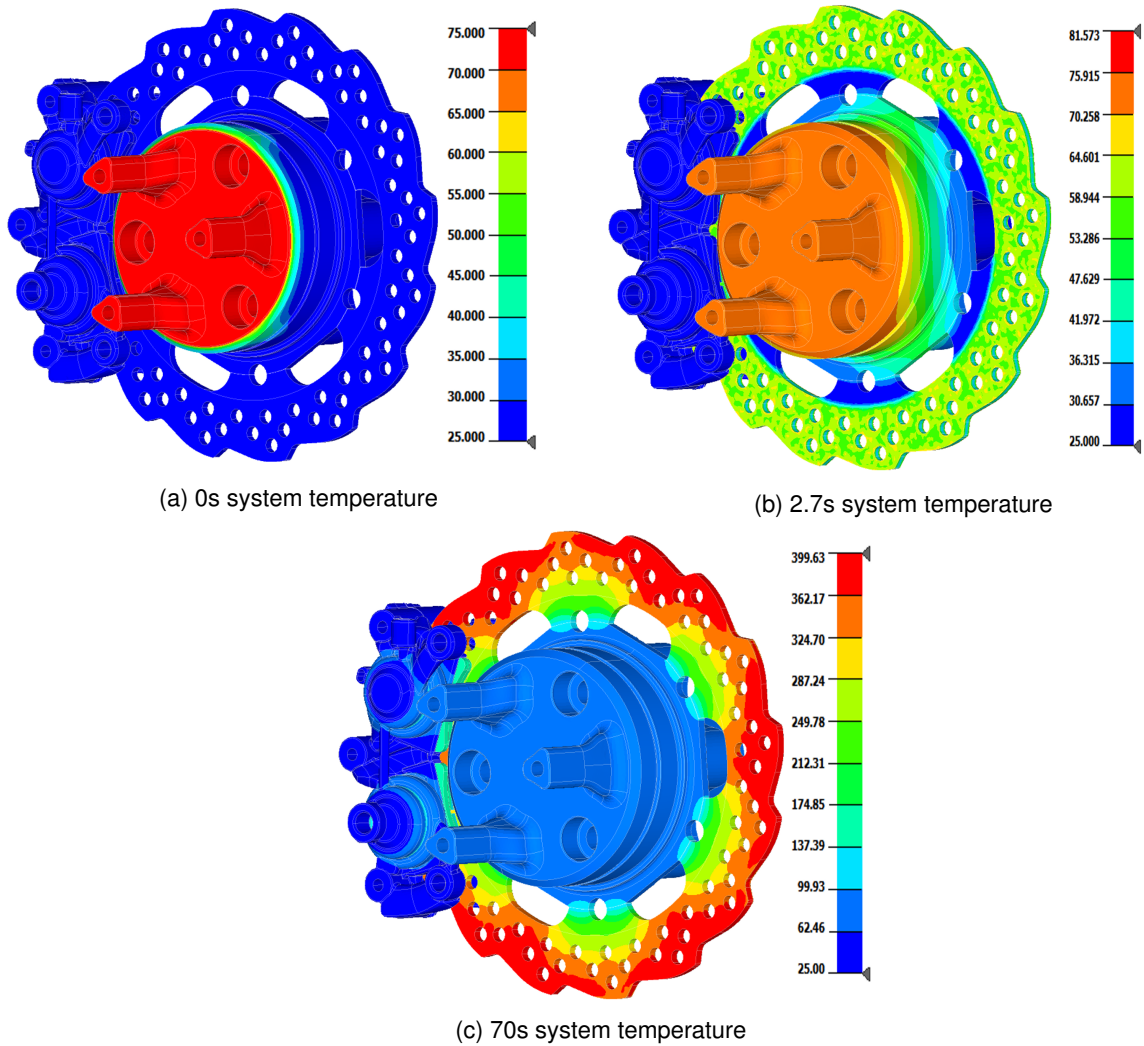


Figure 5.12: Temperature plot at different stages of autocross - Model 2

5.4 Third Model - Aerodynamics and Regeneration influence

The electric motor has some regeneration power that can be switched on, which uses the kinetic energy of the car to recharge the batteries. According to the team, the maximum regeneration power is capped at $15kW$. If that feature is turned on, the car generates energy. If the brake power needed is higher than $15kW$ at any instance, it is considered that the excess braking power is applied mechanically by the brake system. The system 5.17 shows the origin of the braking power, depending on the situation.

$$P_{braking} = \begin{cases} P_{regeneration} & \text{if } P_{braking} \in [0, 15] \\ P_{regeneration} + P_{aero} & \text{if } P_{braking} \in [15, 15 + P_{aero}] \\ P_{aero} + P_{mechanical} + P_{regeneration} & \text{if bigger} \end{cases} \quad (5.17)$$

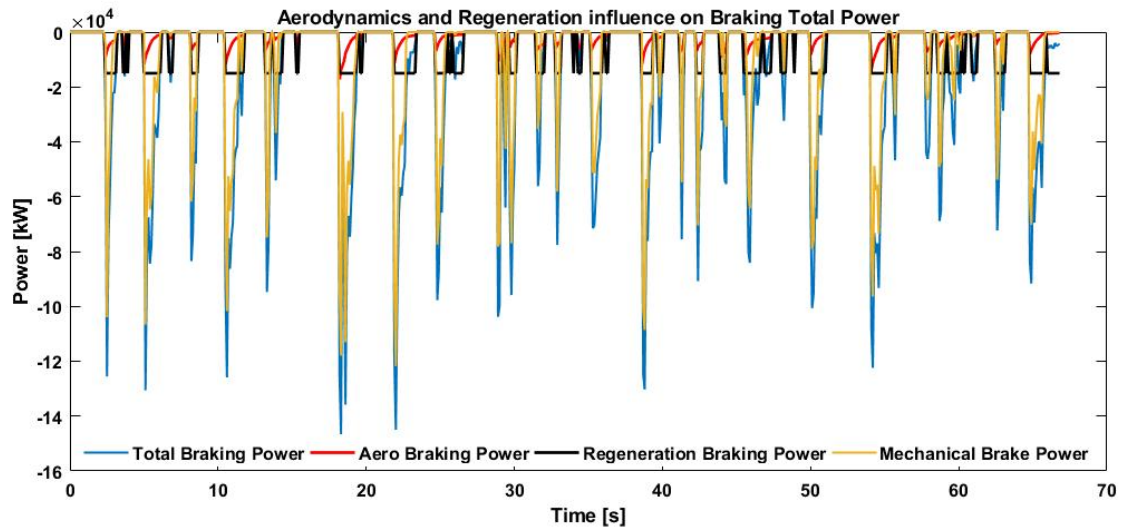


Figure 5.13: Aerodynamics and Regeneration Influence on Braking Total Power

With the regeneration effects, the peak's power difference between the total power and the mechanical power curves is more substantial (figure 5.13). It is expected a significant temperature decrease. Although brake regeneration being usually enabled, it should be considered that the critical and most demanding case that the system is undergoing should be the second model, because brake regeneration is an option that may be disabled if excessive wear is happening on the transmission or in case of high electrical packages temperatures.

5.4.1 Third Model Temperatures

The results are presented in the figures 5.14 and 5.15 that show another reduction in temperatures.

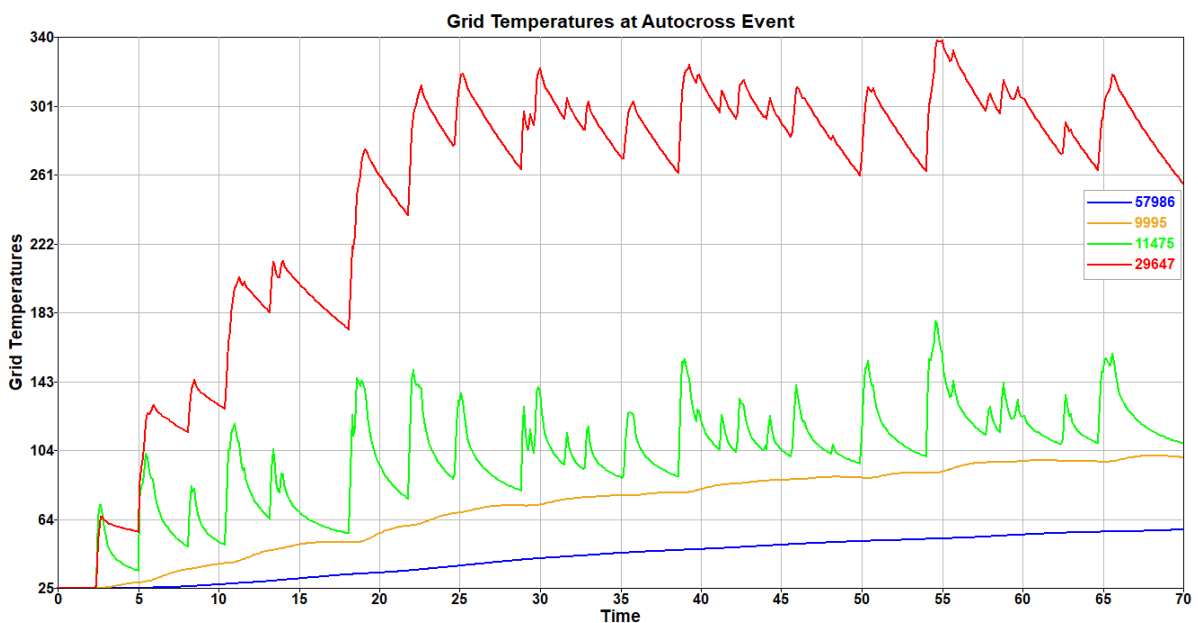
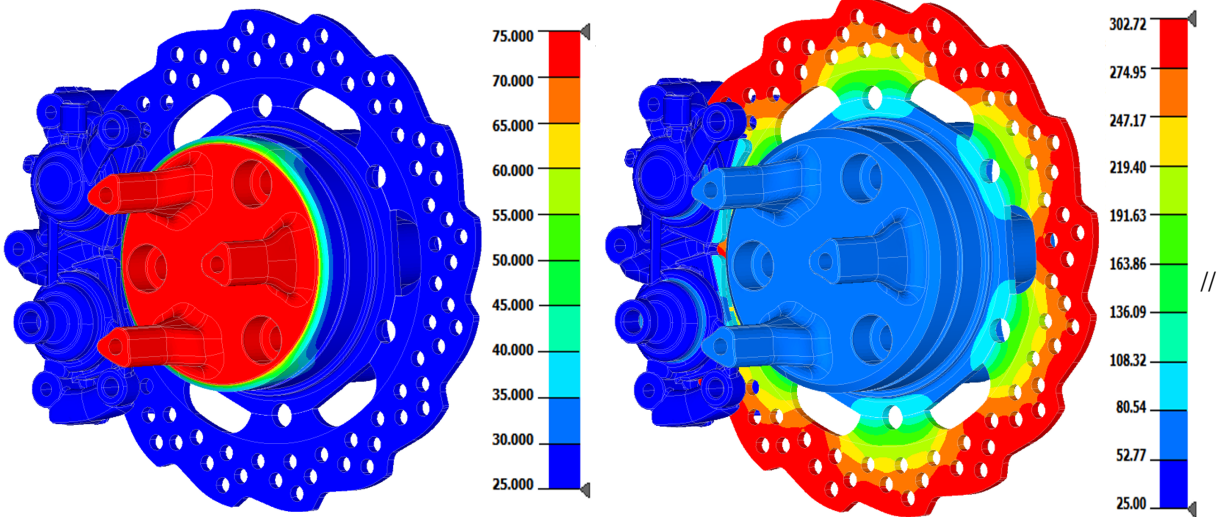
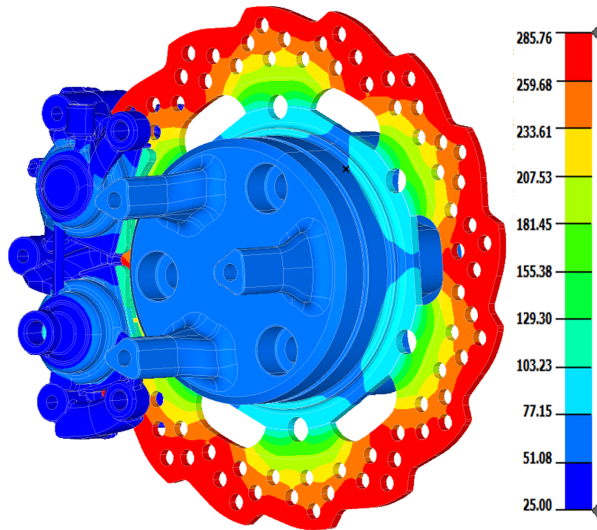


Figure 5.14: Grid temperature Vs Time during an autocross event - Model 3



(a) 0s system temperature

(b) 35s system temperature



(c) 70s system temperature

Figure 5.15: Temperature plot at different stages of autocross - Model 3

5.5 Convergent Temperature

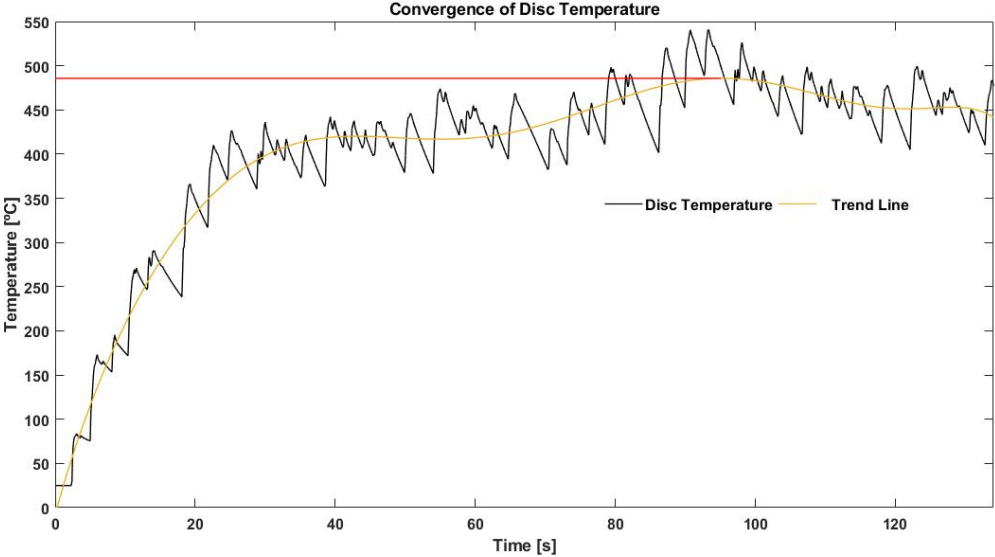


Figure 5.16: Convergence of Disc Temperature

Considering the previous results, the temperature curves tend to lose its slope over the lap and with increasing temperature, pointing to a settled temperature. Therefore it was performed an analysis with two laps in a row to assess if the temperature gets stable under continuous work.

Using the second model data, which is more mechanical demanding than the third model, it can be seen that if two laps of autocross are performed successively, the settling temperature is around 450° C, with some maximum local points, for example, the one indicated by the red line that points to a local maximum temperature of 485 ° C (figure 5.16). At the working temperature range, the heat dissipation rate is higher due to the larger temperature differences. That is the reason why the temperatures kept almost constant over the second lap, since the cooling portions of the curve are steep.

Chapter 6

Manufacturing Approach

The additive manufacturing technologies bring the flexibility of design advantage, but when high tolerances and finishes are needed, there are some adjustments to be made. The combination of additive manufacturing with CNC (Computer Numerical Control) milling/turning technologies is commonly and widely used nowadays. Those processes operate differently since one of them adds material, and the other one removes it.

6.1 3D Printing Design Adjustments

To transform the original final part to the one that should be printed it should be taken into account the features needing tighter tolerances, only achievable with fine machining. Near that features it should be printed material in excess to give room for the machining. Summing, all the thread holes, piston boreholes, backing plate guides and the o-ring seal grooves should be printed with excessive material.

The excessive material must be enough to create the desirable features later; otherwise, the printing time increases in vain, making the whole process of manufacture less optimized.

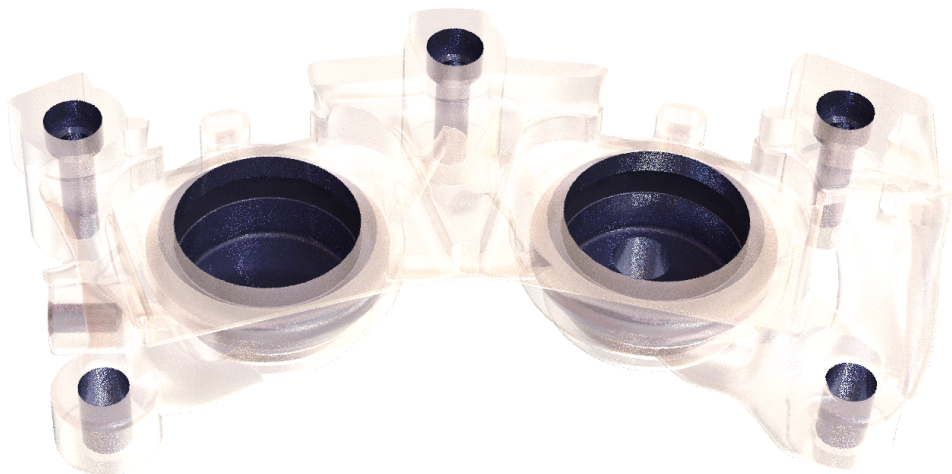


Figure 6.1: Fine tolerance faces of half capiler

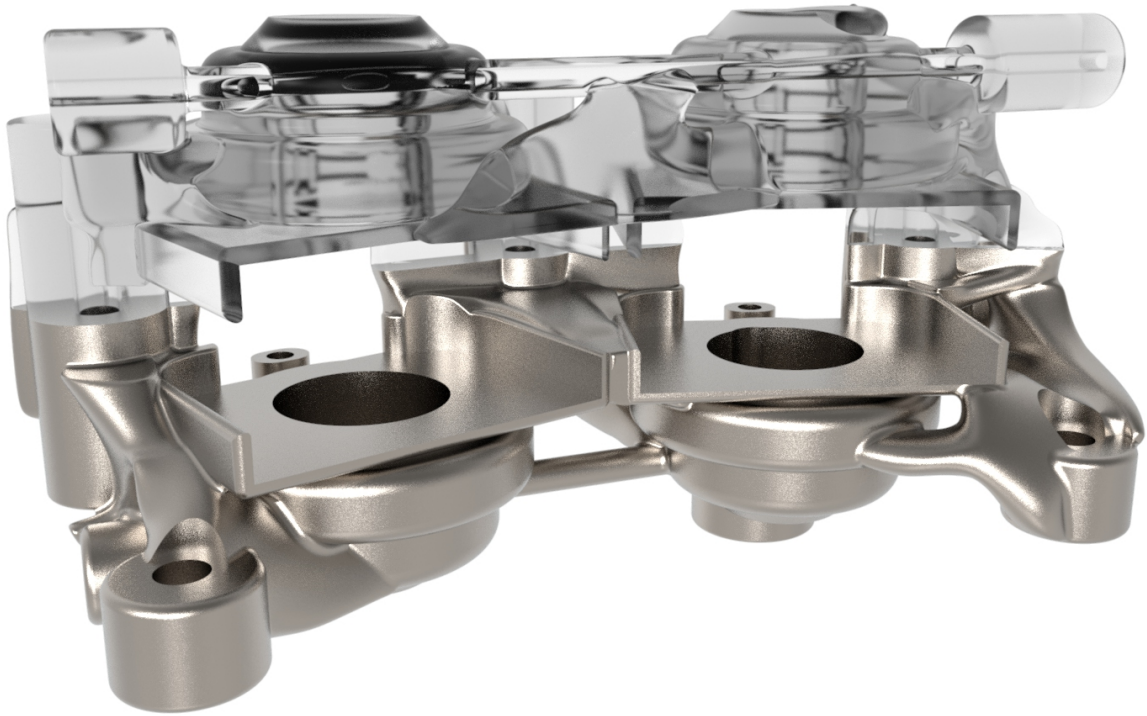


Figure 6.2: Design adaption with excessive material for 3D printing

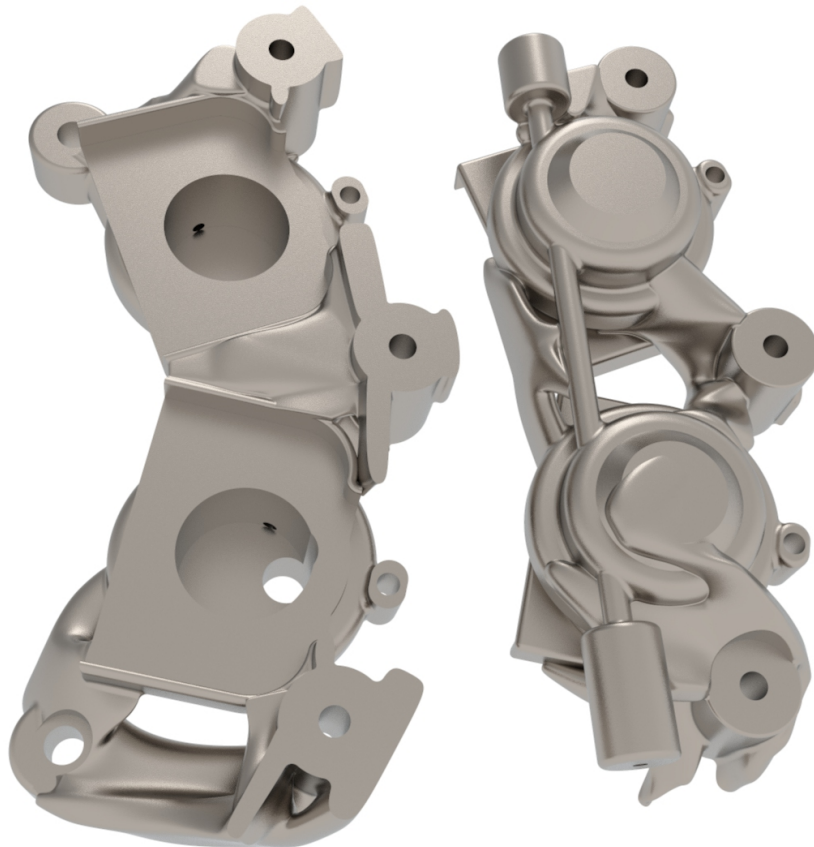


Figure 6.3: Design adaption with excessive material for 3D printing (2)

The figures 6.2 and 6.3 show the design changes that are going to the printing machine. The piston bores were simplified and shrank. All the threaded holes were reduced to a size smaller than the correspondent tap drill for each thread.

6.2 Geometrical and Dimensional Tolerances

6.2.1 Thread Holes

Each one of the holes planned to be threaded should be drilled first to the corrected drill size, to be then tapped to the metric size of the screw.

Knuckle Screw Holes - These holes are threaded with M10x1.5 so the drill size must be 8.5mm.

Halves Connection Screw Holes - For this connection, it is used shoulder bolts with an M6 thread. These shoulder bolts have an 8mm diameter body that passes entirely through one half and part of the other. The goal is to get a tight fit between the halves and the screw, leaving less room for gaps. The thread is only tapped in one half, as shown in figure 6.4. The drill size for the threaded hole must be 5mm.

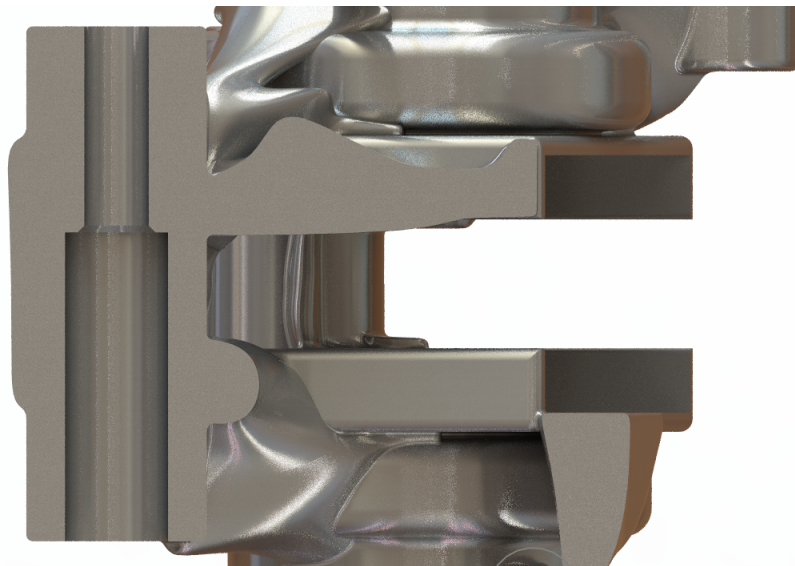


Figure 6.4: Shoulder bolts drill scheme

6.2.2 Piston boreholes

The piston boreholes (figure 6.5) require some specific tolerances to let the pistons work as intended. The central aspect of the tolerances falls upon the o-ring seal. According to the used catalogue, the borehole diameter for the piston must be 25mm with a dimensional tolerance H8, and the maximum diameter that should accommodate the o-ring seal must be 30.9mm with a dimensional tolerance H9.

The pistons, on the other hand, must have a diameter of 25mm with the tolerance f7. The rest of the dimensions needed for the cavity are explained in figure 4.7 from chapter 4.

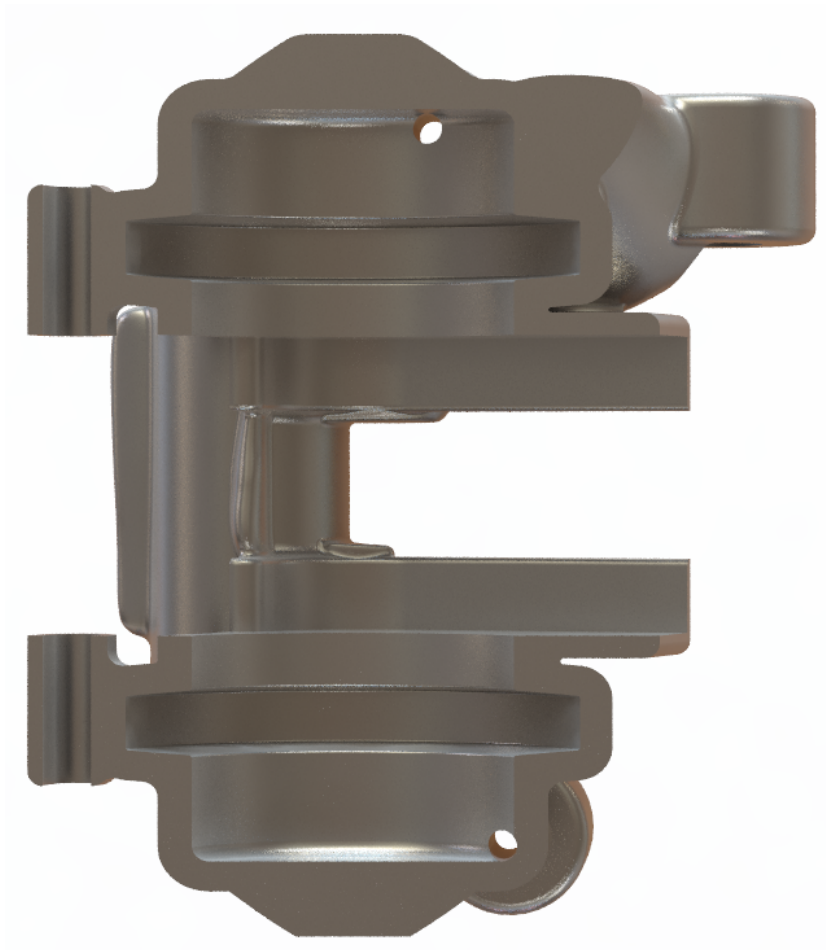


Figure 6.5: Piston boreholes

Apart from those dimensions, there are also some roughness requirements to guarantee the sealing. The groove base and sides must have a mean roughness of $1.6\mu m$ and the contact surface of the piston with the o-ring must have a mean roughness of $0.4\mu m$.

Chapter 7

Alternative Design

7.1 Alternative design obtained by STL editing

During this design process, other techniques more suitable for 3D printing design came up. Currently, it is commonly used STL editing software to shape and prepare parts for 3D printing. This software has many advantages, such as smoothing and wrapping algorithms that can replicate the topology design very quickly. They also have some disadvantages, such as losing the parametric CAD data, resulting in faces or edges not defined, making it difficult for later changes in the design if needed, or some subsequent analysis that may need to be performed.

To explore this software, and looking at the previous results, that are still below the compliance limit, it was decided to run the same optimisation model, but with an additional parameter. It was introduced a constraint of minimum size, that determines the smaller dimensions that any topology member can have, normally acting on its thickness. The minimum dimension was set to $5mm$. Figures 7.1 and 7.2 show the new optimisation responses evolution through the iterations.

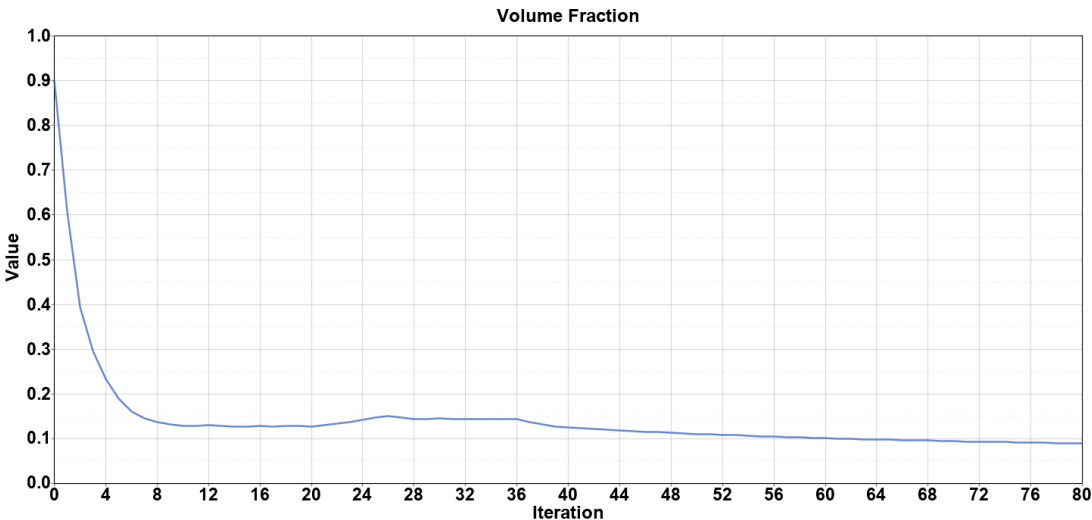


Figure 7.1: Volume fraction response of the alternative optimisation

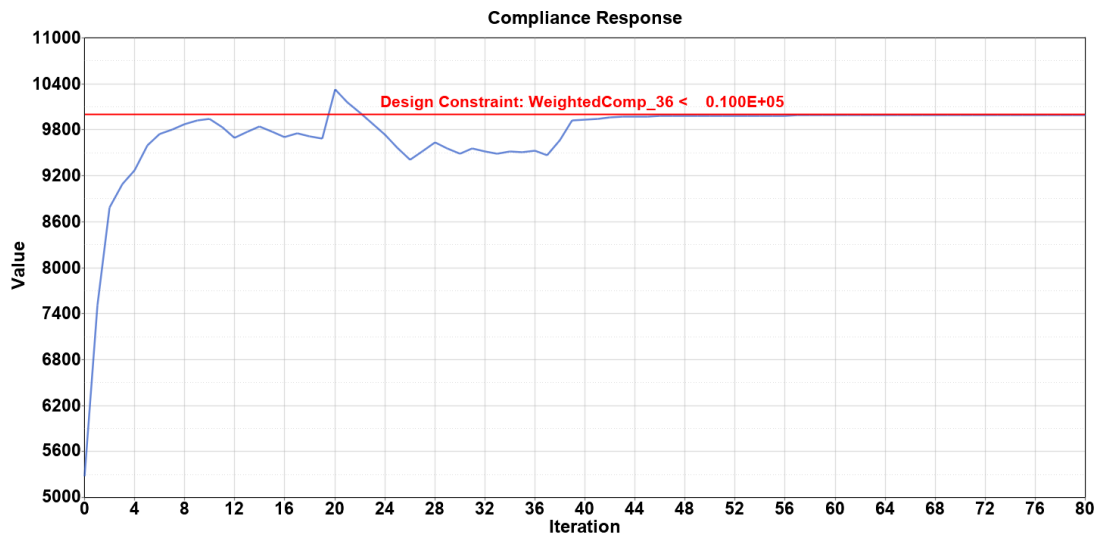


Figure 7.2: Compliance response of the alternative optimisation

The used threshold was the same (0.3) to get a comparable solution with the previously obtained. The figure 7.3 shows some changes due to the minimum size constraint, which result in the elimination of some thin geometries that the previously obtained part had near the middle connection bolt. This constraint also improves the manufacturability since thin regions have more tendency to warp, therefore their elimination results in a cleaner print.

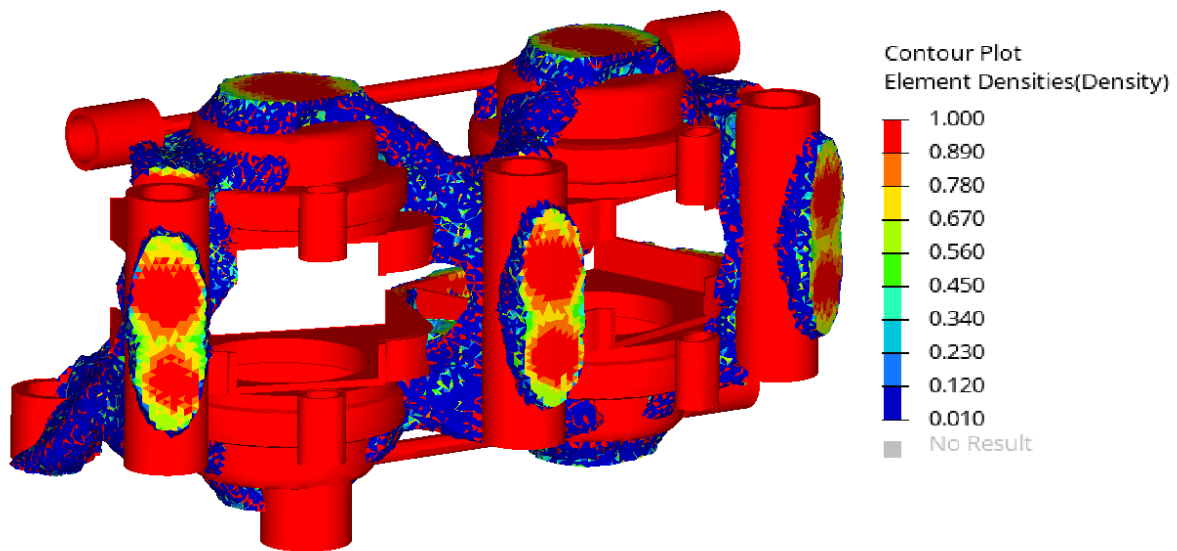


Figure 7.3: Alternative design optimisation isosurface

The software used to recreate this geometry was the trial version of Ansys SpaceClaim which can work directly with facets and perform many operations as if it was cad geometry (Figures 7.4, 7.5, 7.6 and 7.7). This geometry files can be directly fed to the 3D printer, which was not the case since the printable version is simplified. Despite that, this can be used to evaluate the final part weight with this method.

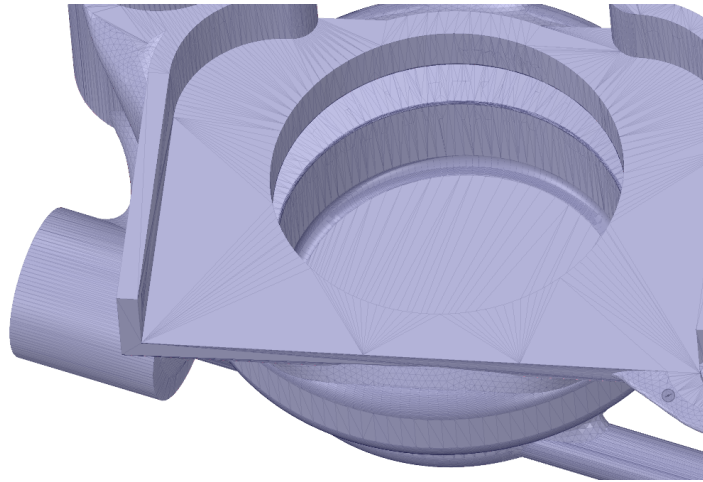


Figure 7.4: Facets geometry representation

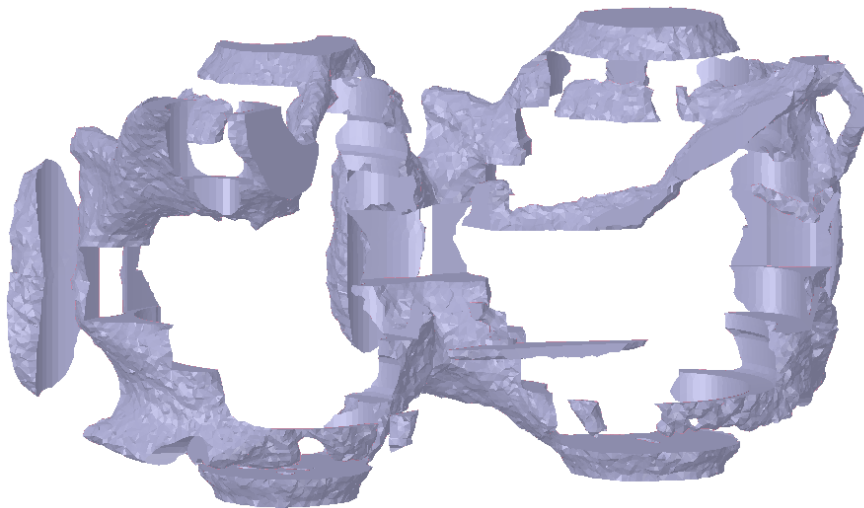


Figure 7.5: SpaceClaim 0.3 density threshold isosurface

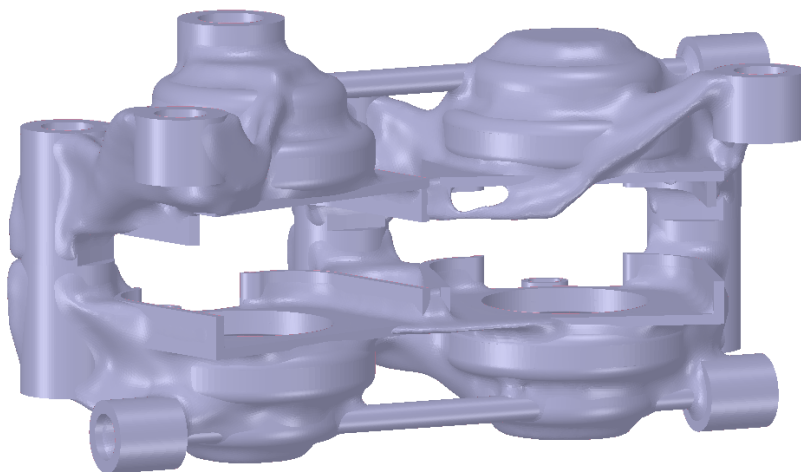


Figure 7.6: Smoothing and wrapping of the design space mesh with the non-design space

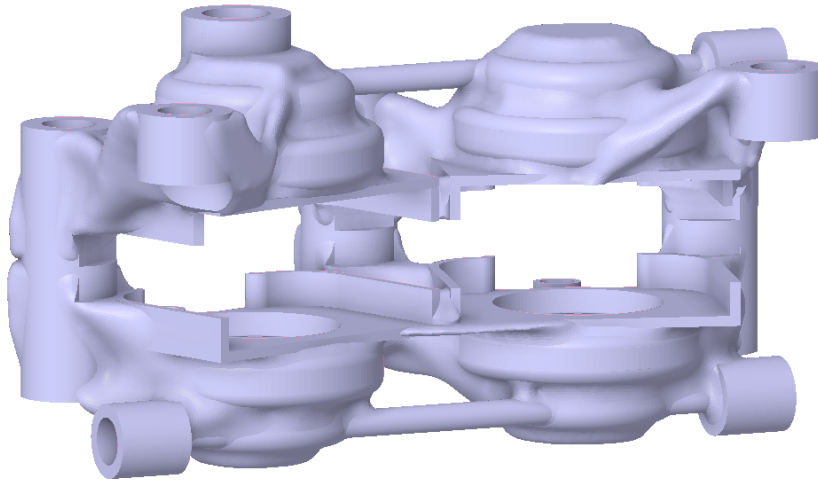


Figure 7.7: Final faceted part

A reanalysis was performed to assure that this new design was, in fact, able to withstand the load case, just like the prior solution. The figure 7.8 shows that the system is inside the established parameters, below the maximum stress defined. The maximum displacement is $0.82mm$, and the measured compliance is $8633N.mm$.

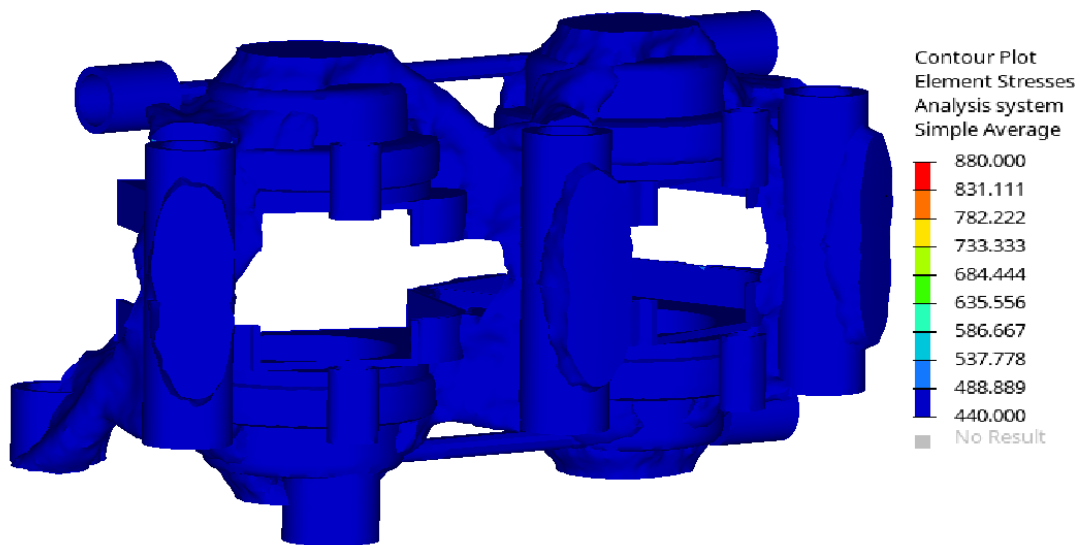


Figure 7.8: Faceted design reanalysis

It is not strictly necessary to repeat the thermal studies since the expected difference of the caliper mass should not be that great to justify the difference in temperatures. Despite that, it may be enough to justify this technology used for the caliper conception if the percentage of mass reduction increases significantly, which is discussed later in the conclusions.

7.2 Final renders

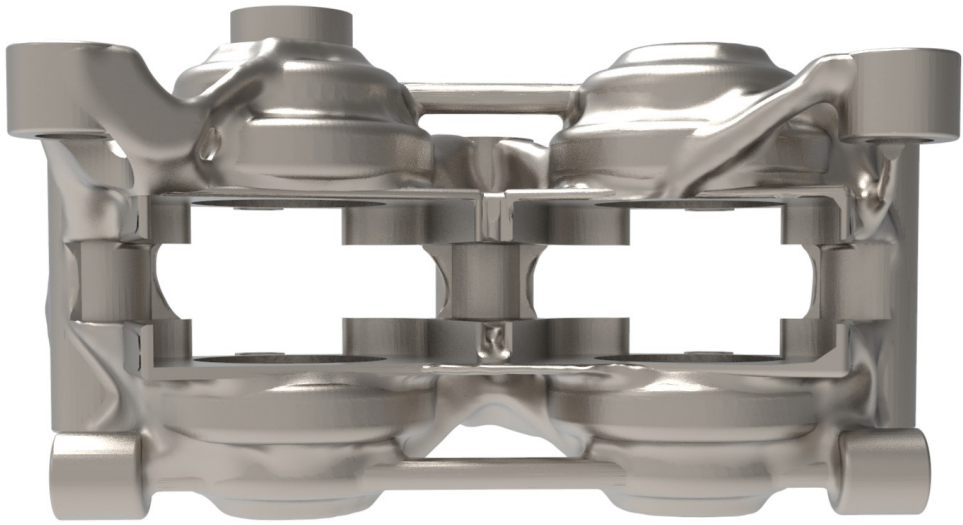


Figure 7.9: Faceted design render view

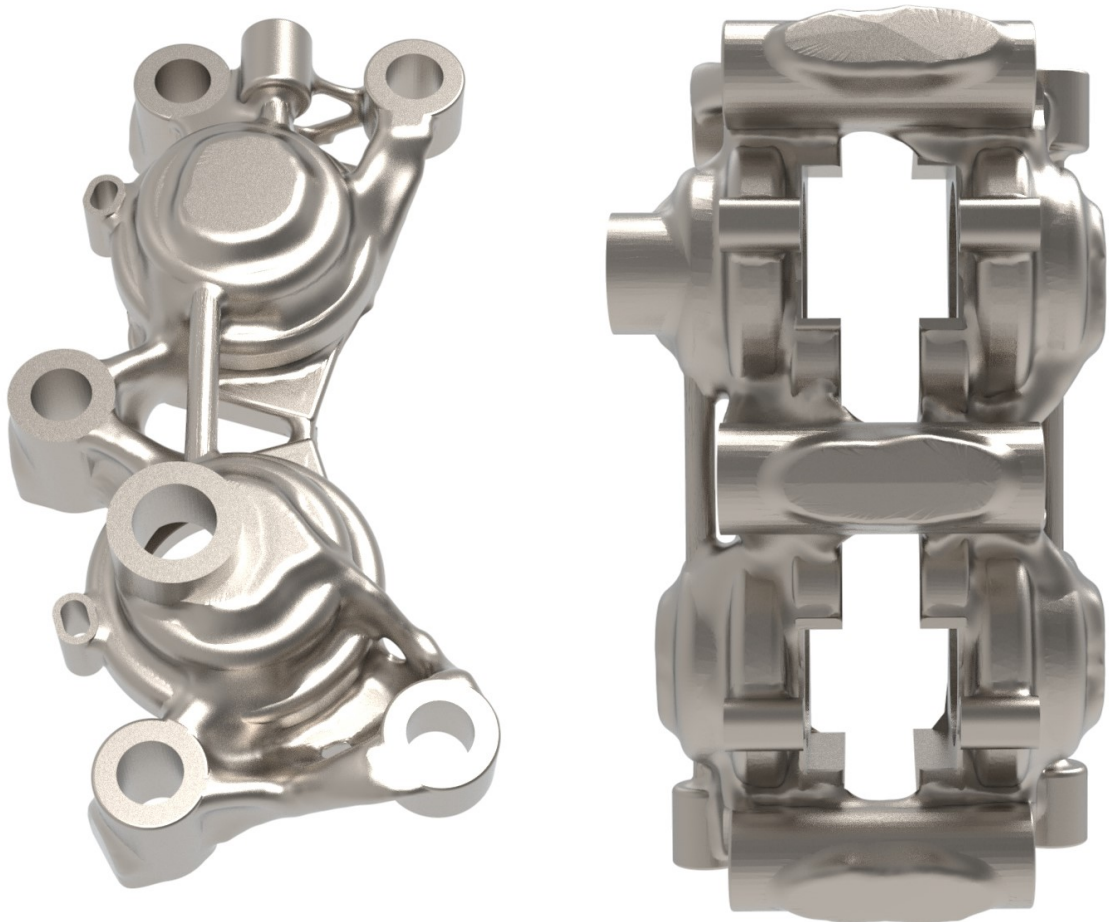


Figure 7.10: Faceted design render view (2)

Chapter 8

Conclusions

8.1 Results Discussion

8.1.1 Detailed comparison between solutions

The current front caliper of the car is the AP Racing CP4227-2S0. It is an aluminium racing caliper made especially for bikes but suitable for the car requirements. It has a similar assembly compared to the 3D printed design. The current has two bleeding valves and two entry banjo fittings, while the thesis design only has one bleeding valve pointing upwards and one entry banjo fitting.



Figure 8.1: AP Racing Caliper

The braking pads, the bleeding valves, the connection bolts, and the fittings are practically the same with only little changes to be made. Therefore the analysis falls upon the caliper and the pistons, that are in this case, the only interchangeable solutions.

After analysing both calipers, the results were regrouped on the tables 8.1 and 8.2.

The compliance of the third design is much lower than the optimisation results. It is crucial to understand that the optimisation results are in the form of a continuous density between 0 and 1 when in reality

Table 8.1: AP Racing caliper analysis

Properties	Value
Compliance	10000 <i>N.mm</i>
Weight (Caliper+Pistons)	400 <i>g</i>
Maximum Displacement	0.82 <i>mm</i>
Selling Price	634€/ <i>unit</i>

Table 8.2: Third design caliper analysis

Properties	Value
Compliance	5674 <i>N.mm</i>
Weight (Caliper+Pistons)	350 <i>g</i>
Maximum Displacement	0.69 <i>mm</i>
Manufacturing Cost	550€ ¹

it can either have the material or not, i.e. the density are only zeros and ones. Since the threshold used was 0.3, all those elements with densities between 0.3 and 1 are converted to a fully dense elements when building the design, which increases the weight and decreases the compliance.

It was possible to reduce the weight of caliper in 12.5%. To further evaluate the cost of the AM solution, it was used the Atzeni and Salmi economic study [33]. It must be clear that this cost analysis is from the production point of view. The following procedure was considered:

- The volume is 110% of the part volume to account for supports and wasted material that the 3D printer used at the building plate;
- It considers that each machine has around five years of linear depreciation to determine its hour cost;
- It considers that the use percentage of the machine will around 60% per year when normally those machines can operate at the 80% range;
- It considers the SLM 280 machine from SLM Solutions with a price tag around 400 000€;
- The build plate size is $280 \times 280 \times 365$ mm. Capable of manufacture two halves, i.e. one caliper at one time.

This machine has several laser configurations, being at its top capable of printing $88\text{cm}^3/\text{h}$ [34]. To get the maximum manufacturing price, it is considered the slowest configuration with only one 400W laser, with maximum build-up rates around $35 - 40\text{cm}^3/\text{h}$. These maximum build-up rates are for a very gross printing which is not desirable.

A study to determine an optimal set of parameters for Ti6Al4V alloy SLM printing realised that for optimal surface quality, the following parameter could be used, with the sacrifice of production rate [35].

Table 8.3: SLM optimal parameters for quality [35]

Parameters	Value
Power	150 <i>W</i>
Scanning Speed	950 <i>mm/s</i>
Hatching Space	0.08 <i>mm</i>
Layer Thickness	0.03 <i>mm</i>

The build-up rate is now calculated as:

$$\dot{V} = S_s \times H_s \times \delta \quad (8.1)$$

¹Calculated further from the production point of view

where S_s , H_s and δ are the scanning speed, hatching space and layer thickness, respectively.

The caliper total volume is $71364mm^3$, meaning that the printable volume is around $78500mm^3$. The maximum build up time will be around:

$$T_{build} = \frac{V_{print}}{\dot{V}} \quad (8.2)$$

$$T_{build} \approx 9.6h$$

Table 8.4: AM final design cost analysis

Number of parts produced per job	-	N	1 (two halves)
Material cost per kg	EUR/kg	M	350
Mass of material per part	kg	U	0.385
Material cost per part	EUR	MP=U×M	135
Machine operator cost per hour	EUR/h	O	20
Set up time	h	A	1.2
Pre-processing cost per part	EUR	AP=A×O/N	24
Depreciation cost per year	EUR/year	C	80000
Hours per year	h/year	H=0.6×365*24	5256
Machine cost per hour	EUR/h	CH=C/H	15.2
Job time	h	T	9.6
Machine cost per job	EUR	CB=CH×T	34.96
Processing cost per part	EUR	CP=CB/N	67.5
Post-Processing time per job	h	B	1.5
Heat treatment cost per job	EUR	HT	20
Post-processing cost per part	EUR	BP=(O×B+HT)/N	50
Total cost per part	EUR	P=MP+AP+CP+BP	≈422

The final cost per caliper demonstrated by the table 8.4 does not include the energy cost, facilities rent and maintenance of the machine, which would also add more cost. According to Zhengdong Liu study, the price expected for the consumables, maintenance, post-processing machines to remove supports and rent are around 80€per part, when merging his data to this study [36].

As a final procedure, the part is milled in the areas of interest. To evaluate the machining cost, it is used the Cost Explanation File (CEF) delivered by the FST Lisboa team on the competitions. The usage of a 3-axis CNC is enough to perform the desired features which have an hourly cost of approximately 24€/h, with every expense accounted [37]. Since this process consists of drilling 10 holes and opening the o-ring grooves, 2hours of machining must be enough margin to consider.

The final cost of the caliper rises to 550€. If the work is done externally, it can be expected a very significant cost increase.

8.1.2 Weight Reduction

At this point in the study, it was achieved some weight reduction, but was that amount expected? After the topology optimisation results, the replication of these results to an organic CAD shape was done manually, which tends to increase the weight to facilitate the design conception. Using the conclusions from the section 8.1.1, it is safe to say there is more room for material removal since the compliance is below the limit, and that can be accomplished in several ways:

- Use programs focused on additive manufacturing techniques with tools capable of smoothing and create the topology design precisely;
- Increase the threshold of the density plot and replicate the design again;
- Decreasing the non-design space volume, by reducing its thickness in some regions that do not need the excessive material.

The second point of view is that, because the design itself is already so much constrained by so many inputs from the current car, the non-design space represents a higher fraction of the total volume, leaving less room for the design space and consequently for its optimisation.

8.1.3 Alternative Solution

This solution was a sort of an answer to the conclusions stated in section 8.1.2. The first point was realised by changing the type of software used to post-process the topology optimisation results. The second point was tested, but no significant differences were found on changing the threshold. The third point approaches a reduction in the thickness of non-design space. However, it was maintained to assure good printing in these regions and eliminate the higher warp probability.

Table 8.5: Alternative design caliper analysis

Properties	Value
Compliance	8633 <i>N.mm</i>
Weight (Caliper+Pistons)	308 <i>g</i>
Maximum Displacement	0.82 <i>mm</i>
Manufacturing Cost	531€ ²

The table 8.5 demonstrates an increase in the fraction of weight reduction when compared to the previous solution, is now situated at 23%. The compliance is still below the maximum constraint because some of the medium density elements are converted to full density.

Table 8.6: AM alternative design cost analysis

Total cost per part	EUR	P=MP+AP+CP+BP	≈403
Other costs associated [36]	EUR	-	80
CNC machining cost [37]	EUR	-	48
Total Cost	EUR	-	531

8.2 Spare Parts Cost

Evaluating the market prices of the spare parts, there is an additional cost associated with the caliper.

²Explained on table 8.6

Table 8.7: Spare parts cost

Part	Market price per unit
Shoulder Bolts x3	0.90€
Bleed Screw x1	5€
Banjo Bolt M8 x2	1.5€
Banjo 8mm 90° x2	5€
Copper Crush Washer M8 x4	0.20€
Banjo Bolt M10 x1	6.25€
Banjo 10mm x1	6.5€
Copper Crush Washer M10 x2	0.20€
Pair of Brake Pads x2	30€
O-rings Parker x4	0.20€
Total	95.45€

A significant part of these components are bought separately from the AP racing solution, so this cost does not influence the comparison established previously.

8.3 Final Conclusions

This study concluded that this application is possible and has a positive impact on car design. For a manufacturer, and through a simple and limited manufacturing cost analysis, it is possible to affirm that the cost of the build may be 16% lower than the buying option from the AP Racing. Despite this cost being lower than the AP racing caliper, it has to be considered that the AP racing price is the selling price with the profit margin and taxes included on top of the manufacturing cost, while the table analysis is the cost from the production point of view. As a Formula Student team, this approach may be valid, since it is possible to negotiate the terms with some sponsors that may not be able to sponsor printed parts fully, but may be able to accept a deal of production costs payment, leaving the profit margin and taxes at the side, in return of the visibility. There is also the possibility of splitting the cost between different sponsors if one is in charge of the material supply and the other in charge of the machinery work.

In the typical industry point of view, this cost analysis will not be acceptable, unless the entity already has this piece of machinery. If the hardware is available, it is possible to produce those components at that price. Otherwise, the costs of ordering these 3D printed components may be estimated by asking for a quote to a known company. As an example, a quote asked to Sculpteo company estimates that the production of one caliper is 1952€. Depending on the batch size, the costs may reduce, but will always be much higher than the previous calculated.

The weight was reduced by 23% while still maintaining compliance 14% below the defined as an objective.

The thermal analysis has served to corroborate the temperature of the disk and its maximum settling point during consecutive runs but also shown that the caliper temperature is within the bearable range for this type of titanium alloy.

8.4 Future Work

The additive manufacturing, especially in the metal material field is still under research for the team. However, there is a lot of studies and development being made in AM field in several industry sectors. The pursuit for a product development lifecycle decrease and to achieve efficient production of prototypes and small batches, led the industry to this type of technologies.

As future work, some interesting points could be left for the team and any person to take into account:

- Given the current range of printable materials, explore the possibility of AM for other car components. If weight reductions in the order of 23% can be achieved, it can be a possible way of decreasing the weight of the car significantly. This approach includes the rear brake calipers.
- Explore the possibility of designing these components in driving (and not driven) approach, i.e. design the calipers first and then the knuckles. Explore the possibility of reducing the front calipers to two pistons, to achieve even more weight losses. This measure would reduce the non-design volume, making the design lighter. However, the reduction in the number of pistons may implicate an increase in its diameter, which may not be compatible with the discs' dimensions.

Bibliography

- [1] M. Hejtmanek. Additive Manufacturing Technologies Utilization in Process Engineering. Master's thesis, České vysoké učení technické v Praze, Czech Republic, 2017.
- [2] Ross Brawn career. URL <https://www.linkedin.com/in/ross-brawn-obe-ba6157123/>.
- [3] R. Limpert. *Brake Design and Safety*. SAE, 3th edition, 2011. ISBN 9780768034387. doi: 10.4271/R-398.
- [4] A. R. Pishdad. Advanced Design of Brake Calipers. Master's thesis, Politecnico di Milano, Italy, 2012.
- [5] Titanium Processing Center. Titanium TI-6AL-4V Properties & Common Uses, 2016. <https://titaniumprocessingcenter.com/titanium-ti-6al-4v-properties-common-uses/>, Last accessed on 21/10/2019.
- [6] M. Peters and C. Leyens. *Titanium and Titanium Alloys*. Wiley, jul 2003. ISBN 9783527305346. doi: 10.1002/3527602119.
- [7] Bugatti Automobiles S.A.S. WORLD PREMIERE: BRAKE CALIPER FROM 3-D PRINTER, 2018. <https://www.bugatti.com/media/news/2018/world-premiere-brake-caliper-from-3-d-printer/>, Last accessed on 21/10/2019.
- [8] Formula Student - IMechE. <https://www.imeche.org/events/formula-student/about-formula-student>, Last accessed on 23/10/2019.
- [9] FS-Germany. Formula Student Rules 2019 V1.1, 2019. URL https://www.formulastudent.de/fileadmin/user_upload/all/2019/rules/FS-Rules_2019_V1.1.pdf. Accessed on 29/10/2019.
- [10] OZ S.p.A. Formula Student Wheels. URL <https://www.ozracing.com/uk/motorsport/formula-student/wheels>. Last accessed on 28/10/2019.
- [11] N. P. Wagh. Design and analysis of modular caliper assembly. Master's thesis, Shivaji University, India, 2005.
- [12] R. Shah, C. Shah, and S. Thigale. Design and analysis of a hydraulic Brake caliper. *International Journal of Mechanical Engineering and Technology*, 8(5):33–41, 2017. ISSN 09766359.

- [13] Robert Bosch GmbH. *Bosch Automotive Handbook*. SAE, 9th edition, 2014. doi: 10.4271/0768081521.
- [14] M. Berry. Shop Work Basics - Bleeding Brakes, 2011. <http://hhh.gavilan.edu/hspenner/iLearnInfo/AMT111/LandingGear/BleedingBrakes.pdf>, Last accessed on 23/10/2019.
- [15] F. Puhn. *Brake Handbook*. HP Books, 1985. ISBN 0-89586-232-8.
- [16] R. Muscoplat. Brake pad backing plate types, 2019. URL <https://ricksfreeautorepairadvice.com/brake-pad-backing-plate-types/>. Last accessed on 28/10/2019.
- [17] V. L. Popov. *Contact Mechanics and Friction*. Springer Berlin Heidelberg, 2nd edition, 2017. ISBN 978-3-662-53080-1. doi: 10.1007/978-3-662-53081-8.
- [18] R. Singh and S. Singh. *Additive Manufacturing: An Overview*. Elsevier, 2017. ISBN 9780128035818. doi: 10.1016/B978-0-12-803581-8.04165-5. URL <https://linkinghub.elsevier.com/retrieve/pii/B9780128035818041655>. Last accessed on 23/10/2019.
- [19] Introduction to 3D Printing - Additive Processes. URL <https://make.3dexperience.3ds.com/processes/powder-bed-fusion>. Last accessed on 23/10/2019.
- [20] M. Islam, B. Boswell, and A. Pramanik. Dimensional accuracy achievable by three-dimensional printing. In *IAENG Transactions on Engineering Sciences*, pages 263–268. CRC Press, apr 2014. doi: 10.1201/b16763-29.
- [21] K. Kamarudin, M. S. Wahab, Z. Shayfull, A. Ahmed, and A. A. Raus. Dimensional Accuracy and Surface Roughness Analysis for AISi10Mg Produced by Selective Laser Melting (SLM). In *MATEC Web of Conferences*, 2016. doi: 10.1051/mateconf/20167801077.
- [22] *O-Ring Handbook*. Parker Hannifin Corporation, 2015. URL <https://www.parker.com/literature/Praedifa/Catalogs/Catalog{ }0-Ring-Handbook{ }PTD5705-EN.pdf>. Last accessed on 29/10/2019.
- [23] A. Olason. Methodology for Topology and Shape Optimization in the Design Process. Master's thesis, Chalmers University of Technology, Sweden, 2010.
- [24] R. Larsson. Methodology for Topology and Shape Optimization : Application to a Rear Lower Control Arm. Master's thesis, Chalmers University of Technology, Sweden, 2016.
- [25] TSF. TABLE OF PRELOADS AND TIGHTENING APPROXIMATE VALUES. URL <http://www.tsftsh.com/assets/files/catalogs/PrecargasWeb.pdf>. Last accessed on 29/10/2019.
- [26] M. Janeček, F. Nový, P. Harcuba, J. Stráský, L. Trško, M. Mhaede, and L. Wagner. The Very High Cycle Fatigue Behaviour of Ti-6Al-4V Alloy. *Acta Physica Polonica A*, 128(4):497–503, oct 2015. ISSN 0587-4246. doi: 10.12693/APhysPolA.128.497.
- [27] R. Budynas and J. K. Nisbett. *Shigley's Mechanical Engineering Design*. McGraw-Hill, 9th edition, 2015. ISBN 978-0-07-352928-8.

- [28] A. Neys. In-Vehicle Brake System Temperature Model. Master's thesis, Chalmers University of Technology, Sweden, 2012.
- [29] F. Talati and S. Jalalifar. Analysis of heat conduction in a disk brake system. *Heat and Mass Transfer*, 45(8):1047–1059, 2009. ISSN 1432-1181. doi: 10.1007/s00231-009-0476-y.
- [30] M. Vidiya and B. Singh. Experimental and Numerical Thermal Analysis of Formula Student Racing Car Disc Brake Design. *Journal of Engineering Science and Technology Review*, 10(1):138–147, feb 2017. ISSN 17919320. doi: 10.25103/jestr.101.19. URL <http://jestr.org/downloads/Volume10Issue1/fulltext191012017.pdf>.
- [31] J. Outinen and P. Mäkeläinen. Mechanical properties of structural steel at elevated temperatures and after cooling down. *Fire and Materials*, 28(24):237–251, mar 2004. ISSN 0308-0501. doi: 10.1002/fam.849.
- [32] L. M. M. d. A. V. de Abreu. Mechanical design of the wheel assembly of an electric Formula Student prototype. Master's thesis, Instituto Superior Técnico, Portugal, May 2019.
- [33] E. Atzeni and A. Salmi. Economics of additive manufacturing for end-usable metal parts. *The International Journal of Advanced Manufacturing Technology*, 62(9-12):1147–1155, oct 2012. ISSN 0268-3768. doi: 10.1007/s00170-011-3878-1.
- [34] SLM Solutions. *Selective Laser Melting Machine SLM 280 2.0*. URL <https://www.slm-solutions.com/en/products/machines/slmr280-20>. Last accessed on 14/10/2019.
- [35] Z. Li, I. Kucukkoc, D. Z. Zhang, and F. Liu. Optimising the process parameters of selective laser melting for the fabrication of Ti6Al4V alloy. *Rapid Prototyping Journal*, 24(1):150–159, jan 2018. ISSN 1355-2546. doi: 10.1108/RPJ-03-2016-0045. URL <https://www.emerald.com/insight/content/doi/10.1108/RPJ-03-2016-0045/full/html>.
- [36] Z. Liu. ECONOMIC COMPARISON OF SELECTIVE LASER MELTING AND CONVENTIONAL SUBTRACTIVE MANUFACTURING PROCESSES. Master's thesis, Northeastern University, Massachusetts, May 2017.
- [37] FST Lisboa. Cost Explanation File (CEF). Technical report, 2019.

Appendix A

Sculpteo Quote

The screenshot shows the Sculpteo website interface. At the top, there is a navigation bar with the Sculpteo logo, links for Services, Material Guide, and Blog, and a user profile section for 'dgompferreira'. A blue button 'Upload a file' is also visible. Below the navigation bar, the main content area displays a quote for a user named 'teste'. The quote includes a table with columns for Model, Scale (xyz), Process, Material, Finish, Color, Varnish, Production, and Prices. Two items are listed: 'teste' and 'teste2'. Both items are made of Titanium 6Al-4V using Laser Melting (Metal) process with a Shot peened finish. The total price is 1952.64 €. The estimated delivery date is Nov. 15, 2019.

Model	Scale (xyz)	Process	Material	Finish	Color	Varnish	Production	Prices
teste	65.8 mm 118.5 mm 35.0 mm	Laser Melting (Metal)	Titanium 6Al-4V	Shot peened	-	-	Standard Ships on Nov. 15, 2019	x € 1034.87 = € 1034.87
teste2	56.7 mm 119.0 mm 30.0 mm	Laser Melting (Metal)	Titanium 6Al-4V	Shot peened	-	-	Standard Ships on Nov. 15, 2019	x € 917.77 = € 917.77

Figure A.1: Sculpteo Quote for the caliper 3D printing

